

New Motifs in DNA Nanotechnology and their Applications

vorgelegt von
Diplom-Ingenieur
Jens Kopatsch

Von der Fakultät III (Prozesswissenschaften)
der Technischen Universität Berlin
zur Erlangung des akademischen Grades

Doktor der Ingenieurwissenschaften
- Dr.-Ing -

genehmigte Dissertation

Promotionsausschuss:

Vorsitzender: Prof. Dr. Roland Lauster

Berichter: Prof. Dr. Ulf Stahl

Berichter: Prof. Dr. Nadrian C. Seeman

Tag der wissenschaftlichen Aussprache: 1. September 2004

Berlin 2004

D 83

Vorveröffentlichungen

Publications:

3D Fractal DNA Assembly from Coding, Geometry and Protection, A. Carbone, C. Mao, P. E. Constantinou, B. Ding, J. Kopatsch, W. B. Sherman, N. C. Seeman. *Natural Computing* 2004

The Design of Self-Assembled 3D DNA Networks. C. Mao, P. E. Constantinou, F. Liu, J. Kopatsch, T. Wang, B. Ding, R. Sha, H. Yan, J. J. Birktoft, R. Sha, H. Zhong, P. S. Lukeman, Y. Pinto, L. Foley, L. A. Wenzler, R. Sweet, M. Becker and N. C. Seeman, *Proceedings of the Electrochemical Society* in press 2004

DX Cohesion in Structural DNA Nanotechnology. P. E. Constantinou, T. Wong, J. Kopatsch, L. B. Israel, C. Mao, B. Ding, R. Sha, X. Zhang, N. C. Seeman. In preparation

Abstracts

Albany 2003 Meeting, The 13th Conversation Structural DNA Nanotechnology, Nadrian Seeman, Hao Yan, Chengde Mao, Ruojie Sha et. al. *Journal of Biomolecular Structure and Dynamics* Vol. 20 Issue 6, June 2003 Page 925

American Crystallographic Association, Annual Meeting 2004,
Abstract: The Design of Self-Assembled 3D DNA Crystals. Nadrian
C. Seeman, Pamela E. Constantinou, Baoquan Ding, Tong Wang,
Jens Kopatsch, Ruojie Sha, Jens J. Birktoft, Furong Liu, Robert
Sweet & Chengde Mao

Patents:

Polygonal nanostructures of polynucleic acid multi-crossover molecules
and assembly of lattices based on double crossover cohesion Pro-
visional US patent application, Nadrian C. Seeman et al.

Acknowledgments

I would like to thank Prof. Dr. Nadrian Seeman for the opportunity to perform my research project at the Chemistry Department of New York University and Prof. Dr. Ulf Stahl for the support of my thesis.

Further I would like to thank all my lab members and former lab members for the good collaboration and time we had together in New York: Banani Chakraborty, Baoquan Ding, Gang Wu, Hong Zhong, Xiaoping Zhang, Xing Wang, Yoel P Ohayon, Jiwen Zheng, Liang Ding, Lisa Israel, Alejandra Victoria Garibotti, Pamela E Constantinou, Ruojie Sha, Shiping Liao, Tong Wang and Wanqiu Shen, Phiset Sa-Ardyen, Loraine Foley and Andrea Giro. A special thanks to Philip Lukeman, Jens Birktoft, Yariv Pinto and William Sherman for scientific discussions, Philip Lukeman, William Sherman and Hans Martin Sieg for proof reading and Jeff Birac for providing the computer aided modelling program GIDEON.

In addition I want to thank Prof. Kathleen Kinnally for the friendly collaboration with the ion-channel project and the people in her laboratory Sonia Martinez-Caballero, Laurent Marc Dejean and Serguei Grigoriev for the friendly work climate.

Zusammenfassung (German Abstract)

Es wurden Versuche mit dem DX-Motiv durchgeführt, um die Mindestlänge von *Sticky Ends* für das *Self-Assembly* zu ermitteln. Weiterhin wurden Kristallisationsversuche mit dem TX-Motiv, ausgestattet mit *Sticky-Ends*, unternommen. Kristallisationsversuche einer TX-Version mit glatten Enden wurden unternommen, um Aussagen über einen eventuell vorhandenen Torsionsstress zu treffen. Von einem Dreiecksmotiv (Chengde-Mao-Dreieck) wurden Gelmobilitätsuntersuchungen von verschiedenen Versionen vorgenommen. Diese Untersuchungen offenbarten möglichen Torsionsstress in einigen der Versionen. Mit drei Helizität-Variationen (Version mit 14nt per innerer Dreiecks-Seitenkante) des Dreiecks wurden Kristallisationsversuche unternommen. Zwei Variationen des Motivs bildeten reproduzierbare Kristalle, die unter Röntgenstrahlen Diffraktion bis zu zehn Ångström zeigten. Ein weiteres Dreiecksmotiv, genannt TXDX, bestehend aus einem Dreieck, aufgebaut aus drei versatzverschränkten TX-Motiven, wurde als vielversprechendes Motiv entwickelt. Die Verbindungen zu anderen TXDX-Dreiecken ist über das DX-Motiv realisiert. Ein- und zweidimensionale Felder konnten nach einer Modifikation, die das *Self-Assembly* auf ein bzw. zwei Dimensionen beschränkt, erzeugt werden. Es sind jeweils drei Variationen für die ein- und zweidimensionalen Felder möglich. Alle wurden erfolgreich erzeugt und mit dem Rasterkraftmikroskop nachgewiesen. Ein rohrartiges Motiv, bestehend aus sechs ca. 30 nm langen DNS-Helices, verbunden durch Überkreuzungen, wurde entwickelt. Dieses Motiv sollte in eine künstliche Membran inkorporieren und als Ionenkanal fungieren. Typisches Ionenkanalverhalten konnte beobachtet werden.

Abstract

Experiments with the well characterized DX motif were undertaken to see which number of nucleotides is necessary for sticky ended assembly. A sticky ended crystallization attempt was made with the TX motif. In addition a crystallization attempt with a blunt ended TX motif was made to disclose a possible torsion stress within the motif. Nondenaturing gel mobility studies of a triangle motif (Chengde Mao triangle) were performed and showed torsion stress in some versions of these molecules. Three molecules that contained 14nt per inner triangle edge, yet have a structure designed to assemble with a different overall helical repeat in the crystal were constructed and crystallization was attempted. Reproducible crystals were obtained from two helicity variations and showed diffraction down to ten Ångström. Another triangle motif, named TXDX triangle, consisting of a triangle based on three TX motifs, connected with a skew, was developed. TXDX triangles were connected with each other using a variation of the DX motif. One and two-dimensional arrays were created after the motif was modified to limit self-assembly to one and two dimensions. Due to the design there are three possible versions of the one and two dimensional arrays. All possible array variations were observed with an atomic force microscope. A tube like motif was designed, consisting of six 30 nm long DNA helices, connected by cross-overs. This motif was supposed to incorporate itself into an artificial membrane and function as an ion channel. Typical ion channel behavior was observed with this motif.

Where nature finishes producing its shapes, there man begins,
with natural things and with the help of nature itself, to create
infinite varieties of shapes.

Leonardo Da Vinci

Contents

1	Introduction	1
1.1	Nanotechnology	1
1.1.1	Introduction to Nanotechnology	1
1.1.2	Self-Assembly	2
1.2	DNA Nanotechnology	3
1.2.1	DNA Structure and Function	3
1.2.2	Holiday Junction and Branch Migration	11
1.2.3	<i>De novo</i> Designed Junctions and Avoidance of Branch Migration	12
1.2.4	2 Dimensional DNA Arrays	14
1.2.5	Other Molecules for DNA Nanotechnology	22
1.3	Nanomechanical Devices based on DNA	26
1.3.1	A Nanomechanical Device Predicated on the B-Z Tran- sition of DNA	26
1.3.2	DNA Nanomechanical Devices Based on Hybridization Topology	27
1.4	DNA Based Computing	29
1.4.1	Introduction to DNA Based Computing	29
1.4.2	DNA Computations with Rectangular Tiles	32

1.4.3	Cumulative XOR Computation with DNA	35
1.5	Crystallography	37
1.5.1	Traditional DNA Crystallography	37
1.5.2	3-Dimensional DNA assembly	37
1.5.3	DNA Cages for Trapping and Characterization of Biomolecules	39
1.6	Ion Channels	40
1.6.1	Ion Channels in Organisms	40
1.6.2	Artificial Ion Channels	41
1.7	Presentation of a Problem	42
1.7.1	DNA Crystallization	42
1.7.2	6 Helix Bundle as an Artificial Ion Channel	42
2	Materials and Methods	43
2.1	Design of New Molecules	43
2.1.1	<i>De novo</i> Design of Sticky Ends	43
2.1.2	<i>De novo</i> Design of DNA Sequences	44
2.1.3	DNA Junctions	44
2.1.4	Computer Aided molecular modeling	44
2.2	From DNA Synthesis to Annealing of Motifs	45
2.2.1	DNA Synthesis	45
2.2.2	Denaturing Gels and DNA Purification	45
2.2.3	Native Gels (Non-Denaturing Gels)	46
2.2.4	Stoichiometry of DNA Strands	47
2.2.5	Fast Annealing of Oligonucleotides for Native Gel Based Studies	48
2.2.6	Slow Annealing of Oligonucleotides	48
2.3	Atomic Force Microscopy	48
2.3.1	Preparation of sample	48

2.3.2	AFM Imaging	49
2.3.3	Post Processing of AFM Pictures	49
2.4	3D Assembly - DNA Crystallization	49
2.4.1	Hanging Drop Crystallization	49
2.4.2	Crystallization with Temperature Control	50
2.4.3	General Crystallization and Crystal Mounting Tech- niques	51
2.4.4	X-Ray Examination of DNA Crystals	52
2.5	Crystallization Experiments	52
2.5.1	3D Assembly with TXA Tiles Under High Magnesium Ion Concentration	52
2.5.2	2D-Assembly of DX Molecules with Short Sticky Ends	53
2.5.3	Crystallization Attempt of Blunt Ended DX Tiles . . .	53
2.5.4	3D Assembly and Gel Studies of Chengde Mao Triangles	54
2.5.5	3D Assembly with a TXDX Triangle Motif and 0D, 1D and 2D examination of the motif	57
2.6	DNA Nanotube as an Artificial Ion Channel	60
2.6.1	Design of a DNA Nanotube for Use as an Artificial Ion Channel	60
2.6.2	DNA Minor Groove Binder	63
2.6.3	Tip Dip and Patch Clamp Experiments	65
3	Results	68
3.1	3D Assembly - DNA Crystallization	68
3.1.1	3D Assembly with TX Tiles Under High Magnesium Ion Concentration	68
3.1.2	2D-Assembly of DX Molecules with Short Sticky Ends	70
3.1.3	Crystallization Attempt of Blunt Ended DX Tiles . . .	72

3.1.4	3D Assembly and Gel Studies of ChengdeMao Triangles	74
3.1.5	3D Assembly with a TXDX triangle motif and 0D, 1D and 2D examination of the motif	82
3.2	DNA Nanotubes	87
3.2.1	DNA Nanotube for Use as an Artificial Ion Channel . .	87
4	Discussion	90
4.1	Crystallization Experiments	90
4.1.1	3D Assembly with TX Tiles Under High Magnesium Ion Concentration	90
4.1.2	2D-Assembly of DX Molecules with Short Sticky Ends	90
4.1.3	Crystallization Attempt of Blunt Ended DX Tiles . . .	91
4.1.4	3D Assembly and Gel Studies of ChengdeMao Triangles	91
4.1.5	3D Assembly with a TXDX Triangle Motif and 0D, 1D and 2D examination of the motif	95
4.2	DNA Nanotube as an Artificial Ion Channel	96
4.3	Conclusion and Outlook	98
4.3.1	3D Assembly	98
4.3.2	6 Helix Bundle	99
5	Bibliography	101
6	Appendix	119
6.1	Gel for XOR Operation	120
6.2	Length Marker for Gel Based Studies	121
6.3	Natrix Formulation from Hampton Research	122
6.4	Crystall Mounting in Capillaries	130
6.5	Netropsin Binding Thermodynamics	132
6.6	Properties and Sequences of Used Sticky Ends	133

6.7	TXDX Triangle Motif with Attached DNA Sequence	136
6.8	Pipetting Strand Combinations for the TXDX Triangle	137
6.9	Calculation of Unique 7mers for the AT-rich sequence	139
6.10	DNA Crystallization Conditions from Literature	144
6.11	Calculation of CDM Triangle Properties	147
6.12	All DNA Strand Sequences used in 5'to 3' Direction	154
6.12.1	Strands for DX 2D Array with Short Sticky Ends	154
6.12.2	Strands used for 3D project with TX Motif	155
6.12.3	Strands for Crystallization of Blunt ended DX Motif	156
6.12.4	DNA Triangle Strands Designed by Prof. ChengDe Mao	157
6.12.5	DNA Strands for Gel-based studies of Triangles	158
6.12.6	DNA Stands for 3D Triangle with 14nt per Edge	160
6.12.7	DNA Strands for 6 Helix Bundle with Netropsin Binding Sites	163
6.12.8	DNA Strands for the TXDX Triangle Motif	166
6.13	Lebenslauf - Curriculum Vitae	171

List of Figures

1.1	Watson-Crick base pairing*. Adenine pairs with thymine (upper part of the figure) and guanine pairs with cytosine (lower part)	4
1.2	Adenine self pairing*	4
1.3	Adenine can pair with uracil in Hoogsteen base paring*	5
1.4	Adenine can pari with uracil in reversed Hoogsteen base paring*	5
1.5	Adenine can pair with thymine in reversed Watson-Crick base pairing*	6
1.6	Guanine can pair with uracil in sheared Watson-Crick base pairing*. The cytosine position in regular Watson-Crick pairing is drawn in red.	6
1.7	B-DNA double helix*.B-DNA is the most stable helical form of DNA formed by a random sequence. The right side of the figure shows a view down the helical axis.	7
1.8	A-DNA helix* can form under dehydrating conditions. The right side of the figure is a view down the helical axis.	8

*Picture obtained from public sources

1.9	D-DNA is shown* in the left side of the picture and can occur with alternating A and T sequences . Z-DNA (right side*) is formed by GC rich sequences under high salt conditions. The Z-DNA back bone is left handed.	9
1.10	DNA triplex* formed by three DNA strands. Hoogsteen base pairing is involved in this structure.	10
1.11	Quadruplex DNA* are found in the end of eukaryontic chromosomes and contain G-rich repetitive sequences.	11
1.12	Branch migration [†] . Crossing-over of homologous areas (II) of two double helices (I), followed by branch migration (II-III) of the Holliday junction and resolution (IV) lead to two possible products (V). VI shows a possible ligation step.	11
1.13	Four arm junction with symmetry minimization [†] . It does not possess the symmetry necessary to perform branch point migration.	13
1.14	Three arm junctions with sticky ends. Ligation studies show that regular three arm junctions (left side) equipped with sticky ends tend to cyclize. Bulged three arm junctions (right side) show less tendency to cyclize.	13
1.15	Sticky ended cohesion [†] . Two DNA helices with complementary sticky ends can associate due to Watson-Crick base pairing and can optionally be ligated together.	15
1.16	Basic concept of self assembly [†] . A motif can associate to form a larger predicted complex due to specific sticky ends.	16

[†]Picture kindly provided by Prof. Dr. Seeman

1.17	Different types and nomenclature of DNA double crossover molecules [†] . The first character 'D' stands for double crossing over, the second character refers to the relative orientations of their two double helical domains, 'A' for antiparallel and 'P' for parallel. The third character refers to the number (modulus 2) of helical half-turns between crossovers, 'E' for an even number and 'O' for an odd number. A fourth character is needed to describe parallel double crossover molecules with an odd number of helical half-turns between crossovers. The extra half-turn can correspond to a major (wide) groove separation, designated by 'W,' or an extra minor (narrow) groove separation, designated by 'N.'	17
1.18	Assembly principle of a 2D-DNA array consisting of two different DX tiles [†] . A hairpin, serving as a topographic label, is incorporated into the blue tile.	18
1.19	AFM picture of a 2D DX array [†] . The hairpin on every second tile can be clearly seen and shows the predicted spacing.	18
1.20	TX motif consisting of three helices connected by 4 cross-overs, shown in a blunt ended version.	19
1.21	Assembly principle of a 2D array consisting of two different TX tiles [†] . A hairpin, serving as a topographic label, is incorporated into the red tile.	20
1.22	AFM picture a 2D DNA array consisting of TX tiles. The hairpin on every second tile can be clearly seen and shows the predicted spacing.	20
1.23	Schematic picture of parallelogram assembly [†] . Four junctions can be combined into a rhombus like motif.	21

1.24	AFM picture of parallelogram array [†] . The rhombus like structure can be distinguished.	21
1.25	The DNA strands in this molecule [†] have the connectivity of a cube. It consists of six cyclic strands. The cube is created by ligating two ends of two quadrilaterals to form a belt-like molecule. The nucleotides are represented by white dots (nucleic base) in this drawing, the colored dots represent the sugar phosphate backbone of the DNA strands with one color per strand.	22
1.26	The DNA strands in this molecule [†] have the connectivity of a truncated octahedron. The truncated octahedron is viewed down the four fold axis of one of the squares. The edges of the truncated octahedron consist of two full turns of dsDNA. The complete truncated octahedron contains 14 cyclic strands of DNA and each cyclic strand corresponds to a face of the truncated octahedron. The nucleotides are represented by white dots (nucleic base) in this drawing, the colored dots represent the sugar phosphate backbone of the DNA strands.	23

- 1.27 Borromean rings made of DNA[†]. Borromean rings are special because if one of the three rings is destroyed it will free the other two rings while leaving them intact and not connected to each other. The conventional nodes in Borromean rings (a) have been replaced by three nodes, derived from 1.5 turns of DNA double helix (b). The stereoscopic representation (c) is shown in the middle part of the picture. A stereoscopic view of the synthesized DNA molecule with hairpins is shown in the lower part of the picture (d). The hairpins contain sequences for restriction enzymes that can be used for digestion and, depending on the restriction site used, release of the other two DNA rings. 25
- 1.28 A nanomechanical device predicated on the B-Z transition of DNA[†]. Twenty nucleotide pairs of this helix can be converted into Z-DNA and induce a nanomechanical movement of the rigid DX tiles. The part acting as a bridge between the tiles is shown in yellow. The relative movement of the DX tiles is caused by the transition of right handed B-DNA to left handed Z-DNA (induced with Hexaamminecobalt(III) chloride) and can be measured with FRET (Fluorescence resonance energy transfer of donor and acceptor molecules attached to the DX molecules in the appropriate place marked by green and purple dots). The upper part of the figure shows the bridge DNA in B Form (right handed) and the lower part shows it in Z-Form (left handed). 26

1.29	Nanomechanical device based on hybridization topology [†] . Left side (a): The letters A, B, C and D, along with the color coding, show that the bottom of the JX ₂ motif (C and D) are rotated 180° relative to the PX motif. The set strands are shown in green, they can be removed by the addition of biotinylated green fuel strands (biotin indicated by black circles, process step I). The addition of the purple set strands (process step II) converts the unstructured intermediate into the JX ₂ motif. In process step III the JX ₂ molecule is converted to the unstructured intermediate by the addition of biotinylated yellow fuel strands. The PX device is restored and the cycle completed by the addition of green set strands (IV). Right side (b): AFM observation of the cycle with DNA trapezoids attached as a marker.	28
1.30	Graph with 7 nodes. Arrows indicate possible connections between two nodes.	29
1.31	Algorithmic assembly by Wang tiles [†] , each edge pairs with another edge of the same color. If this rule is strictly employed the assembly mimics the operation of a Turing machine. The mosaic on the bottom shows the principle of an addition. The 5th, 9th and 14th columns of the mosaic in the first row show a special tile, which corresponds to the sum of 5 + 9. Based on a perfect assembly concerning the edge color pairing rule, the 3rd special tile in the first row marks the result of the addition: 14.	33

1.32	XOR calculation with DNA [†] . (a) shows a triple crossover molecule that contains a reporter strand. (b) shows the several TX molecules used in the operation. The final result is found by ligating the reporter strand, amplifying it with PCR, treating it with restriction enzymes and examining it on a gel.	35
1.33	3D Assembly with TX molecules [†] . Assembly in the 3rd dimension can be achieved by connecting the middle helix with sticky ends which enable another 90° rotated TX tile do connect.	38
1.34	DX tiles can be arranged to fill 3D space when each DX is rotated 135° relative to the next DX [†]	38
1.35	DNA cages containing oriented guests [†] . If DNA crystals can be created they might be able to capture biomolecules and serve as crystallization scaffolding.	39
2.1	Example of a CDM triangle with 17nt per inner triangle edge. The basic design of this molecule was thought up by Prof. Chengde Mao. If equipped with sticky ends then this motif can assemble along each helical DNA axis and fill space. . . .	56
2.2	DNA triangle handedness by Dr. William Sherman. The CDM triangle can occur in two different conformations (left or right handed), depending on the number of nt per inner triangle edge.	56
2.3	Computer generated model of a TXDX triangle tile. The motif is shown in a blunt ended version.	58
2.4	Top view of a computer generated model of a TXDX triangle tile.	59

2.5	Computer generated model of one side of the TXDX triangle tile. The TXDX triangle consists of three of such “sub-motifs,” connected with a skew. This “sub-model” lacks some strand nicks of the actual TXDX triangle.	59
2.6	End view of a computer generated model of the 6 helix bundle. Six DNA helices are connected via cross-overs. Each helix has 9 full turns of DNA, the motif consists of 19 strands.	60
2.7	Angled view of a computer generated model of the 6 helix bundle. Six DNA helices are connected via cross-overs. Each helix has 9 full turns of DNA, the motif consists of 19 strands.	61
2.8	Molecular structure of Netropsin*.	64
2.9	Stereoscopic picture of a dsDNA Crystal structure with Netropsin attached in the minor groove*.	64
2.10	The tip dip method. Ion channels can be reconstituted into bilayers formed at the tip of a microelectrode in a method called tip-dip. A microelectrode is submerged in a bath. Lipids (typically in an organic solvent like decane) are layered on top of the bath and allowed to form a monolayer on the bath surface (A). The microelectrode is raised out of the bath (B). A bilayer is formed like a sandwich as the microelectrode is again returned to the bath (C). Channels are added to the bath and insert spontaneously (not shown).**	66
3.1	Light microscope picture of annealed TX crystals under polarized light	69

**Picture Kindly Provided by Prof. Dr. Kinnaly

3.2	Light microscopy picture of TX crystals grown with a combination of slow temperature decrease and hanging drop vapor diffusion.	69
3.3	AFM picture of a DX array with short sticky ends. Picture scale 1.1 μm x 1.1 μm	70
3.4	AFM picture of a DX array with short sticky ends. Picture scale 595 nm X 595 nm	71
3.5	Light microscope picture of a crystallization attempt via hanging drop vapor diffusion of a blunt ended DX tile (upper part of the drop). Crystals were grown in Natrix kit buffer 26. . . .	72
3.6	Light microscope picture of a crystallization attempt via hanging drop vapor diffusion of a blunt ended DX tile (lower part of the drop). Crystals were grown in Natrix kit buffer 26. . . .	73
3.7	Light microscope picture of a crystallization attempt via hanging drop vapor diffusion of a blunt ended DX tile. Crystals were grown in Natrix kit buffer 44.	73
3.8	Picture of a gel (5% polyacrylamide) study of CDM triangles with 13 nt and 14 nt per inner edge. Lane 1 contains <i>HaeIII</i> digested pBR marker, lanes 2-5 show the 13 nt triangle with a logarithmically decreasing concentration from 12 μM to 1.5 μM , lanes 6-9 show the same for the 14 nt triangle. 10 μl were loaded.	74
3.9	Picture of a gel (5% polyacrylamide) study of CDM triangles with 15 nt per inner edge. Lane 1 contains <i>HaeIII</i> digested pBR marker, lanes 2-5 CDM triangle, 12 μM to 1.5 μM logarithmic concentration series). 10 μl were loaded.. . . .	75

3.10	Picture of a gel (5% polyacrylamide) study of CDM triangles with 17 nt and 18 nt per inner edge. Lane 1 contains <i>Hae</i> III digested pBR marker, lanes 2-5 show the 17 nt triangle, lanes 6-9 show the 18 nt, both with logarithmically decreasing concentration from 12 μ M to 1.5 μ M. 10 μ l were loaded.	76
3.11	Light microscope picture of crystals from system CDM-A (polarized light). Crystals were grown in Natrix kit buffer 5. . . .	77
3.12	Light microscope picture of crystals from system CDM-B (polarized light). Crystals were grown in Natrix kit buffer 45. . . .	77
3.13	Light microscope picture of crystals from system CDM-C (polarized light). Crystals were grown in Natrix kit buffer 19. . . .	78
3.14	X-ray diffraction pattern form a CDM-A triangle system	78
3.15	X-ray diffraction pattern form a CDM-B triangle system. . . .	79
3.16	Light microscope picture of crystals from system CDM-B _{1BE} (polarized light). Crystals were grown in Natrix kit buffer 19. . . .	80
3.17	Composite of 10 X-ray diffraction patterns collected from system CDM-B _{1BE}	81
3.18	Picture of a gel (5% acrylamided) study of the TXDX triangle motif. The motif is blunted “around the clock.” Lane 1 shows <i>Hae</i> III digested pBR marker, lane 2 the 10 bp ladder marker, lanes 3-8 contain a logarithmic concentration series of the blunted TXDX triangle 0.1 μ M - 2 μ M. 10 μ l were loaded.	82
3.19	Atomic force microscopy picture of 2D arrays consisting of TXDX triangles (flavor A).	83
3.20	Atomic force microscopy picture of 2D arrays consisting of TXDX triangles (flavor B)	84

3.21	Atomic force microscopy picture of 2D arrays consisting of TXDX triangles (flavor C)	85
3.22	Atomic force microscopy picture of 2D arrays consisting of TXDX triangles flavor B	86
3.23	Current trace at 50 mV showing ion channel behaviour (800 pS transitions). Sample contained 5 μ l 6HB (0.1 μ M) and 1 x Netropsin bundle saturation.	87
3.24	Current trace at 50 mV showing ion channel behaviour (800 pS and 2 nS transitions). Sample contained 5 μ l 6HB (0.1 μ M) and 1 x Netropsin saturation.	88
3.25	Current trace at 50 mV showing ion channel behaviour (200 pS, 600 pS and 1 nS transitions). Sample contained 5 μ l 6HB (0.1 μ M) and 1 x Netropsin saturation.	88
4.1	Sierpinsky carpet. A 2D fractal derived from a square by cutting it into 9 equal squares with a 3-by-3 grid, removing the central piece and then applying the same procedure ad infinitum to the remaining 8 squares.	93
4.2	The Menger sponge or the Sierpinsky cube fractal [‡] is the 3D version of the Sierpinsky carpet . It may be possible to assemble a version of the sponge out of DNA.	94
4.3	A parallelogram consisting of four 6 helix bundles. This might be a promising motif because it may offer the possibility to cross conductor paths on a nanometer scale.	99
6.1	XOR calculation with DNA [†]	120
6.2	Capillary crystal mounting step 1*	130

[‡]Rendered Cube Picture Kindly provided by Prof. Dr. Alessandra Carbone

6.3	Capillary crystal mounting step 2*	131
6.4	Sequence and strand structure of TXDX triangle.	136

List of Tables

2.1	Buffer compositions	46
2.2	Buffer compositions	47
2.3	Triangles designed and synthesized based on a basic design by Prof Chengde Mao	55
3.1	TXDX Triangle distances	86
6.1	pBR <i>Hae</i> III digested marker fragment sizes	121
6.2	Natrix Buffer Compositions	122
6.3	Sequence dependent Netropsin binding energies.	132
6.4	Sticky ends for the DX Motif for 2D Arrays	133
6.5	Sticky ends for the CDM Triangle Motif for 3D Assembly . . .	134
6.6	Sticky ends for the TxDx Triangle Motif	134
6.7	Sticky Ends for the TXA Motif for 3D Assembly	135
6.8	Strand combinations for the 3D TXDX Triangle	137
6.9	Calculation of unique 7 mers	139
6.10	DNA Crystals and Crystallization Conditions	144
6.11	CDM Triangle Properties with Minimal Turns.	147
6.12	CDM Triangle Properties with 1 Turn.	149
6.13	CDM Triangle Properties with 1 Turn.	151
6.14	CDM Triangle Properties with 1 Turn.	152

Nomenclature

π	The mathematical constant π 3.14, the ratio of a circle's circumference to its diameter
σ	Conductivity if used within a equation
0D	0-dimensional, molecule without sticky ends
1D	1-dimensional, molecule designed to form linear structure
2D	2-dimensional, m Designed to form an array
3D	3-dimensional, molecule designed to fill space
6HB	6 helix bundle
A	Adenin
A	Area if used in ion channel equations
AFM	Atomic force microscope
arrang.	arrangement
ATP	Adenosinetriphosphate
C	Cytosin

c small c, Brominated Cytosin if used within a DNA Sequence

CDM Prof. Chengde Mao

Compl. Complementary

conc. Concentration

DNA Deoxyribonucleic acid

ds Double stranded

DX DNA Tile consisting of two helices connected by two cross-overs

FRET Fluorescence resonance energy transfer

G Conductance in Siemens [S], inverse of resistance

G Guanine

helicity Number of nucleotides per DNA full turn

helicity Number of nucleotides per DNA full turn

HPLC High pressure liquid chromatography

IV Current - voltage curve

junc. Junction

l Length if used in equations

M Molarity $\text{g} \times \text{mol}^{-1}$

min. Minute[s]

mRNA messenger ribonucleic acid

n.a.	Not available
NMR	Nuclear magnetic resonance
No.	Number
nt	Nucleotides
NYU	New York University
PAGE	Polyacrylamid gel electrophoresis
PCR	Polymerase chain reaction
PEG	Polyethylene glycol
RNA	Ribonucleic acid
S	Siemens - unit of measurement for electric conductance, being the inverse of ohm
SEQUIN	A program designed by Prof. Seeman to assign nucleic acids SE- Quences INteractively
ss	Single stranded
T	Thymin
t	small t, Brominated Thymin if used within a DNA Sequence
TX	DNA Tile consisting of three helices connected by four cross-overs
U	Uracil
x	x direction in TXDX Triangle arrays
y	y direction in TXDX Triangle arrays

Chapter 1

Introduction

1.1 Nanotechnology

1.1.1 Introduction to Nanotechnology

Nanotechnology is described as the art and science of building complex devices and structures with atomic precision [17]. The prefix nano itself stands for one billionth ($\frac{1}{1000000000}$). In general the term nanoscience and nanotechnology are used for structures in the 1-100 nm size range which are artificially synthesized by a variety of physical, chemical and mechanical methods [14] [23].

Two approaches to create structures on a nanoscale are possible:

- Bottom Up
- Top Down

The so called top down approach to nanostructures employs manufacturing methods such as lithography to create smaller and smaller structures, down to nanostructures. The bottom up approach is the manufacturing of

nanomaterials directly on a molecular scale. The synthesis of nanoscale structures uses a variety of methods: molecular precursors as chemical or physical vapor deposition, gas condensation, chemical precipitation, aerosol reactions, biological templating, processing of bulk precursors (mechanical attrition, crystallization from the amorphous state, phase separation), and from nature (biologically mimicked systems) [68]. Siegel [68] gives three properties by which nanoscale materials are determined:

- The ability to control the size and the size distribution of the desired nanoscale structures
- The compositions of the constituent phases in a nanostructure material
- The control of the nature of the interfaces created between constituent phases and the interactions across the interfaces

Microtechnologists are trying to build miniature mechanical devices, store information in less space and develop computers that offer more operations \times time⁻¹ \times space⁻¹. This kind of engineering requires control of matter on a molecular level. The IBMTM logo has been made of single atoms, positioned by an AFM (Atomic force microscope) tip [21]. A single, propeller-like molecule's rotation at high speeds within a supramolecular lattice has been observed with scanning tunneling microscopy (STM) [25]. Such molecular propellers may lead to the development of nanomechanical devices. These achievements show the possibilities of nanotechnology and the need for control on a molecular level.

1.1.2 Self-Assembly

One approach to nanoscale structures is the assembly of simple and complex structures via molecular self-assembly. Molecular self assembly uses non co-

valent interactions in both solid and liquid states to form larger aggregates of atomic or molecular units with specific geometries [14]. This “bottom up” approach to the assembly of nanostructures uses molecular recognition to build a wide variety of structures. The process of self-assembly is widely used in biological systems. The self-assembly of viruses may be given as an example. The nanometer scale is used by the living cell to construct its components, which often cohere by non bonded interactions, such as microtubes, filaments built from protein subunits and formation of the double helix [86].

1.2 DNA Nanotechnology

1.2.1 DNA Structure and Function

Nucleotide Base Pairing

DNA (Deoxyribonucleic acid), in its double-stranded form is the genetic material of most organisms and organelles, although phage and viral genomes may use single-stranded DNA, single stranded RNA (ribonucleic acid) or double stranded RNA [103]. The backbone of the DNA is formed by sugar-phosphate molecules. At the C1-position of the ribose a nucleic base is attached. The most common nucleic bases are shown in fig. 1.1 in Watson-Crick base pairing. The Watson-Crick DNA structure model was founded on the idea that adenine (A) pairs to thymine (T) by hydrogen bonding, and guanine (G) to cytosine (C) and hence the content of G always equals the content of C as T equals A (Chargaff’s rule). Currently, DNA Nanotechnology is mainly based on Watson-Crick base paring (see fig. 1.1) but this pairings are not the only pairs that form nor is the A-T pair even among the most stable. Just about any base can hydrogen bond to any other base

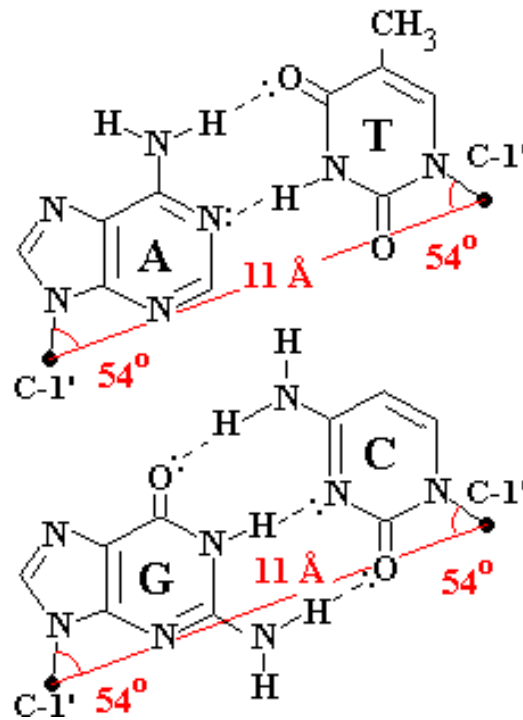


Figure 1.1: Watson-Crick base pairing*. Adenine pairs with thymine (upper part of the figure) and guanine pairs with cytosine (lower part)

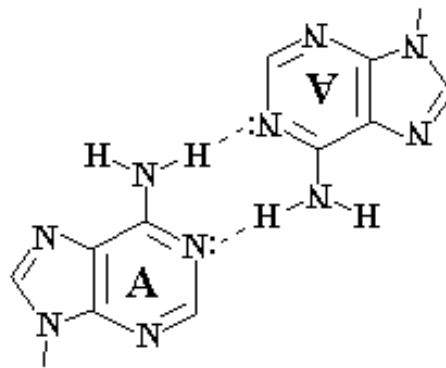


Figure 1.2: Adenine self pairing*

including self-pairs. Fig. 1.2 shows an Adenine base pairing with another Adenine base, fig. 1.3 shows Hoogsteen base pairing and fig. 1.4 shows re-

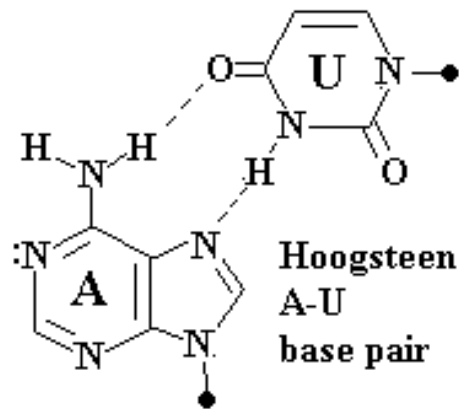


Figure 1.3: Adenine can pair with uracil in Hoogsteen base pairing*

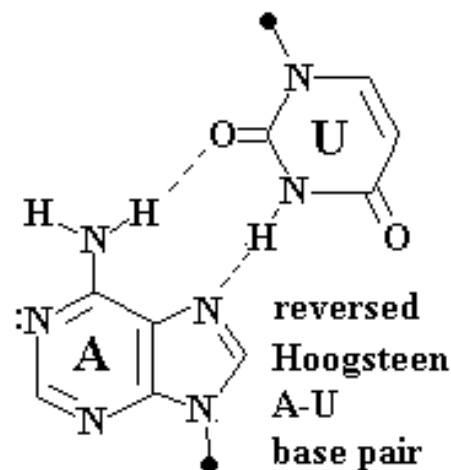


Figure 1.4: Adenine can pair with uracil in reversed Hoogsteen base pairing*

versed Hoogsteen base pairing. Reversed Watson-Crick base pairing is shown in fig. 1.5, sheared Watson-Crick base pairing can be seen in fig. 1.6. The Watson-Crick base pairing G-C and A-T shares a unique geometry, both C-1' Atoms are 10.8 Å apart from each other. This allows complementary (concerning the Watson-Crick base pairing) sequences to form a double DNA helix with the least amount of helix backbone disturbance. With the ex-

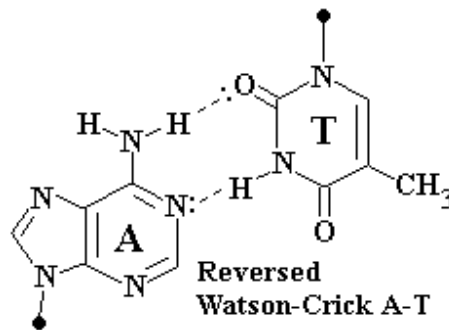


Figure 1.5: Adenine can pair with thymine in reversed Watson-Crick base pairing*

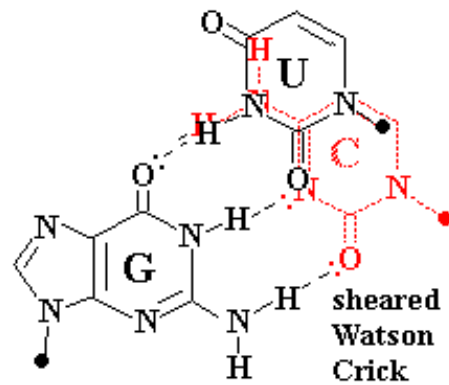


Figure 1.6: Guanine can pair with uracil in sheared Watson-Crick base pairing*. The cytosine position in regular Watson-Crick pairing is drawn in red.

ception of unusual motifs such as quadruplexes or triplexes, Watson-Crick paired helices are usually at a thermodynamical minimum relative to other structures due to base stacking, hydrogen bonding and minimal helix distortion. If paired DNA strands are heated complementary sequences can maintain a double helix form at the highest temperature before dissociation. In contrast, if a solution containing DNA strands is allowed to cool from high temperature, complementary DNA sequences will be the first to form double

stranded DNA helices corresponding to the most thermodynamically stable product. In aqueous solution the H-Bond formation alone does not provide sufficient energy to form a stable double helix. Base stacking provides another -16.0 to $-61.6 \frac{kJ}{mol}$ per 4 complementary bases (two 2mers), depending on the base sequence.

B-DNA

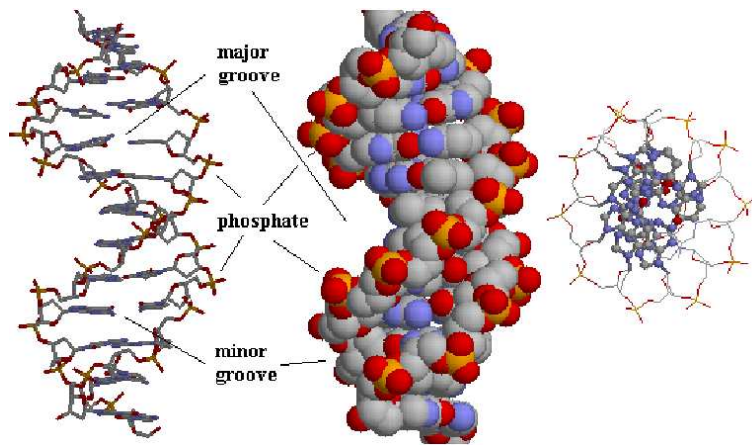


Figure 1.7: B-DNA double helix*. B-DNA is the most stable helical form of DNA formed by a random sequence. The right side of the figure shows a view down the helical axis.

B-DNA is shown in fig. 1.7. Under physiological conditions B-DNA is the most stable helical form of DNA formed by a random sequence. The two strands run in opposite directions and the bases project towards each other like the rungs of a ladder due to Watson-Crick complementary base pairing. In its B molecular form the helix is 2.0 nm in diameter with a pitch of 3.6 nm [100]. One full turn in the double helical structure corresponds to 10.5 nucleotides in solution and 10.0 nucleotides in crystal form [100].

A-DNA

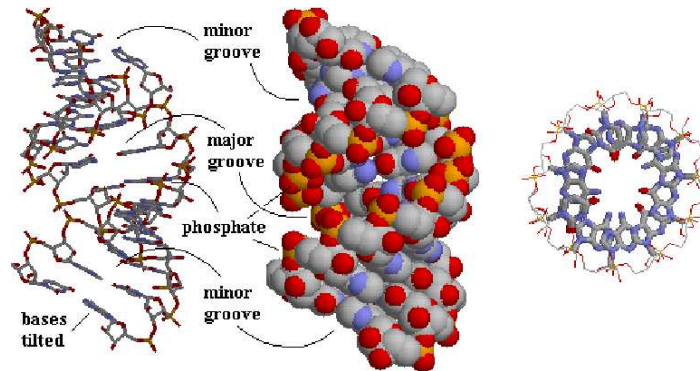


Figure 1.8: A-DNA helix* can form under dehydrating conditions. The right side of the figure is a view down the helical axis.

Under dehydrating conditions DNA can form A-DNA, as seen in fig. 1.8. A-DNA corresponds also to the conformation of dsRNA due to avoidance of steric interference of 2'O. DNA/RNA hybrids form a structure similar to A-DNA. In A-DNA the helix has 11 nt per DNA full turn.

C-DNA

C-DNA can occur under low relative humidity and in the absence of excess salt and in the presence of Li-ions [61]. The C-DNA helix has $9\frac{1}{3}$ nucleotides per full turn. A structural model of C-DNA displays the displacement of the bases to the outside of the helix in the major groove and the development of a very deep minor groove.

D-DNA and Z-DNA

Alternating T and A sequences can form D-DNA. Promoter sites are AT rich and AT rich regions are less stable compared to GC containing sequences.

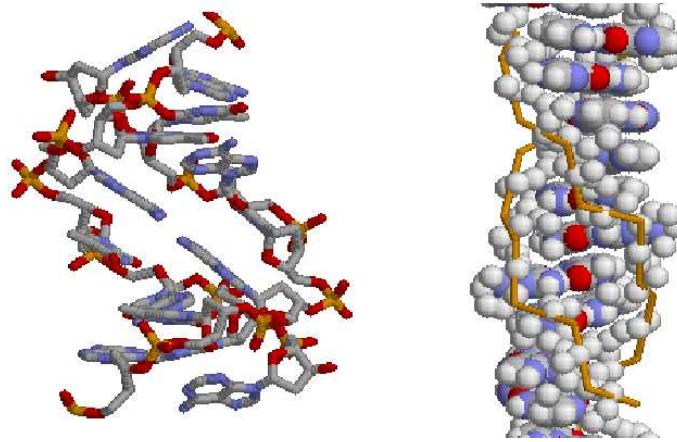


Figure 1.9: D-DNA is shown* in the left side of the picture and can occur with alternating A and T sequences . Z-DNA (right side*) is formed by GC rich sequences under high salt conditions. The Z-DNA back bone is left handed.

These sequences can switch from normal B-DNA to D-DNA in high ionic concentrations or under the influence of binding proteins. In D-DNA a full turn corresponds to 8 bp. At high salt concentrations Z-DNA is formed from GC rich sequences with strictly alternating purine pyrimidine sequences. Z-DNA has 12 bp per DNA full turn [77]. In contrast to standard DNA backbone conformations Z-DNA has a left-handed sense. Z-DNA has a zigzag backbone due to C sugar conformation compensating for G glycosidic bond conformation and a narrow minor groove [77].

PNA

Peptide nucleic acid (PNA) can be synthesized and possesses polyaminoethylglycine, a polymer of amide bonds [22] and is given as an example of a nucleic acid with a backbone not found in nature. PNA is not degraded by any known enzyme and offers unique features for antisense expression blockers. Many

other derivatives have been synthesized and might be applied to DNA nanotechnology due to the advantage of the non-ionic backbone, resistance to enzyme degradation and hydrophobic properties. PNA-DNA hybrids are more stable than RNA-DNA and hence PNA can be used to displace a hybridized strand.

DNA Triplex

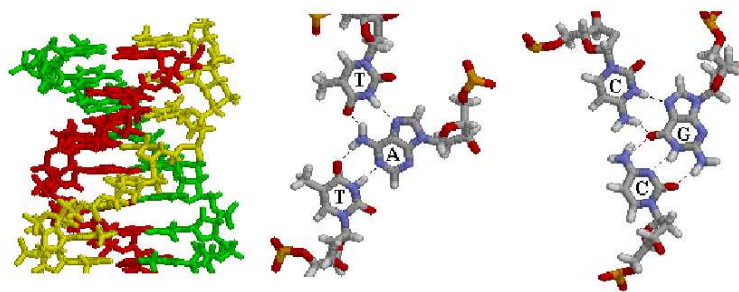


Figure 1.10: DNA triplex* formed by three DNA strands. Hoogsteen base pairing is involved in this structure.

Base triplets can form due to the accessible wide major groove of B-DNA and exposed access to the Hoogsteen face of the base pair purines 1.10. The third (yellow) strand runs parallel to the red purine strand in fig. 1.10. The CCG triplex has protonated C in the Hoogsteen position.

DNA quadruplex and G quartets

Quadruplexes consisting of guanine are found as terminating sequences at the end of eukaryotic chromosomes [106]. Telomeres contain G-rich repetitive sequences and are synthesized by telomerases using RNA templates. The four strands of the quadruplex are associated through guanine quartets. Each

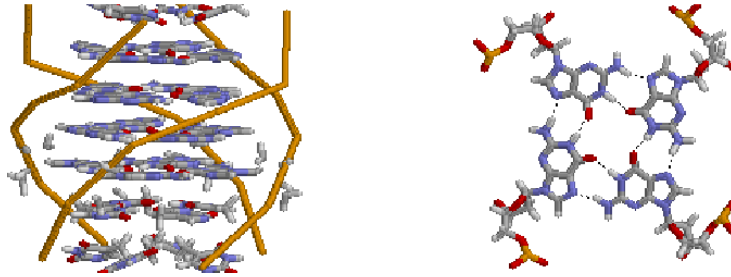


Figure 1.11: Quadruplex DNA* are found in the end of eukaryotic chromosomes and contain G-rich repetitive sequences.

guanine pairs with its Watson-Crick face to H-bond to the Hoogsteen face of its neighbor.

1.2.2 Holiday Junction and Branch Migration

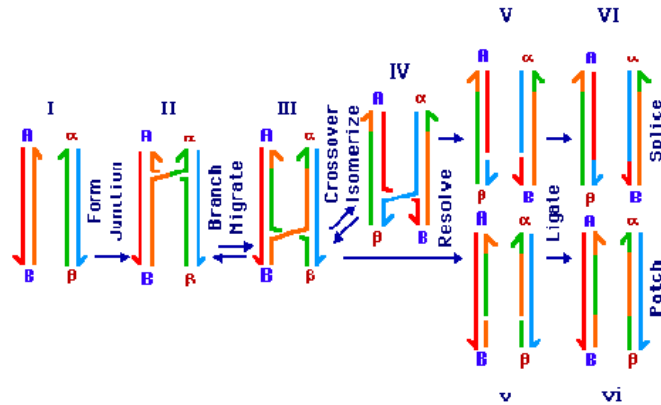


Figure 1.12: Branch migration[†]. Crossing-over of homologous areas (II) of two double helices (I), followed by branch migration (II-III) of the Holliday junction and resolution (IV) lead to two possible products (V). VI shows a possible ligation step.

One of the main properties of the DNA in organisms is that it is a long (*E. coli* 1.3 mm [100]), unbranched and linear molecule. Branched DNA occurs in replication and in the process of genetic recombination when the homologous areas of two double helices cross over (fig. 1.12). Both replicative and recombinational intermediates are normally unstable due to internal sequence symmetries, which allow their resolution to double helices, via the process of branch point migration [96]. Fig. 1.12 shows the process of crossing over and branch migration as it occurs during genetic recombination. Both helices consisting of homologous regions carry flanking markers, A and B in the strands on the left, and a and b on the right. Fig. 1.12 I shows two double helices, II shows the crossing over of the homologous sequences, III shows a state formed by branch migration and IV a state reached by cross-over isomerization. V shows two possible end products formed from state III and IV and finally VI as the two possible final ligated products.

1.2.3 *De novo* Designed Junctions and Avoidance of Branch Migration

Fig 1.13 shows a four-arm junction that is the equivalent to the Holliday structure [38] found in the process of genetic recombination. The Holliday structure, as found in the process of recombination, has two-fold sequence symmetry. In contrast, the sequence shown in fig. 1.13 prevents branch migration through sequence symmetry minimization [84] and does not contain the two-fold symmetry necessary to perform branch migration. Arrowheads indicate 3'-ends. Each strand is paired with two other strands and labeled with Arabic numerals, the four arms are numbered with roman numerals. The base pairing is symbolized by a dot between complementary bases. This junction can not perform branch migration because there is no homologous

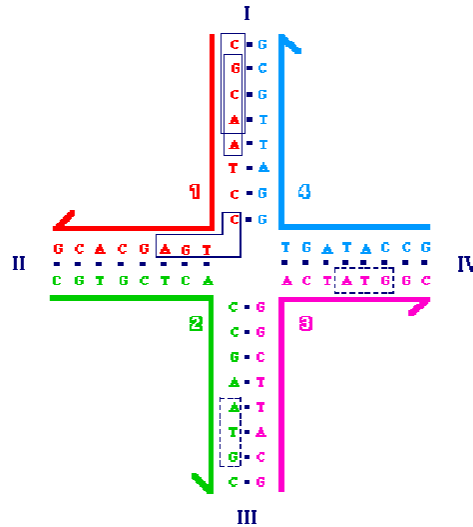


Figure 1.13: Four arm junction with symmetry minimization[†]. It does not possess the symmetry necessary to perform branch point migration.

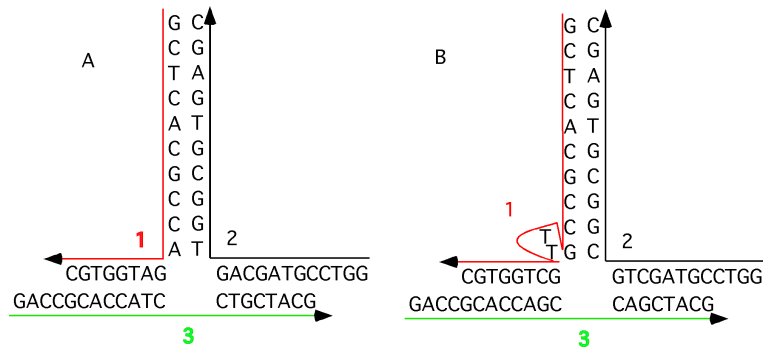


Figure 1.14: Three arm junctions with sticky ends. Ligation studies show that regular three arm junctions (left side) equipped with sticky ends tend to cyclize. Bulged three arm junctions (right side) show less tendency to cyclize.

two-fold sequence symmetry flanking the central branch point. Furthermore all tetramer (4mer) segments are unique.

It is possible to design oligonucleotides that preferentially form a three arm junction via Watson-Crick base pairing [84, 57]. Fig. 1.14 A shows a three arm junction with sticky ends and fig. 1.14 B shows a bulged 3 arm junction. Three arm junctions are not able to perform branch migration. The three arm junctions equipped with sticky ends are able to form linear complexes and also several cyclic products because they are flexible about a bending axis and maybe twist-wise as well [57]. Bulged three arm junctions are less likely to cyclize [54]. Further, junctions with five [105], six [105], eight, ten and twelve arms (unpublished) have been designed and constructed in Prof Seeman's laboratory.

1.2.4 2 Dimensional DNA Arrays

Requirements and Basic Concept

Three key elements necessary for the control of three dimensional structure in molecular construction are given by Li et al. [51]:

- The predictable specificity of intermolecular interactions between components
- The local structural predictability of intermolecular compounds
- The structural rigidity of the components

The first two requirements make DNA excellent building blocks because sticky ended association directed by Watson-Crick base pairing between sticky ended molecules has been used successfully to direct intermolecular specificity [15] and the ligated or unligated product is double helical B-DNA,

whose geometric properties are well known [4].

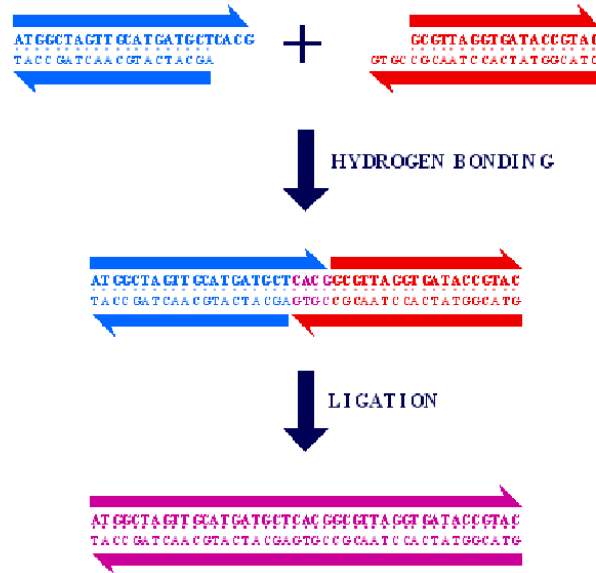


Figure 1.15: Sticky ended cohesion[†]. Two DNA helices with complementary sticky ends can associate due to Watson-Crick base pairing and can optionally be ligated together.

Fig. 1.15 shows sticky ended cohesion moderated by Watson-Crick base pairing and optional final ligation step. The basic concept of assembly of complex structures from individual tiles can be seen in fig. 1.16. It has been reported that one of the key problems when using branched DNA as a construction medium is that branched junctions seem to be extremely flexible molecules [57, 71]. Ligated three and four arm junctions (using conventional sticky end methods) show a series of macro cyclic products [56]. Thus, a key goal is to find DNA structures that lack the ability to cyclize.

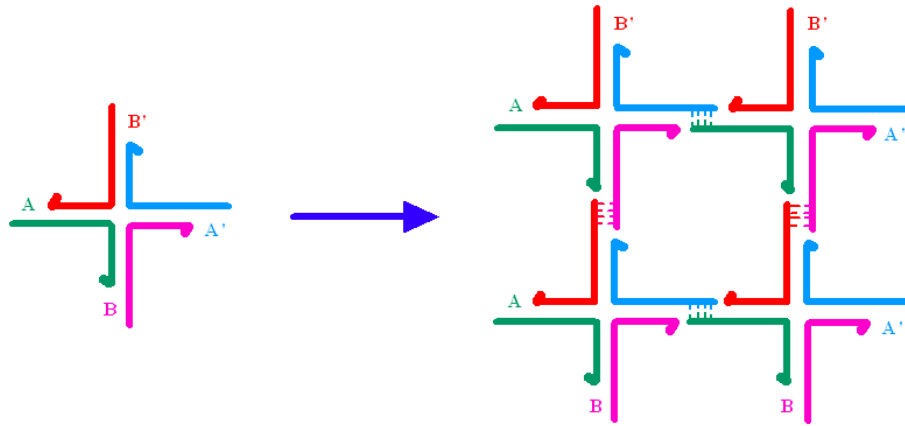


Figure 1.16: Basic concept of self assembly[†]. A motif can associate to form a larger predicted complex due to specific sticky ends.

Double Crossover molecules

Different types of double crossover (DX) molecules are shown in fig. 1.17. DX molecules consist of two helices connected by four arm junctions. The first character 'D' stands for double crossing over, the second character refers to the relative orientations of their two double helical domains, 'A' for antiparallel and 'P' for parallel. The third character refers to the number of helical half-turns between crossovers, 'E' for an even number and 'O' for an odd number. The two double crossover molecules on the right side in fig. 1.17 show parallel double crossover molecules with an odd number between crossovers, 'W' indicates the extra half turn corresponds to a major groove separation, 'N' indicates a minor groove separation. Arrowheads indicate 3' ends of DNA strands in fig. 1.17. It has been shown that DAE molecules can be ligated extensively without showing a large propensity to cyclize [51]. Parallel double crossover molecules are not well behaved on non-denaturing gels, unless their ends have been closed off in hairpin loops. Antiparallel double crossover

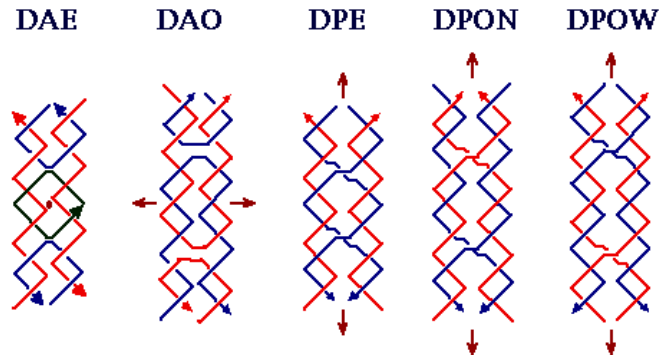


Figure 1.17: Different types and nomenclature of DNA double crossover molecules[†] The first character 'D' stands for double crossing over, the second character refers to the relative orientations of their two double helical domains, 'A' for antiparallel and 'P' for parallel. The third character refers to the number (modulus 2) of helical half-turns between crossovers, 'E' for an even number and 'O' for an odd number. A fourth character is needed to describe parallel double crossover molecules with an odd number of helical half-turns between crossovers. The extra half-turn can correspond to a major (wide) groove separation, designated by 'W,' or an extra minor (narrow) groove separation, designated by 'N.'

molecules appear to be stable molecules[51].

2 Dimensional DNA Arrays with DX Molecules

A DNA hairpin can be incorporated into a DX molecule. The hairpin is perpendicular to the DX tile and is inserted between cross-overs, using a bulged 3-arm junction [84, 57]. Double cross-over molecules have been successfully

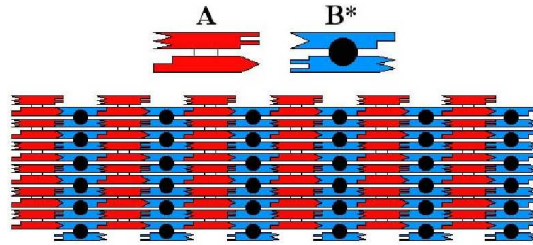


Figure 1.18: Assembly principle of a 2D-DNA array consisting of two different DX tiles[†]. A hairpin, serving as a topographic label, is incorporated into the blue tile.

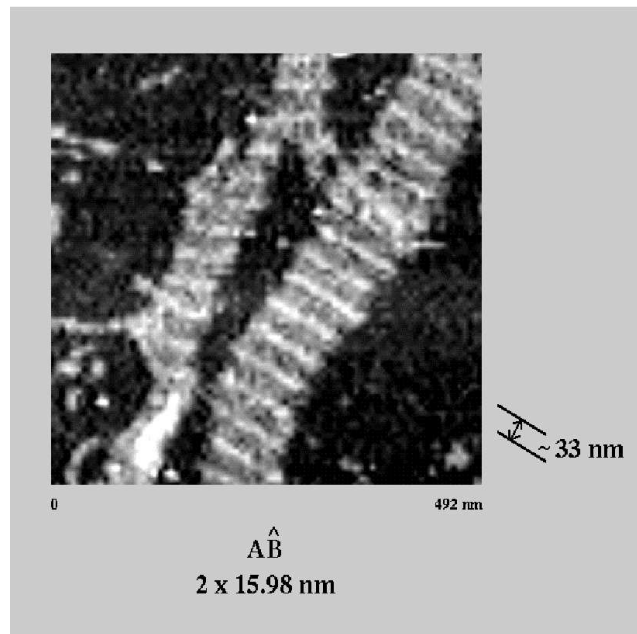


Figure 1.19: AFM picture of a 2D DX array[†]. The hairpin on every second tile can be clearly seen and shows the predicted spacing.

used to build 2D DNA lattices. By using a DX molecule with a hairpin in every 2nd tile, serving as a topographic label, stripes above the surface at

intervals have been produced [108]. Fig. 1.18 shows how the DX molecules assemble in a chessboard like structure, fig. 1.19 shows an AFM picture of the produced array. Further, arrays with four tiles and a topographic label on every 4th tile have been produced with the predicted spacing [108].

2 Dimensional DNA Arrays with TX Molecules

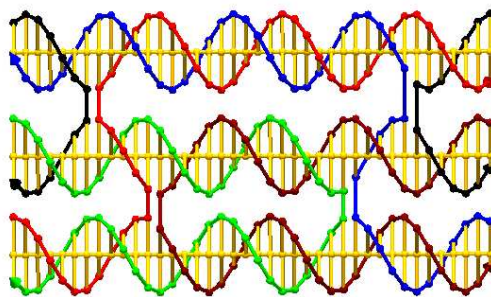


Figure 1.20: TX motif consisting of three helices connected by 4 cross-overs, shown in a blunt ended version.

Three DNA helices can be connected by four cross-overs to form a TX molecule as shown in fig. 1.20. Like DX molecules the TX molecules can assemble into 2 dimensional arrays. The principle of the array assembly is shown in fig. 1.21. An AFM picture of a produced array is shown in fig. 1.22 [45].

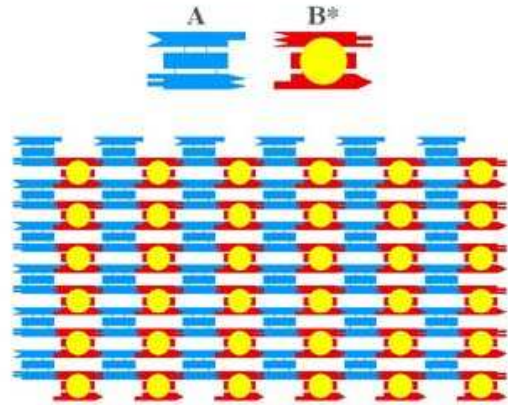


Figure 1.21: Assembly principle of a 2D array consisting of two different TX tiles[†]. A hairpin, serving as a topographic label, is incorporated into the red tile.

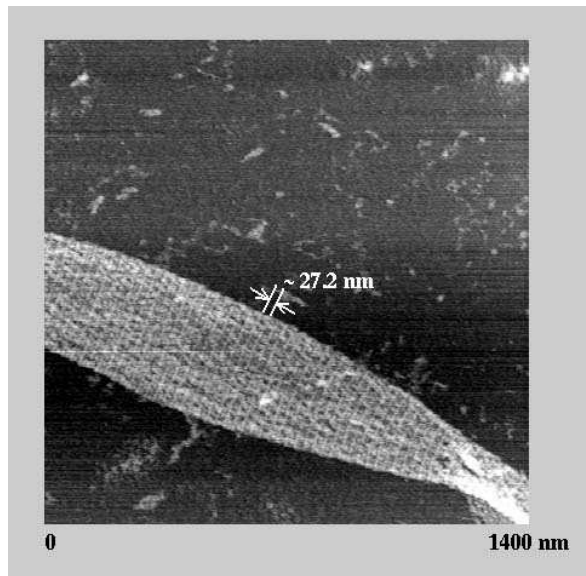


Figure 1.22: AFM picture a 2D DNA array consisting of TX tiles. The hairpin on every second tile can be clearly seen and shows the predicted spacing.

2 Dimensional DNA Arrays with Parallelograms

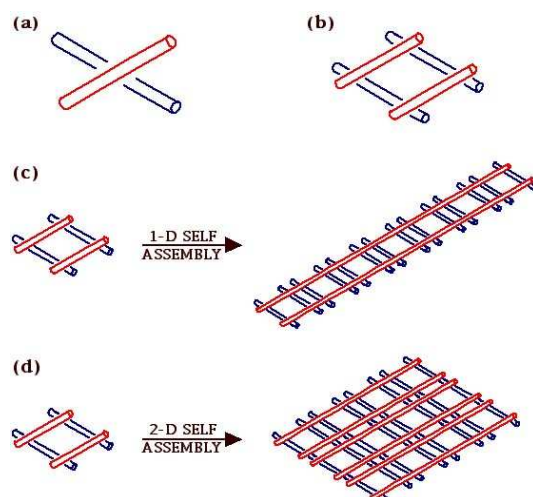


Figure 1.23: Schematic picture of parallelogram assembly[†]. Four junctions can be combined into a rhombus like motif.

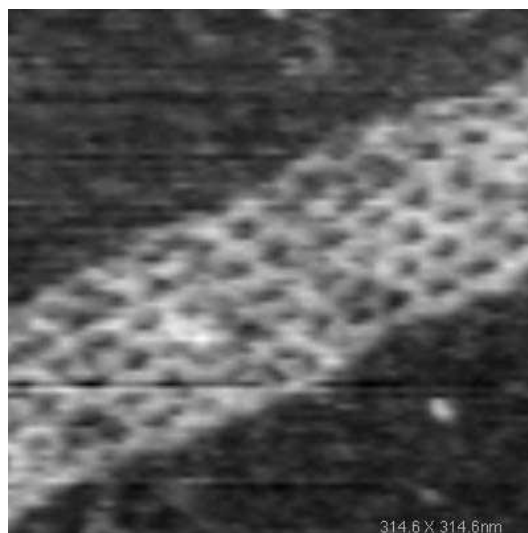


Figure 1.24: AFM picture of parallelogram array[†]. The rhombus like structure can be distinguished.

The Holliday junction forms a stacked structure in the presence of mag-

nesium ions, see fig. 1.23 (a). Four junctions can be combined into a rhombus like motif (b) and can form a linear (1d) array (c) or a crystal (2d array) (d), depending on the provided sticky ends. An AFM picture of a 2d array is shown in fig. 1.24.

1.2.5 Other Molecules for DNA Nanotechnology

DNA Cube

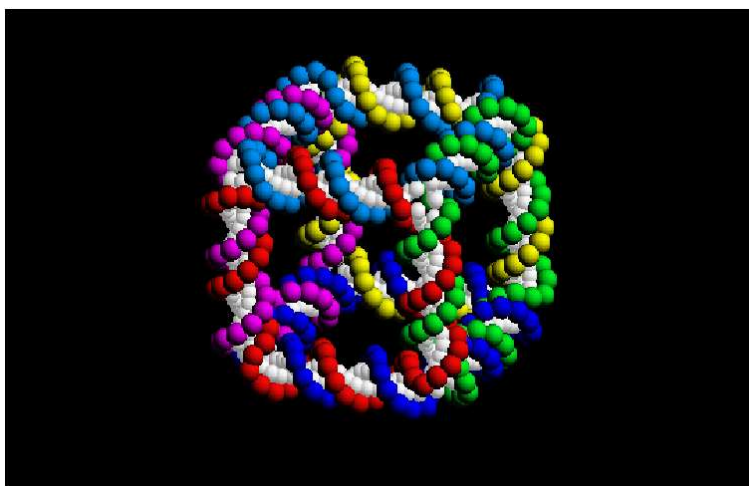


Figure 1.25: The DNA strands in this molecule[†] have the connectivity of a cube. It consists of six cyclic strands. The cube is created by ligating two ends of two quadrilaterals to form a belt-like molecule. The nucleotides are represented by white dots (nucleic base) in this drawing, the colored dots represent the sugar phosphate backbone of the DNA strands with one color per strand.

The helices of the molecule shown in fig. 1.25 have the connectivity of a cube. It consists of six cyclic strands. The cube is created by ligating two ends of two quadrilaterals to form a belt-like molecule that has to be

purified to remove side products [83]. The nucleotides are represented by white dots (nucleic base) in this drawing, the colored dots represent the sugar phosphate backbone of the DNA strands with one color per strand. The successful synthesis has been reported in Nature [83].

DNA Truncated Octahedron

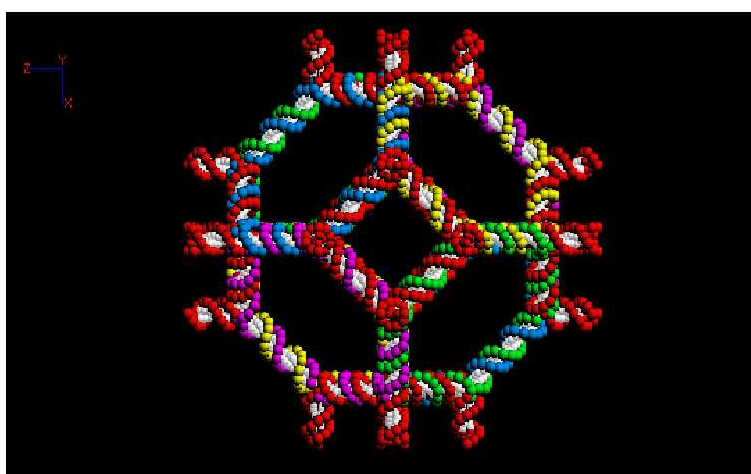


Figure 1.26: The DNA strands in this molecule[†] have the connectivity of a truncated octahedron. The truncated octahedron is viewed down the four fold axis of one of the squares. The edges of the truncated octahedron consist of two full turns of dsDNA. The complete truncated octahedron contains 14 cyclic strands of DNA and each cyclic strand corresponds to a face of the truncated octahedron. The nucleotides are represented by white dots (nucleic base) in this drawing, the colored dots represent the sugar phosphate backbone of the DNA strands.

The molecule shown in fig. 1.26 consists of DNA helices with the connectivity of a truncated octahedron. The structure, containing six squares and

eight hexagons, has been successfully synthesized with DNA (fig. 1.26) [116]. The truncated octahedron shown in fig. 1.26 is viewed down the four fold axis of one of the squares. The edges of the truncated octahedron consist of two full turns of dsDNA. The complete truncated octahedron contains 14 cyclic strands of DNA and each cyclic strand corresponds to a face of the truncated octahedron. The nucleotides are represented by white dots (nucleic base) in this drawing, the colored dots represent the sugar phosphate backbone of the DNA strands. The truncated octahedron has 36 edges and each vertex contains a DNA hairpin of DNA extending from it, drawn in red. Those strands correspond to the squares that form the squares. The backbones of the strands that form the hexagons are drawn in different colors (yellow (upper right), cyan (upper left), magenta (lower left) and green (lower right)). The molecular weight of the truncated octahedron has been reported at 790,000 Daltons [116].

Borromean Rings Made out of DNA

Fig. 1.27 shows Borromean rings made of DNA. Borromean rings are special because if one of the three rings is destroyed it will free the other two rings while leaving them intact and not connected to each other. The conventional nodes in Borromean rings have been replaced by three nodes, derived from 1.5 turns of DNA double helix. Fig. 1.27 c is the stereoscopic representation of fig. 1.27 b. Fig. 1.27 d is the stereoscopic view of the synthesized DNA molecule with hairpins. The hairpins contain sequences for restriction enzymes that can be used for digestion and, depending on the restriction site used, release of the other two DNA rings. This work is published in Nature [58].

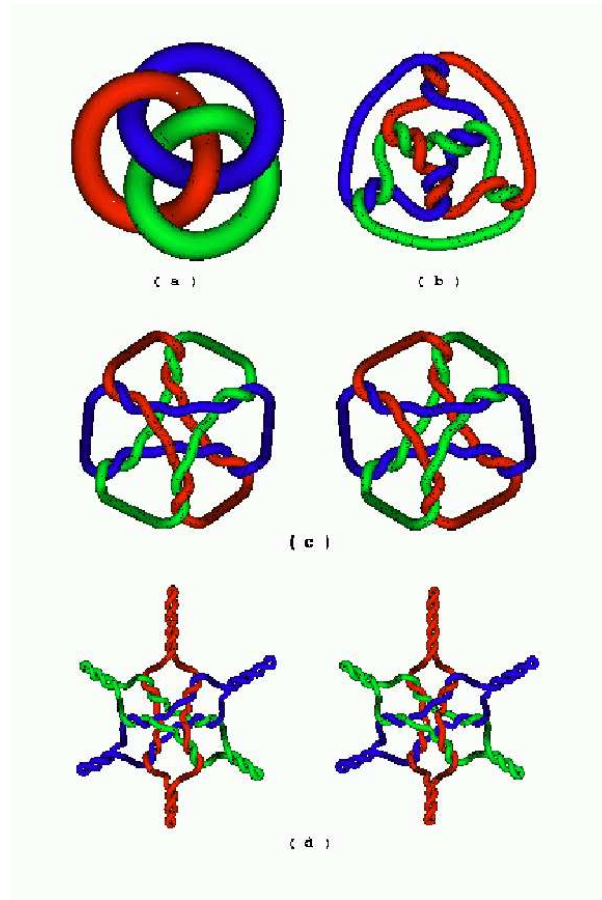


Figure 1.27: Borromean rings made of DNA[†]. Borromean rings are special because if one of the three rings is destroyed it will free the other two rings while leaving them intact and not connected to each other. The conventional nodes in Borromean rings (a) have been replaced by three nodes, derived from 1.5 turns of DNA double helix (b). The stereoscopic representation (c) is shown in the middle part of the picture. A stereoscopic view of the synthesized DNA molecule with hairpins is shown in the lower part of the picture (d). The hairpins contain sequences for restriction enzymes that can be used for digestion and, depending on the restriction site used, release of the other two DNA rings.

1.3 Nanomechanical Devices based on DNA

1.3.1 A Nanomechanical Device Predicated on the B-Z Transition of DNA

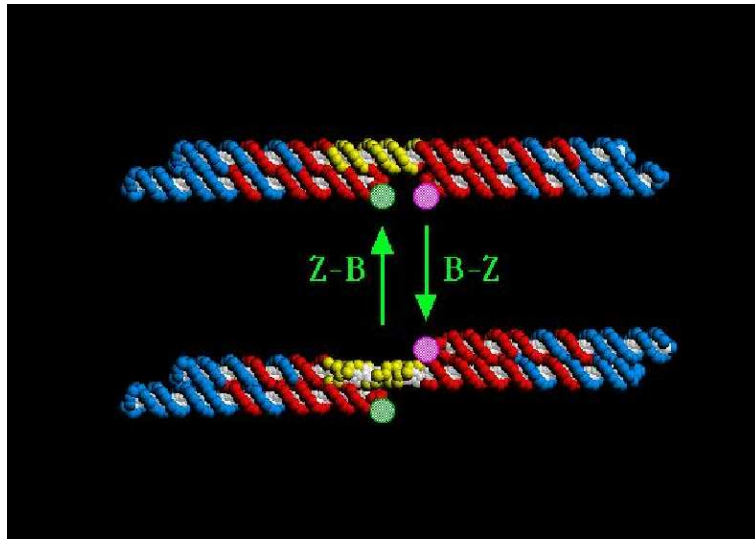


Figure 1.28: A nanomechanical device predicated on the B-Z transition of DNA[†]. Twenty nucleotide pairs of this helix can be converted into Z-DNA and induce a nanomechanical movement of the rigid DX tiles. The part acting as a bridge between the tiles is shown in yellow. The relative movement of the DX tiles is caused by the transition of right handed B-DNA to left handed Z-DNA (induced with Hexaamminecobalt(III) chloride) and can be measured with FRET (Fluorescence resonance energy transfer of donor and acceptor molecules attached to the DX molecules in the appropriate place marked by green and purple dots). The upper part of the figure shows the bridge DNA in B Form (right handed) and the lower part shows it in Z-Form (left handed).

DNA has been shown to be a material useful for the assembly of arrays on the nanometer scale. It is desirable to assemble nanomechanical devices from the same material. The simplest device is a rigid object that can respond to an external signal. A device based on DNA has been constructed that consists of two DX molecules connected by a DNA double helix with 4.5 full turns (fig. 1.28) [59]. Twenty nucleotide pairs of this helix can be converted into Z-DNA [77] and induce a nanomechanical movement of the rigid DX tiles. The part acting as a bridge between the tiles is shown in yellow in fig. 1.28. The relative movement of the DX tiles is caused by the transition of right handed B-DNA to left handed Z-DNA and can be measured with FRET (Fluorescence resonance energy transfer of donor and acceptor molecules attached to the DX molecules in the appropriate place marked by green and purple dots). The upper part of fig. 1.28 shows the bridge DNA in B Form (right handed) and the lower part shows it in Z-Form (left handed). The transition was induced with the addition of Hexaamminecobalt(III) chloride to the solution and reversed by dialyzing Hexaamminecobalt(III) chloride away [59].

1.3.2 DNA Nanomechanical Devices Based on Hybridization Topology

A new form of nanomolecular, sequence-dependent device based on DNA was introduced as “Molecular DNA tweezers” [115]. Based on this basic concept of set and unset strands further sequence dependent devices using a motif called PX with the advantage of rigidity have been designed. The PX motif, postulated to be involved in genetic recombination, consists of two helical domains formed by four strands that flank a central dyad. See molecule and sequence-depended device cycle in fig. 1.29 (left side (a)). Every possi-

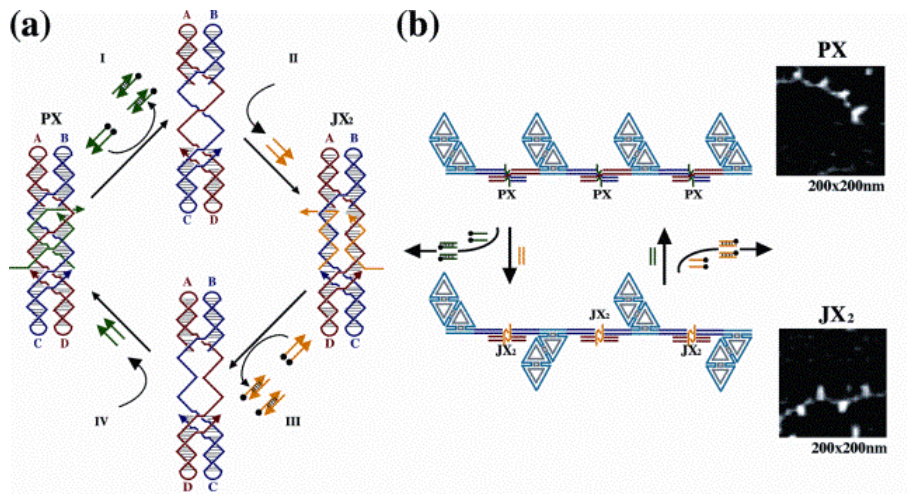


Figure 1.29: Nanomechanical device based on hybridization topology[†]. Left side (a): The letters A, B, C and D, along with the color coding, show that the bottom of the JX₂ motif (C and D) are rotated 180° relative to the PX motif. The set strands are shown in green, they can be removed by the addition of biotinylated green fuel strands (biotin indicated by black circles, process step I). The addition of the purple set strands (process step II) converts the unstructured intermediate into the JX₂ motif. In process step III the JX₂ molecule is converted to the unstructured intermediate by the addition of biotinylated yellow fuel strands. The PX device is restored and the cycle completed by the addition of green set strands (IV). Right side (b): AFM observation of the cycle with DNA trapezoids attached as a marker.

ble crossover occurs between the two helical domains of the PX motif. The JX₂ motif is similar to the PX motif but lacks two crossovers in the middle (see fig. 1.29 (right side of (a))). The letters A, B, C and D, along with the color coding, show that the bottom of the JX₂ motif (C and D) are rotated

180° relative to the PX motif. Fig. 1.29 (a) illustrates the principles of device operation. The set strands are shown in green (fig. 1.29). They can be removed by the addition of biotinylated green fuel strands (biotin indicated by black circles, process step I). The addition of the purple set strands (process step II) converts the unstructured intermediate into the JX_2 motif. In process step III the JX_2 molecule is converted to the unstructured intermediate by the addition of biotinylated yellow fuel strands. The intermediates between step I to II and step III to IV are identical. The PX device is restored and the cycle completed by the addition of green set strands (process step IV, fig. 1.29). Fig. 1.29 (b): shows an AFM observation of the cycle with DNA trapezoids attached as a marker.

1.4 DNA Based Computing

1.4.1 Introduction to DNA Based Computing

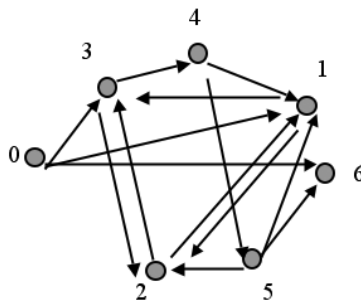


Figure 1.30: Graph with 7 nodes. Arrows indicate possible connections between two nodes.

DNA based computing exploits DNA molecules to solve mathematical problems. DNA based computing was first demonstrated by Adleman in

“Molecular computation of solutions to combinatorial problems” [3] to solve the Hamiltonian path problem¹. Hamilton’s problem is NP-complete² and hence also NP-hard³. In the Hamiltonian path problem, a path in a given graph has to be found from node 1 to node N that passes every node only once. Every node has to be visited but is not allowed to be visited more than once. The Hamiltonian path problem does not include the problem of finding the shortest path through a given graph what would correspond to the traveling sales man problem⁴ Fig. 1.30 shows a graph with 7 nodes.

¹Hamiltonian problem (Or “Hamilton’s problem”) A problem in graph theory posed by William Hamilton: given a graph, is there a path through the graph, which visits each vertex precisely once (a “Hamiltonian path”)? Is there a Hamiltonian path which ends up where it started (a “Hamiltonian cycle” or “Hamiltonian tour”) Entry from Free Online Dictionary of computing [39]

²NP-complete - (NPC, Nondeterministic Polynomial time complete) A set or property of computational decision problems, which is a subset of NP (i.e. can be solved by a nondeterministic Turing Machine in polynomial time), with the additional property that it is also NP-hard. Thus a solution for one NP-complete problem would solve all problems in NP. Many (but not all) naturally arising problems in class NP are in fact NP-complete. There is always a polynomial-time algorithm for transforming an instance of any NP-complete problem into an instance of any other NP-complete problem. So if you could solve one you could solve any other by transforming it to the solved one. Entry from Free Online Dictionary of computing [39]

³NP-hard - A set or property of computational search problems. A problem is NP-hard if solving it in polynomial time would make it possible to solve all problems in class NP in polynomial time. Some NP-hard problems are also in NP (these are called “NP-complete”), some are not. If you could reduce an NP problem to an NP-hard problem and then solve it in polynomial time, you could solve all NP problems. Entry from Free Online Dictionary of computing [39]

⁴traveling salesman problem: Given a set of towns and the distances between them, determine the shortest path starting from a given town, passing through all the other towns and returning to the first town. This is a famous problem with a variety of solutions of varying complexity and efficiency. The simplest solution (the brute force approach)

Adleman suggested [3] the following algorithm to solve the problem:

1. Generate random path through the graph
2. Keep only those paths that begins with v_{in} and end with v_{out}
3. If the graph has n vertices, then keep only those paths that enter exactly n vertices
4. Keep only those paths that enter all of the vertices at least once.
5. If any path remains, say 'yes', otherwise say 'no'.

Adleman solved this problem by representing each vertex i in the graph with a random 20mer sequence of DNA O_i . He created an oligonucleotide for each edge in the graph $i \rightarrow j$ that was the 3' 10 mer of O_i (for $i > 0$, otherwise it was all of O_i) followed by the 5' 10 mer of O_j ($j < 6$, otherwise it was all of O_j). The 20mer oligonucleotide with the sequence complementary to O_i was denoted $\underline{O_i}$. All $\underline{O_i}$ and $O_i \rightarrow j$ sequences were ligated together (step 1), followed by a PCR with primers O_0 and $\underline{O_6}$ (step 2). Thus, only those molecules encoding paths that begin with vertex 0 and end with vertex 6 were amplified. By separation on an agarose gel (only the 140 bp bands, representing exactly 7 vertices, were kept) step 3 was realized. By affinity purification with a biotin-avidin magnetic beads system all the encoded paths

generates all possible routes and takes the shortest. This becomes impractical as the number of towns, N , increases since the number of possible routes is $!(N-1)$. A more intelligent algorithm (similar to iterative deepening) considers the shortest path to each town, which can be reached in one hop, then two hops, and so on until all towns have been visited. At each stage the algorithm maintains a "frontier" of reachable towns along with the shortest route to each. It then expands this frontier by one hop each time. Entry from Free Online Dictionary of computing [39]

that miss a vertex of the path were eliminated (step 4). The remaining product was PCR amplified and run on a gel. A band would indicate that a path exists (step 5). DNA computing might be superior in some tasks comparing to traditional von Neumann computers⁵ because it is massively parallel. In particular some optimization and code breaking algorithms [2, 78] can take full advantage of parallel computing.

1.4.2 DNA Computations with Rectangular Tiles

Rectangular tiles, known as Wang tiles, with programmable interactions can mimic the operation of a given Turing machine⁶ [109, 107]. Fig. 1.31 shows

⁵von Neumann architecture - A computer architecture conceived by mathematician John von Neumann, which forms the core of nearly every computer system in use today (regardless of size). In contrast to a Turing machine, a von Neumann machine has a random-access memory (RAM) which means that each successive operation can read or write any memory location, independent of the location accessed by the previous operation. A von Neumann machine also has a central processing unit (CPU) with one or more registers that hold data that are being operated on. The CPU has a set of built-in operations (its instruction set) that is far richer than with the Turing machine, e.g. adding two binary integers, or branching to another part of a program if the binary integer in some register is equal to zero (conditional branch). The CPU can interpret the contents of memory either as instructions or as data according to the fetch-execute cycle. Von Neumann considered parallel computers but recognized the problems of construction and hence settled for a sequential system. For this reason, parallel computers are sometimes referred to as non-von Neumann architectures. A von Neumann machine can compute the same class of functions as a universal Turing machine. Entry from Free Online Dictionary of computing [39]

⁶Turing Machine - A hypothetical machine defined in 1935-6 by Alan Turing and used for computability theory proofs. It consists of an infinitely long “tape” with symbols (chosen from some finite set) written at regular intervals. A pointer marks the current position and the machine is in one of a finite set of “internal states”. At each step the

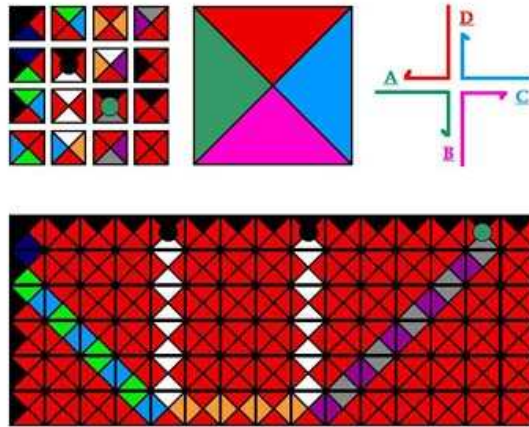


Figure 1.31: Algorithmic assembly by Wang tiles[†], each edge pairs with another edge of the same color. If this rule is strictly employed the assembly mimics the operation of a Turing machine. The mosaic on the bottom shows the principle of an addition. The 5th, 9th and 14th columns of the mosaic in the first row show a special tile, which corresponds to the sum of $5 + 9$. Based on a perfect assembly concerning the edge color pairing rule, the 3rd special tile in the first row marks the result of the addition: 14.

machine reads the symbol at the current position on the tape. For each combination of current state and symbol read, a program specifies the new state and either a symbol to write to the tape or a direction to move the pointer (left or right) or to halt. In an alternative scheme, the machine writes a symbol to the tape *and* moves at each step. This can be encoded as a write state followed by a move state for the write-or-move machine. If the write-and-move machine is also given a distance to move then it can emulate an write-or-move program by using states with a distance of zero. A further variation is whether halting is an action like writing or moving or whether it is a special state. Without loss of generality, the symbol set can be limited to just “0” and “1” and the machine can be restricted to start on the leftmost 1 of the leftmost string of 1s with

Wang tiles in the left upper section, as designed in 'Tilings and Patterns' [31]. The edges of the tiles are colored. Some contain up to four different colors, some consist of only one color. The assembly principle of Wang Tile assembly is based on the idea that each edge pairs with another edge of the same color. If this rule is strictly employed the assembly mimics the operation of a Turing machine. The mosaic on the bottom in fig. 1.31 shows the principle of an addition. The 5th, 9th and 14th columns of the mosaic in the first row show a special tile, which corresponds to the sum of $5 + 9$. Based on a perfect assembly concerning the edge color pairing rule, the 3rd special tile in the first row marks the result of the addition: 14. The tiles 2 to 8 in the top row have to be unique to assure that the right result is presented. It was pointed out by Prof. Winfree that such operations might be performed with DNA structures, equipped with sticky ends representing the colored tile edges. Fig. 1.31 shows in the upper right the J1 junction, a symmetry minimized equivalent of the Holliday structure, equipped with sticky ends. Such structures might put the theory in practice. The J1 structures tend to cyclize [51] and hence might not be the preferred structures. Structures created by Prof. Yan, that form a cross like structure like the Holliday junction with the DX motif [114] might be more suitable to act as Wang tiles.

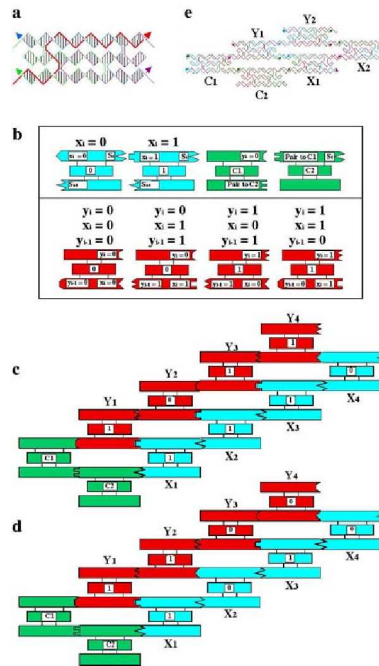


Figure 1.32: XOR calculation with DNA[†]. (a) shows a triple crossover molecule that contains a reporter strand. (b) shows the several TX molecules used in the operation. The final result is found by ligating the reporter strand, amplifying it with PCR, treating it with restriction enzymes and examining it on a gel.

1.4.3 Cumulative XOR Computation with DNA

A cumulative XOR computation with DNA has been reported [85]. A cumulative XOR operation is defined as:

strings of 1s being separated by a single 0. The tape may be infinite in one direction only, with the understanding that the machine will halt if it tries to move off the other end. All computer instruction sets, high level languages and computer architectures, including parallel processors, can be shown to be equivalent to a Turing Machine and thus equivalent to each other in the sense that any problem that one can solve, any other can solve given sufficient time and memory. Entry from Free Online Dictionary of computing [39]

$$Y(i) = XOR[Y(i-1), X(i)] \quad (1.1)$$

The result is 1 if the two inputs are different ((0 and 1) or (1 and 0)), the result is 0 if they are the same ((1 and 1) or (0 and 0)). The calculation was performed with the components shown in fig. 1.32, the actual gel can be seen in appendix fig. 6.1. Fig. 1.32 (a) shows a triple crossover molecule that contains a reporter strand [45]. The reporter strand is drawn in red color. Fig. 1.32 (b) shows the several TX molecules used in the operation. Input X(i) tiles are drawn in light blue, their value is shown at the center of each tile. The value '1' is presented by a restriction site for *EcoRV* and a '0' is presented by a restriction site for *PvuII* in the tile. All x tiles were equipped with unique sticky ends. The X(i) tiles were allowed to associate randomly, giving, for a four-bit problem, 16 different final answer strands. The X-tiles connect to the Y tiles by the two green connector tiles. The four red Y TX answering tiles, corresponding to the two different inputs, are shown under b in fig. 1.32. The X and C (input) tiles assemble first in the annealing protocol due to longer sticky ends. Fig. 1.32 shows two calculations performed in section (c) and (d). In (c), the inputs are X(1) = 1; X(2) = 1; X(3) = 1; X(4) = 0. This should lead to Y(1) = 1; Y(2) = 0; Y(3) = 1; Y(4) = 1. In (d), the input values are X(1) = 1; X(2) = 0; X(3) = 1; X(4) = 0, leading to Y(1) = 1; Y(2) = 1, Y(3) = 0; Y(4) = 0. The final result is found by ligating the reporter strand, amplifying it with PCR, treating it with restriction enzymes and examining it on a gel (for gel see appendix fig. 6.1).

1.5 Crystallography

1.5.1 Traditional DNA Crystallography

Relatively large quantities of material are required for X-ray crystallography. 5-10 mg of high purity material are considered typical for a crystallization screening [64]. These quantities can today be easily obtained with automated DNA synthesis [64]. At least 95% purity is considered necessary to obtain high quality crystals [64]. Most DNA strands for crystallization are purified via HPLC to remove unwanted blocking agents, precursors and truncated sequences [64]. HPLC purification achieves reasonable purity for DNA strands up to 20nt, for longer sequences PAGE purification becomes necessary [64]. Nearly all the DNA crystals reported to public crystals databases are of duplex DNA [64]. Probably less than 20% of all tried sequences can be successfully crystallized and even small changes in the sequence may result in a failure to crystallize [64]. Successful oligonucleotide crystallization has been performed in a quite narrow range of crystallization conditions. A crystallization buffer kit can be commercially obtained from Hampton Research that includes a matrix of 48 of the most common DNA crystallization buffers based on a double screening procedure suggested by Scott et al. [81]. An overview of common crystallization conditions and concentrations based on the protein data bank from the institute of molecular biotechnology (Jena, Germany) is given in the appendix (s. tbl 6.10 and tbl. 6.10).

1.5.2 3-Dimensional DNA assembly

One of the questions arising with 3-dimensional DNA assembly is how to fill space. In contrast to traditional crystallization, a sticky ended approach is taken to assemble rigid, predicted periodic structures to fill space. The

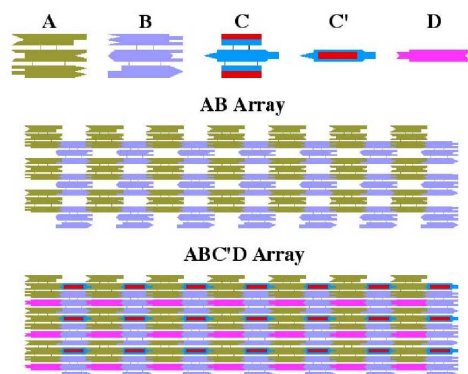


Figure 1.33: 3D Assembly with TX molecules[†]. Assembly in the 3rd dimension can be achieved by connecting the middle helix with sticky ends which enable another 90° rotated TX tile do connect.

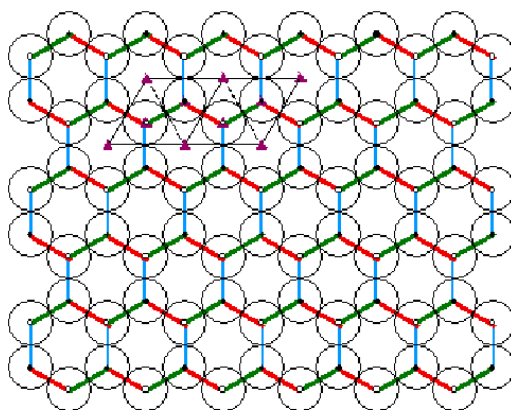


Figure 1.34: DX tiles can be arranged to fill 3D space when each DX is rotated 135° relative to the next DX[†].

TX motif (s. fig. 1.20) can be used to fill space. The assembly in the first two directions is the same as for 2 dimensional arrays (s. fig. 1.22), the 3rd dimension can be achieved by exchanging the closed loops of the middle helix with sticky ends which enable another 90° rotated TX tile to connect with it (s. fig. 1.33). Crystals have been grown from this motif but showed poor

diffraction (data not published). Another motif able to fill space is the DX motif (s. fig. 1.17), where each DX tile is rotated 135° , relative to the next DX tile, which corresponds to 4 nt (assembly principle see fig. 1.34). Once poor diffraction for this system was observed by Prof. Mao but could never be repeated (data not published, data not shown).

1.5.3 DNA Cages for Trapping and Characterization of Biomolecules

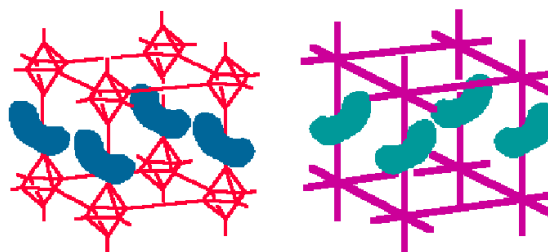


Figure 1.35: DNA cages containing oriented guests[†]. If DNA crystals can be created they might be able to capture biomolecules and serve as crystallization scaffolding.

Crystallization as applied to proteins has been described as a “black art” or alchemy [64]. Things have improved since then, but crystallization of proteins is still a very work intensive process that requires a high investment of work power and protein substance and still, diffracting crystals might not be achieved. One use of space filling DNA tiles assembled via sticky ends might be the capturing of trapped, oriented guest molecules within the DNA framework. Fig. 1.35 shows two connected networks that function as a scaffold and contain trapped, oriented guest molecules. Proteins or other biological macromolecules that are hard to crystallize might be forced this

way into crystallization and could be examined with x-rays. The left cage in fig. 1.35 consists of octahedra and a truncated cube, the right network consists only of a cube. Each network is meant to represent an infinite network to be constructed from DNA. The kidney-shaped objects represent the guest molecules, their structure could be resolved via x-rays as long as they are parallel within the crystals. The octahedra cage and the cube cage in fig. 1.35 are given as examples but other motifs may be used for the trapping of biomolecules as long as they fill space and diffract down to a reasonable resolution.

1.6 Ion Channels

1.6.1 Ion Channels in Organisms

Ion channels are macromolecular pores in cell membranes [36]. The model of embedded proteins in membranes was suggested by Singer and Nicolson [90]. Membrane proteins are either an integral membrane protein or an assembly of several proteins, consisting of sub-units. The arrangement is typically circular with a water filled pore, perpendicular to the lipid bilayer membrane. Ion channels bear the same relation to electric signaling as enzymes bear to metabolism [36]. There are three major types of gated ion channels:

- Ligand gated - open or close in response to signalling molecules
- Stretch/Mechanically gated - react to mechanical signals
- Voltage gated - act in response to changes in the charge

Channel behaviour can be examined via the patch clamp technique which allows examination of single ion channels and recording of macroscopic currents in the pA-scale. In this technique, a fine pipette with a tip diameter of

only of few μm is pressed against a cell membrane and a part of the membrane is sucked into the pipette. In this way Neher and Sakmann [66] were able to trap ion channels in the membrane and make single channel recordings. They were awarded the Nobel price for their efforts in 1993. A single ion channel conducts about 10 million ions per second which corresponds to a few pA. Ion channels are implicated in many diseases and are a major drug target [36].

1.6.2 Artificial Ion Channels

Artificial ion channels might be used to build artificial molecular machines and nanometer devices [13]. A few artificial ion channels were already created [13, 6, 101, 102]. Flomenbom and Klafter [24] discuss single stranded DNA movement through a nanopore and a possible application as a new fast sequencing method. Further, artificial ion channels might be suitable for monitoring mRNA (messenger ribonucleic acid) *in vivo* by recording a current spectrum when the mRNA passes through an artificial nanopore.

1.7 Presentation of a Problem

1.7.1 DNA Crystallization

Preliminary steps to 3D assembly have been performed in Prof. Seeman's laboratory. Crystallization attempts with the TX and DX motifs were undertaken. Further crystallization attempts to be undertaken can be categorized into the following categories:

- Further crystallization attempts of known and already examined motifs
- Development and application of new crystallization techniques
- Development of new motifs for sticky ended DNA crystallization

The overall goal is to achieve a system that assembles via sticky ends reproducible and in a designed fashion into a 3 dimensional crystal lattice that shows diffraction, when exposed to x-rays, down to a high resolution ($\leq 3 \text{ \AA}$).

1.7.2 6 Helix Bundle as an Artificial Ion Channel

Preliminary experiments with six DNA duplexes, connected by crossovers, that can self assemble into a hollow bundle have been performed and a tube like structure could be observed, consisting of the annealed 6 helix bundle and connected by sticky ends [62], see section Materials and Methods for further description of the motif and pictures (section 2.6). This motif was to be redesigned to explore its possible application as an artificial ion channel.

Chapter 2

Materials and Methods

2.1 Design of New Molecules

2.1.1 *De novo* Design of Sticky Ends

Sticky ends are normally obtained through DNA digestion by restriction enzymes, a basic process used in genetic cloning [100]. Sticky ends obtained from digestion with restriction enzymes have the disadvantage that they are self-complementary because most restriction enzymes cut palindromic sequences. For building defined structures with DNA molecules the sticky ends were designed *de novo* applying the following rules:

- All sticky ends should be the same length (number of nucleotides)
- same $\frac{GC}{AT}$ content
- reaction energy ΔG for different sticky ends differs by less than 30%
- never more than two guanosines in a stretch
- not self-complementary

The free reaction energy of all sticky ends designed in this thesis were calculated with the HyTherTM webpage, described by Santa Lucia [72, 79].

2.1.2 *De novo* Design of DNA Sequences

New sequences were engineered using the SEQUIN program. The SEQUIN (assign nucleic acids SEquences INteractively) program is based on the so called CRITON-SEEMAN algorithm [82] which uses CRTION elements for the new assignment of nucleotides. The program is written in FORTRAN77 by Prof. Seeman and was run on a SGI ORIGIN 200 workstation with 4 x 180 MHz IP27 RISC processors and 256 MB RAM.

2.1.3 DNA Junctions

For the branch points in new motifs the well known and characterized junction J1 (see fig. 1.13) was used if possible or symmetry minimized junction to prevent branch migration.

2.1.4 Computer Aided molecular modeling

The computer program GIDEON, written by Jeffrey Birac, was used for computer aided design of new motifs (to be published). It was run on dual processor G4 Mac computers.

2.2 From DNA Synthesis to Annealing of Motifs

2.2.1 DNA Synthesis

All strands were synthesized on an Applied Biosystems 380 B, an Applied Biosystems 394 DNA/RNA, a PerSeptive Biosystems Expedite automatic DNA synthesizer or obtained from IDT Integrated DNA Technologies and deprotected for at least 24 hours in 10 ml ammonium hydroxide solution at 60°C.

2.2.2 Denaturing Gels and DNA Purification

All used DNA strands were PAGE purified. The denaturing gels contained $8.3 \frac{\text{mol}}{\text{l}}$ urea, were run at 55°C and contained between 10% and 20% acrylamide (19:1 acrylamide:bisacrylamide), depending on the length of the sequences. Gels were run on at $28.6 \frac{\text{V}}{\text{cm}}$ with constant voltage (for running and sample buffer see tbl. 2.1). The bands were visualized with ethidium bromide and UV light, the target band was cut out and eluted over night in a 1.5 ml reaction tube in elution buffer (see tbl. 2.1). The elution buffer with the eluted DNA was butanol extracted 6 times to remove ethidium bromide traces. The aqueous solution was added to a new tube and ethanol was added (3:1). The DNA was finally precipitated by incubation of the tubes in dry ice for one hour, spun at 14,000 g for 30 minutes, the supernatant was discarded, the DNA dried and resuspended in double distilled water, filtered through a 0.22 μm filter and dialyzed in a mini dialysis unit from PIERCE (Slide-A-Lyzer™ 3500 MWCO) over night.

Table 2.1: Buffer compositions

Buffer	Ingredients
Running buffer pH 8.0	89 mM TrisHCl 89 mM boric acid 2 mM EDTA
Sample buffer	10 mM NaOH 1 mM EDTA 0.1 % xylene cyanol as a tracking dye
Elution buffer pH 8.0	500 mM Ammonium acetate 10 mM $[\text{CH}_3\text{COO}]_2 \text{Mg} \cdot 4 \text{H}_2\text{O}$ 2 mM EDTA

2.2.3 Native Gels (Non-Denaturing Gels)

Native gels contained between 4 % and 10 % acrylamide (19:1, acrylamide: bisacrylamide) and were run with 10-14 $\frac{\text{V}}{\text{cm}}$ (constant voltage) at room temperature (21°C), for sample and running buffer see tbl.2.2. The bands were visualized with stainsall dye obtained from Sigma. pBR322 *Hae*III digested length marker from SIGMA (see Appendix tbl. 6.1) and/or 10 base pair ladder from InvitrogenTM was used for native gel studies as a reference (10bp ladder contains DNA fragments from 330 bp to 10 bp in 10 pb steps, the fragments 100 bp and 330 bp appear three times brighter on a gel).

Table 2.2: Buffer compositions

Buffer	Ingredients
Sample buffer pH 8.0	40 mM TrisHCl 20 mM acetic acid 2 mM EDTA 12.5 mM magnesium acetate
Running buffer pH 8.0	40 mM Tris-acetate 2 mM EDTA 12.5 mM magnesium acetate

2.2.4 Stoichiometry of DNA Strands

The optical density of each strand was measured after purification (2.2.2) with a Spectronic Genesys 5 spectrophotometer at 260 nm wavelength. The concentration of each strand was estimated with Lambert Beer's law ($1 \text{ OD} = 35 \mu\text{l} \times \text{g}^{-1} \times \text{cm}^{-1}$) and an average molecular weight of $330 \text{ g} \times \text{mol}^{-1} \times \text{nucleic base}^{-1}$. If necessary, the stoichiometry was corrected by titrating pairs of strands that should bind to each other by Watson-Crick base pairing. The amount used of one of the strands was varied by using different volumes of one of the strands (e.g. $\frac{\text{volumestrand1}}{\text{volumestrand2}}$: $\frac{1}{0.8}, \frac{1}{0.9} \dots \frac{1}{1.4}$). The mixed strands were annealed by the annealing protocol given in 2.5 and visualized by native gel electrophoresis and Stains All™ solution from SIGMA. The absence of a monomer band was taken to indicate the titration end point.

2.2.5 Fast Annealing of Oligonucleotides for Native Gel Based Studies

The strands that were to form a complex or an array were pipetted stoichiometrically (s. 2.2.4) into a reaction tube, buffer was added and the volume finalized with double distilled, 0.22 μm filtered water. The reaction tubes were then exposed to the following temperatures:

- 90 °C for 5 min.
- 65 °C for 15 min.
- 35 °C for 20 min.
- 21 °C (room temperature) for 20 min.

2.2.6 Slow Annealing of Oligonucleotides

The strands were stoichiometrically (see 2.2.4) mixed, buffer was added and the volume finalized with double distilled, 0.22 μm filtered water. The tube was closed with a clip, placed in a 2 liter vessel of boiling water for 2 minutes. Then the vessel with the tube was transferred to a Styrofoam box (3.5 cm wall thickness) and left there for 2-4 days. This slow cool down process was intended to enable the strands to find their complements that correspond to the lowest energy level and therefore form the desired motif or array.

2.3 Atomic Force Microscopy

2.3.1 Preparation of sample

5 μl were carefully pipetted onto the surface of a freshly cleaved piece of mica (Ruby Red Mica Sheets from Electron Microscopy Sciences). After

adsorption times between 1 - 20 min., 5-6 drops of double distilled and 0.22 μm filtered water were carefully placed on the mica surface, forming a big drop on the mica, stabilized by the surface tension. The mica was picked up and the drop shaken off. A filter paper was moved to the edge of the mica, removing the remaining liquid by capillary forces. The prepared sample was examined under the AFM within the next ten minutes.

2.3.2 AFM Imaging

AFM imaging was done under isopropanol in a fluid cell on a NanoScope IV model from Digital Instruments Inc.. Si_3N_4 cantilevers with integral tips coated from NanoProbesTM Digital Instruments Inc. were used as scanning tips.

2.3.3 Post Processing of AFM Pictures

All images were processed with the WSxMTM computer software obtained from Nanotec Electronica (<http://www.nanotec.es>). All AFM pictures were flattened and the contrast was adjusted. All shown AFM pictures are computerized close ups from AFM acquired data.

2.4 3D Assembly - DNA Crystallization

2.4.1 Hanging Drop Crystallization

Hanging drop crystallization was performed with 12 well crystallization plates obtained from Hampton Research. The motif was pre-annealed (2.2.6) with 0.1 x Cacodylate buffer and 10 mM Mg^{2+} . The crystallization buffer in the well was 300 μl . 2 μl of the sample was pipetted on a siliconized glass

cover slide from Hampton research and 2 μl of the same buffer as in the well was added to the sample and mixed on the cover slide. Silicon Grease from DOW Corning was put between the side of the well and the cover slide was pressed on the grease with the sample on the bottom of the cover slide, the grease prevents any exchange with the outer atmosphere. The DNA concentration in the sample (hanging drop) will increase due to vapor diffusion until the concentration of salts, buffers and precipitant is the same as in the well. The increase of DNA concentration will often force the DNA to crystallize or precipitate. Hampton recommends a DNA concentration of 12 mg x ml⁻¹, leading to a final concentration of 6 mg x ml⁻¹. Dilution series were done with each motif and concentrations between 24 mg x ml⁻¹ and 1 mg x ml⁻¹. The hanging drop crystallization technique was done with TAE, HEPES and Cacodylate buffers in the presence of magnesium ions. Further the Natrix Kit, a matrix of common crystallization conditions was used [81]. The Natrix Kit, offered by Hampton Research, was used for crystallization attempts of several motifs. It consists of 48 unique buffer, salt and precipitant combinations, covering a broad range of solutions that have already been successfully used to crystallize nucleic acids [81]. For the composition of all 48 buffer solutions see Appendix 6.3.

2.4.2 Crystallization with Temperature Control

Crystal Annealing in Reaction Tubes

Crystals were annealed in buffer (either HEPES, TAE or Cacodylate with Mg²⁺ concentrations from 10 mM to 100 mM) with the same protocol used for 2D arrays (see 2.2.6). The DNA concentrations were between 1 μM and 4 μM .

Crystallization with Hanging Drop and Temperature Control

In addition, a hybrid technique using parts of hanging drop crystallization and crystallization with temperature control was used. The tile was pre-annealed (2.2.6) with 0.1 x Caccodylate buffer and 10 mM Mg^{2+} . A 12 well crystallization plate from Hampton was prepared the same way as described in 2.4.1. A Petri dish with 45°C water was put on the top over the cover slides and the plate was put in an incubator (Torrey Pines Scientific ECHOTerm™) at 45°C and cooled down to 37°C with $0.1 \frac{^{\circ}\text{C}}{\text{hour}}$ controlled temperature decrease. The preheated Petri dish prevents condensation on the cover slide caused by the higher water volume in the Petri dish compared to the volume in the wells.

2.4.3 General Crystallization and Crystal Mounting Techniques

Crystal Mounting in Loops

Crystals were transferred to different buffers with increasing content of anti-freeze (e.g. PEG, Glycerol, $(\text{NH}_4)_2\text{SO}_4$) to prevent the formation of water crystals during flash cooling. When the crystal environment reached the final anti-freeze agent concentration, the crystal was captured under a light microscope with a loop (CryoLoop™ from Hampton Research) and put immediately in liquid nitrogen for 30 seconds. Finally the loop was put into a cap (CrystalCap from Hampton Research) and stored in liquid nitrogen until exposed to x-rays.

Crystal Mounting in Capillaries

Crystals were sucked into a capillary (Quartz capillaries from Hampton Research, different diameters), pretreated with SigmaCoat (SIGMA). The liquid around the crystal was removed with a micro wick (Hampton Research). A small reservoir of buffer was kept in the capillary to prevent the crystal from drying. The capillaries were sealed and kept at 20°C until exposed to x-rays. The crystal mounting technique is shown in appendix fig. 6.2 and fig. 6.3.

2.4.4 X-Ray Examination of DNA Crystals

All crystals were examined by x-rays at the National Synchrotron Light Source, department of energie (NSLS Brookhaven/Long Island). The diffraction was collected at the National Light synchrotron beamline X8C on a MarCCD collector. The wavelength was 1.1Å exposure times were between 2 and 20 minutes.

2.5 Crystallization Experiments

2.5.1 3D Assembly with TXA Tiles Under High Magnesium Ion Concentration

The TXA (fig. 1.20) motif for 3D assembly is a modified version of the TXA motif that was developed in my master thesis [45]. The middle helix was cut to allow 3D assembly by connecting to another, 90° rotated TXA via sticky ends (see fig. 1.33). The modified design, the sequence assignment and the design of the sticky ends were made by Pamela Constantinou. Crystals were obtained but diffracted at low resolution. The same motif was to be used for crystallization experiments with higher magnesium ion concen-

tration. The experiments performed should examine the possibility of aiding 3D assembly by increasing magnesium ion concentrations (50 mM and 100 mM Mg^{2+} instead of 10 mM Mg^{2+}). The crude strands for the TX motif were obtained from Pamela Constantinou, purified (2.2.2) and slow annealed (2.2.6) with Caccodylate buffer and 4 μM DNA tile concentration. In addition a crystallization attempt with a hanging drop/annealing combination (2.4.2) was done with Cacodylate Buffer and the Natrix Kit. For sequences see Appendix 6.12.2, for sticky end sequences properties see Appendix (Tbl. 6.4).

2.5.2 2D-Assembly of DX Molecules with Short Sticky Ends

After many unsuccessful sticky ends guided crystallization attempts with different motifs the question arose how many nucleotides are sufficient for 3 dimensional assembly. To answer this question the well known and characterized DX motif was modified and equipped with sticky ends consisting of only 3 nt to see if this will be enough to form a 2-dimensional array. The sequences were designed according to sections 2.1.1, 2.1.3 and 2.1.2, synthesized and purified according to sections 2.2.1 and 2.2.2, slow annealed(2.2.6, HEPES, 10 mM Mg^{2+}), AFM examined (2.3.1,2.3.2) and the pictures post processed (2.3.2). For sequences see Appendix 6.12.1, for sticky end sequences and properties see Appendix, Tbl. 6.7.

2.5.3 Crystallization Attempt of Blunt Ended DX Tiles

Due to difficulties obtaining x-ray diffraction via sticky ended interactions, a blunt ended DAE tile was to be examined. A resolved crystal structure would reveal any bending or torsion stress within the tile. It was designed

according to sections 2.1.1, 2.1.3 and 2.1.2, synthesized and purified according to sections 2.2.1 and 2.2.2. A crystallization attempt was made with the hanging drop crystallization technique (2.4.1), selected crystals were mounted in loops (2.4.3) and exposed to x-rays (2.4.4). For sequences and brominated sequences see appendix 6.12.3.

2.5.4 3D Assembly and Gel Studies of Chengde Mao Triangles

Gel Based Studies of Blunt Ended ChengdeMao Triangles

A new motif for DNA Nanotechnology was invented by Prof. Chengde Mao [55] from Purdue University. The motif takes into account that DNA crystals prefer to grow in the direction of the helical axis (an example of one CDM triangle is given in fig. 2.1). The DX and TX motifs used for 3D assembly have the disadvantage that they have to grow in one direction perpendicular to the helical axis. The triangle of Prof. Mao fills 3 dimensional space with a helical axis growing in all three dimensions. Unfortunately the motif seemed to be unstable when examined by native PAGE. A crystallization attempt based on a triangle with 2 full turns between triangles, 16 nt per triangle edge and an assumption of 10.5 nt per DNA full turn with the Natrix kit done by Prof. Mao gave crystals with well defined faces. When exposed to x-rays in the Brookhaven National Light Synchrotron they showed diffraction but the wrong space group. Dr. W. Sherman performed calculations concerning the CDM triangles and their geometrical properties (s. appendix 6.11). Based on these assumptions 5 blunt ended triangles (13 nt, 14 nt, 15 nt, 17 nt and 18 nt per inner triangle edge) were designed according to sections 2.1.3 and 2.1.2, synthesized and purified according to

Table 2.3: Triangles designed and synthesized based on a basic design by Prof Chengde Mao

Name of triangle	nt per inner triangle edge	assumed helicity	full turns between triangles	length of sticky ends	triangle handedness
CDM-C	14	10.5	1	4	left
CDM-A	14	10.5	2	5	left
CDM-B	14	10.0	2	4	left

sections 2.2.1 and 2.2.2, slow annealed(2.2.6 with TAE 10 mM Mg^{2+}) and examined by native PAGE (s. 2.2.3).

3D Assembly with ChengdeMao Triangles with 14 nt per inner triangle edge

Using the assumption of 14 nt per inner triangle edge three different triangles were designed (see tbl. 2.3). Please note that the triangle with 14 nt per inner triangle corresponds to a left handed triangle (s. fig. 2.2) based on the calculations of Dr. Sherman (s. 6.11). The triangles were designed according to sections 2.1.3 and 2.1.2, synthesized and purified according to sections 2.2.1 and 2.2.2. The crystallization attempts were made with slow annealing (1 x Cacodylate Buffer, 10 mM Mg^{2+}) and with a hanging drop/annealing combination (2.4.2). Crystals obtained via hanging drop/annealing combination were examined by x-rays(2.4.4) with a synchrotron. For DNA sequences see appendix 6.12.6, for sticky end sequences and properties see 6.5.

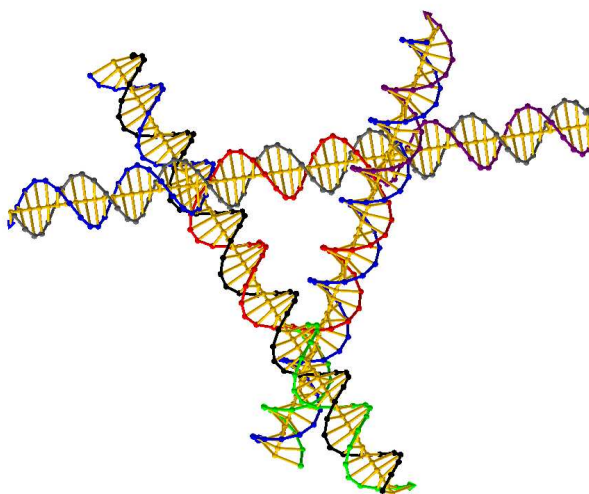


Figure 2.1: Example of a CDM triangle with 17nt per inner triangle edge.

The basic design of this molecule was thought up by Prof. Chengde Mao. If equipped with sticky ends then this motif can assemble along each helical DNA axis and fill space.

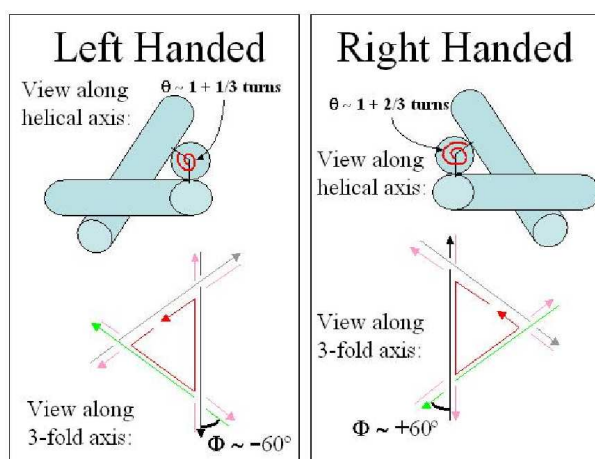


Figure 2.2: DNA triangle handedness by Dr. William Sherman. The CDM triangle can occur in two different conformations (left or right handed), depending on the number of nt per inner triangle edge.

3D Assembly of a ChengdeMao Triangle with One Direction Blunted

A triangle system, as thought up by Prof. Chengde Mao, grows into three axes along the helical axes. One direction was blunted to see how such a system that is expected to grow only in 2 dimensions react to a crystallization approach. For system CDM-A either strand CDM-S4-14A was exchanged with strand CDM-S4-14A-BE or strand CDM-S6-14A was exchanged with strand CDM-S6-14A-BE. For system CDM-B strand CDM-S1-14B exchanged with strand CDM S6-14B-BE. The strands were synthesized and purified according to sections 2.2.1 and 2.2.2. The crystallization attempts were made with slow annealing (1 x Cacodylate Buffer, 10 mM Mg^{2+}) and with a hanging drop/annealing combination (2.4.2). Crystals obtained via hanging drop/annealing combination for system CDM-B were examined via x-rays (2.4.4) with a synchrotron. For DNA sequences see appendix 6.12.6.

2.5.5 3D Assembly with a TXDX Triangle Motif and 0D, 1D and 2D examination of the motif

Stimulated by the design of Prof. Chengde Mao a new triangle was thought up that grows into space along the helical axes but is based on more rigid motifs (DX, s. fig. 1.17 and TX, s. fig 1.20). The triangles inner motif consists of three TX tiles, connected by bulged three arm junctions (2 per edge). The triangle corners extend via a rigid DX motif to the next triangle. The triangle is shown in fig. 2.3, a top view is given in fig. 2.4. Fig. 2.5 shows a side view of a “sub-motif” of the triangle. The triangle consists of three of such “sub-motifs”, connected with a skew. The “sub-motif” is only given for better understanding, it does not show how the actual connections between

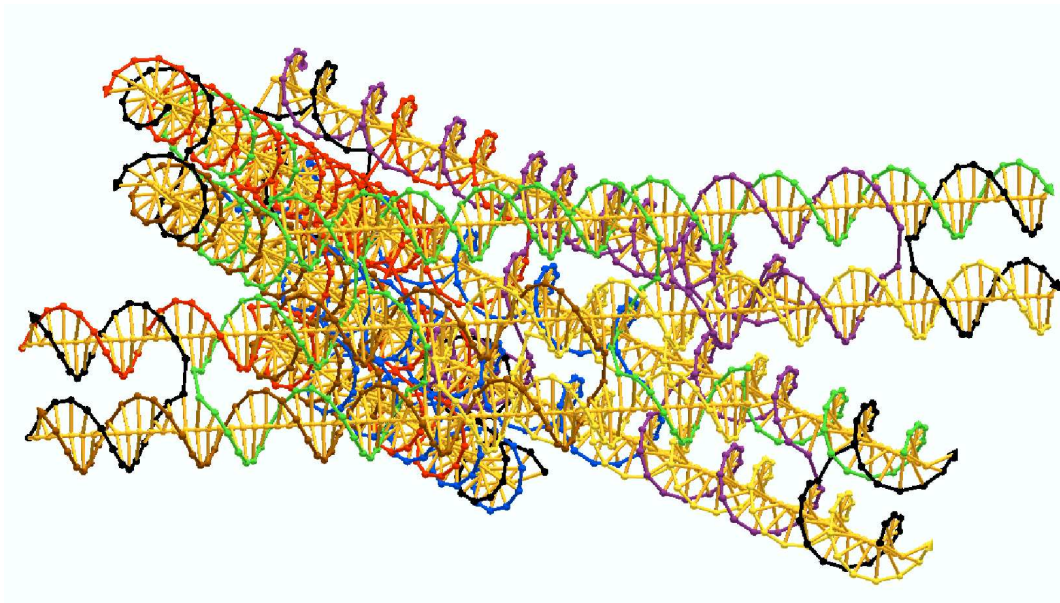


Figure 2.3: Computer generated model of a TXDX triangle tile. The motif is shown in a blunt ended version.

the three “sub-motifs”. A drawing with the attached DNA sequence, the position of the bulged 3arm connections is shown in the appendix (s. fig. 6.4). The triangle motif could be designed that the strand nicks possess perfect three fold symmetry but the nicks were set instead on positions that surround the nick with G and/or C bases. The triangle was designed according to sections 2.1.3, 2.1.2, 2.1.4, synthesized and purified according to sections 2.2.1 and 2.2.2. A blunt ended tile was examined on a native gel (2.2.3), 1D and 2D arrays were AFM examined (1 X HEPES Buffer, 10 mM Mg^{2+} , 2.3.1, 2.3.2). Please note that there are 3 flavors for the 1D motif as well as for the 2D motif (see section 6.8). All three possible flavors for 1D and 2D assembly were examined. Crystallization attempts (3D) were made with slow annealing (1 x Cacodylate Buffer, 1 x TAE Buffer or HEPES Buffer, each had 10 mM Mg^{2+}) and with a hanging drop/annealing combination (2.4.2). For DNA

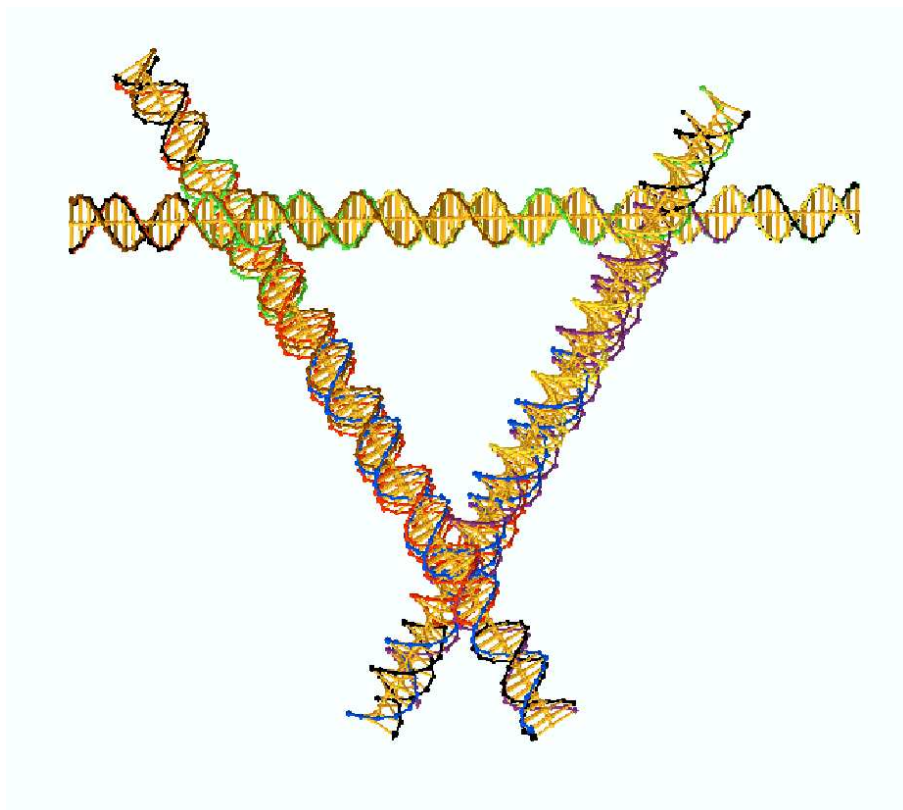


Figure 2.4: Top view of a computer generated model of a TXDX triangle tile.

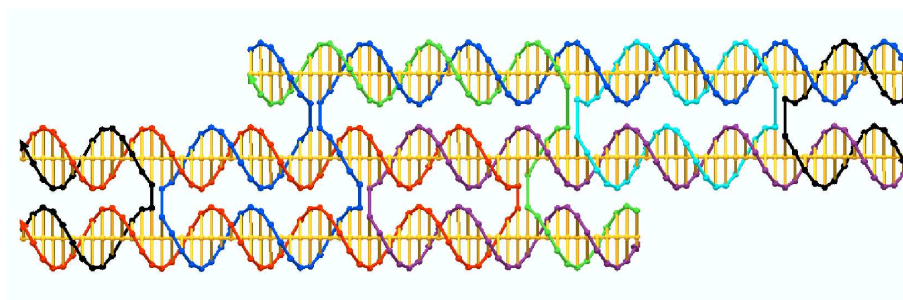


Figure 2.5: Computer generated model of one side of the TXDX triangle tile. The TXDX triangle consists of three of such “sub-motifs,” connected with a skew. This “sub-model” lacks some strand nicks of the actual TXDX triangle.

sequences see appendix 6.12.8, for sticky end sequences and properties see 6.6, for pipetting strand combinations (how to get 0D, 1D, 2D and 3D motifs) see appendix, section 6.8.

2.6 DNA Nanotube as an Artificial Ion Channel

2.6.1 Design of a DNA Nanotube for Use as an Artificial Ion Channel

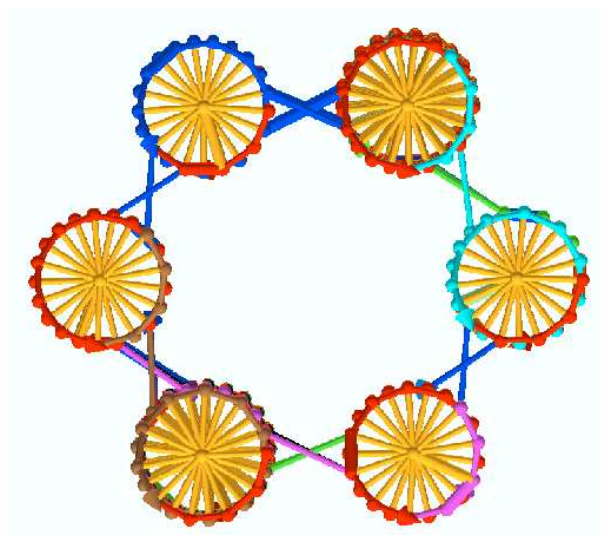


Figure 2.6: End view of a computer generated model of the 6 helix bundle. Six DNA helices are connected via cross-overs. Each helix has 9 full turns of DNA, the motif consists of 19 strands.

A motif can be constructed that links six helices together to form a bundle or a tube. A version of this motif, containing six helices with 9 full turns, connected by cross-overs that form a bundle has been designed by Prof.

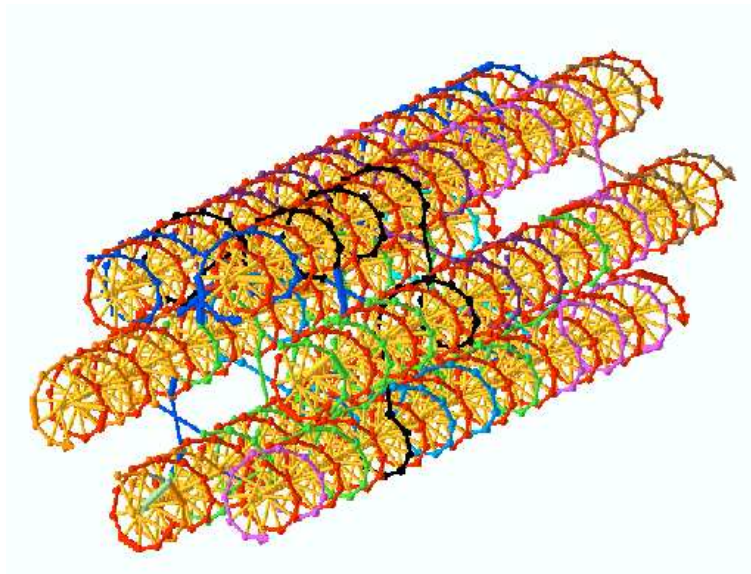


Figure 2.7: Angled view of a computer generated model of the 6 helix bundle.

Six DNA helices are connected via cross-overs. Each helix has 9 full turns of DNA, the motif consists of 19 strands.

Seeman, preliminary experiments for 1D and 2D assembly were done by former student Frederick Mathieu. A new version was designed with GIDEON (2.1.4) with an additional 4 cross-overs to increase the rigidity of the motif. A GIDEON model of the motif is shown in fig. 2.6 and fig. 2.7. The modified motif does not contain any sticky ends. An AT-rich sequence is placed outside of the three inner middle turns which in combination with netropsin, a minor groove binder (see section 2.6.2) should make this region hydrophobic. In this context, an AT-rich sequence shall be defined as consisting only of A's and T's. The position of the outside sequence in the 6 helix bundle molecule was found by computer aided molecular modeling with GIDEON. Three full turns of each helix require eighteen 8 nt long AT-rich ds sequences. Further, the AT-rich sequences should be unique to assure that the motif will form

properly. Each unique 8mer, flanked by G/C's, consists of two unique 7mers.

Calculation of unique 8mer (example):

- All possible 7mers were calculated and converted to binary code:

Decimal	Binary	Sequence	Complementary
015	0001111	5'AAATTTT	3'TTTAAAA
021	0010101	5'AATATAT	3'TTATATA
043	0101011	5'ATATATT	3'TATATAA
106	1101010	5'TTATATA	3'AATATAT

- All sequences that contain more than three A or T in a row were eliminated:

021	0010101	5'AATATAT	3'TTATATA
043	0101011	5'ATATATT	3'TATATAA
106	1101010	5'TTATATA	3'AATATAT

- All sequences that would occur twice if the complementary sequences are taken into account were eliminated:

021	0010101	5'AATATAT	3'TTATATA
043	0101011	5'ATATATT	3'TATATAA

- 18 unique 8mers were calculated (appendix tbl. 6.9), each consisting of two unique 7mers:

AATATATA

All possible unique 8mers, fulfilling all restrictions, can be described with

regular expression¹ (see eqn. 2.1).

$$/[(A | T)\{8\} - (AAAA|TTTT)]/ \quad (2.1)$$

All AT-rich sequences were assigned first, based on the calculated unique 8mer and the remaining molecule sequences were designed according to sections 2.1.3 and 2.1.2, synthesized and purified according to sections 2.2.1 and 2.2.2 and slow annealed (sec. 2.2.6, HEPES, 10mM Mg²⁺). The annealed sample was either AFM examined (2.3.1, 2.3.2, 2.3.2), native gel examined (2.2.3) or used for tip-dip bilayer experiments (2.6.3). For DNA strands sequences see section 6.12.7.

2.6.2 DNA Minor Groove Binder

Netropsin is known to bind the minor groove of DNA, the molecular formula is shown in fig. 2.8. Several short ds DNA helices have been crystallized with Netropsin [5]. It binds to the minor groove and is able to distinguish between DNA sequences (appendix, tab. 6.3) and preferably binds to AT rich sequences. Netropsin displaces the spine of hydration in the minor groove and may make the DNA slightly hydrophobic. Resolution of crystal structures with netropsin show one netropsin molecule in the minor groove but NMR (nuclear magnetic resonance) studies show that two netropsin molecules bind to the AT-rich minor groove in solution [11]. Fig. 2.9 shows a stereoscopic

¹Any description of a pattern composed from combinations of symbols and the three operators: Concatenation - pattern A concatenated with B matches a match for A followed by a match for B. Or - pattern A-or-B matches either a match for A or a match for B. Closure - zero or more matches for a pattern. The earliest form of regular expressions (and the term itself) were invented by mathematician Stephen Cole Kleene in the mid-1950s, as a notation to easily manipulate “regular sets”, formal descriptions of the behaviour of finite state machines, in regular algebra. Entry from Free Online Dictionary of computing [39]

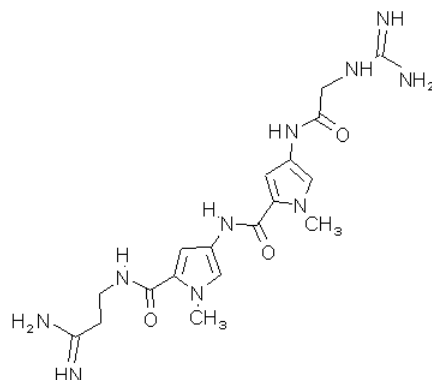


Figure 2.8: Molecular structure of Netropsin*.

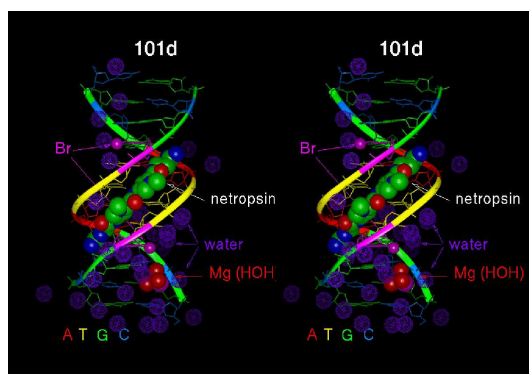


Figure 2.9: Stereoscopic picture of a dsDNA Crystal structure with Netropsin attached in the minor groove*.

image of a resolved crystal structure of dsDNA with netropsin.

Netropsin was obtained from SIGMA and used in different concentrations, based on the assumption of two bound netropsin molecules per 4mer (consisting of A's and T's). For Tip Dip experiments, 100 μl (0.1 μM) of the 6HB was slow annealed. After 24, hours netropsin was added into the tube with the annealed sample and the tube was incubated for another 24 hours at room temperature. Netropsin concentrations were between 0.5 and 8 times

total bundle saturation. The outer side of one turn consists of a 8mer AT-rich sequence, 4 netropsin molecules are expected to bind for total saturation. The bundle has three 8mers binding sites per helix and consists of 6 helices. Hence for 1 mol 6HB 72 mol of netropsin are considered total bundle saturation, based on the oversimplified model that every netropsin binds to the expected binding site. The association constant for an AT-rich sequence is 10^7 M^{-1} , for a sequence containing GC is only 10^4 M^{-1}

2.6.3 Tip Dip and Patch Clamp Experiments

The possible behavior of the 6HB as an ion channel was examined with tip dip, following published protocols [92, 33]. A 6 cm long silver wire was cleaned with a scourer and AgCl coated via electrolysis in a 1 M AgCl solution. The silver wire was mounted into the tip and a pulled glass capillary (Sutter Instrument Corporation, Model P-87 Micropipette puller, Capillaries: World Precision Instruments Inc. Glass 1mm, 4in Item 1B100F-4), filled with HEPES buffer (1 M KCl for symmetric, 150mM KCl for asymmetric conditions) was put over the silver wire into the tip. A well of a 96 well microtiter plate was filled with buffer(1 M KCl, HEPES pH 7.4) and 1 μl of a n-decane/lipid (soy phosphatidylcholin from Avanti Lipids Inc.) mixture was layered on top of the filled well. The tip was lowered and raised into the solution with a Brinkmann micromanipulator. If raised two times into the solution with the lipid layer, a lipid bilayer may form on the tip (s. fig. 2.10), characterized by current insulating behavior. The whole system was insulated against noise with a metal case by WARNER Instrument Corporation and with a BenchMate 2200 vibration free platform.

The voltage-clamp recordings were made with a 3900A Integrating Patch Clamp (Dagan, Minneapolis, MN). Signals were monitored with a Tektronix

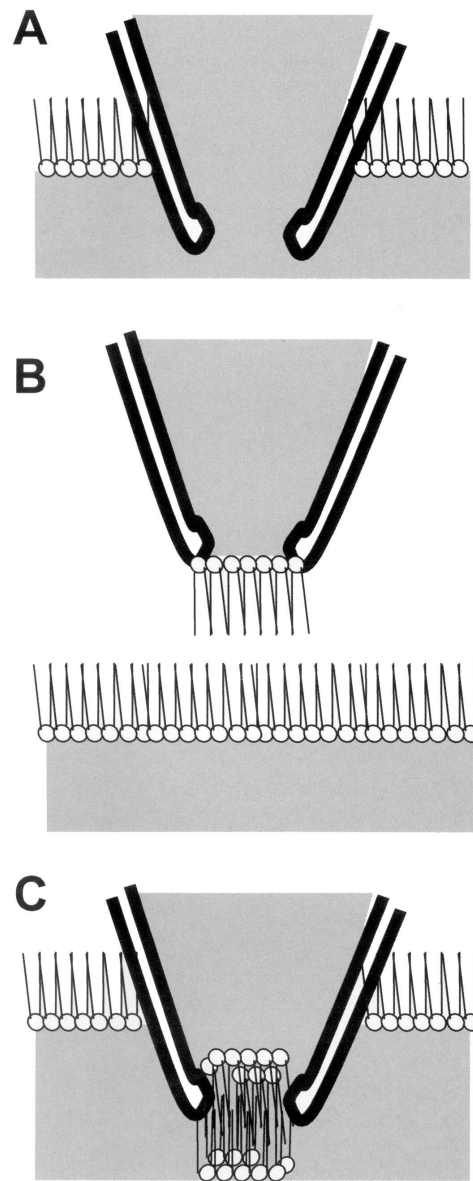


Figure 2.10: The tip dip method. Ion channels can be reconstituted into bilayers formed at the tip of a microelectrode in a method called tip-dip. A microelectrode is submerged in a bath. Lipids (typically in an organic solvent like decane) are layered on top of the bath and allowed to form a monolayer on the bath surface (A). The microelectrode is raised out of the bath (B). A bilayer is formed like a sandwich as the microelectrode is again returned to the bath (C). Channels are added to the bath and insert spontaneously (not shown).**

TDS 320 Two Channel Oscilloscope, a Tektronix 2201 Digital Storage Oscilloscope and filtered at 1 kHz with the four-pole Bessel low-pass filter. The output was channeled into a DIGIDATA 1322A (Axon Instruments) and the digital output signal was visualized and stored using Clampex 8.2 software (Axon Instruments, run on a Dell Pentium 4 1.8 GHz 512 MB Ram and Windows XPp). Ohmic behavior was recorded under symmetric and asymmetric conditions with the Tektronix TDS 320, noise analysis was done with WinEDR (public domain Strathclyde Electrophysiology Software package, supplied free of charge to academic users by Dr. John Dempster, of the University of Strathclyde in Glasgow, U.K.). Control experiments were done with the same 6HB but without the presence of netropsin. Further controls were done with netropsin alone and a 90mer dsDNA helix.

Chapter 3

Results

3.1 3D Assembly - DNA Crystallization

3.1.1 3D Assembly with TX Tiles Under High Magnesium Ion Concentration

Fig. 3.1 shows TX crystals, obtained by slow annealing in Cacodylate buffer (4 μmol DNA concentration, 100 mM Mg^{2+}). The crystals are needle shaped and roughly 50 μm in length. The crystals singly extinguished under plane polarized light but showed no diffraction when exposed to x-rays. Fig. 3.2 shows TX crystals, obtained by a slow annealing - hanging drop combination 2.4.2 with Natrix buffer number 5 and 4 μmol DNA concentration. The crystals look feather shaped. The size of the crystals is up to 0.5 mm in length. The crystals singly extinguished under plane polarized light but showed no diffraction when exposed to x-rays.

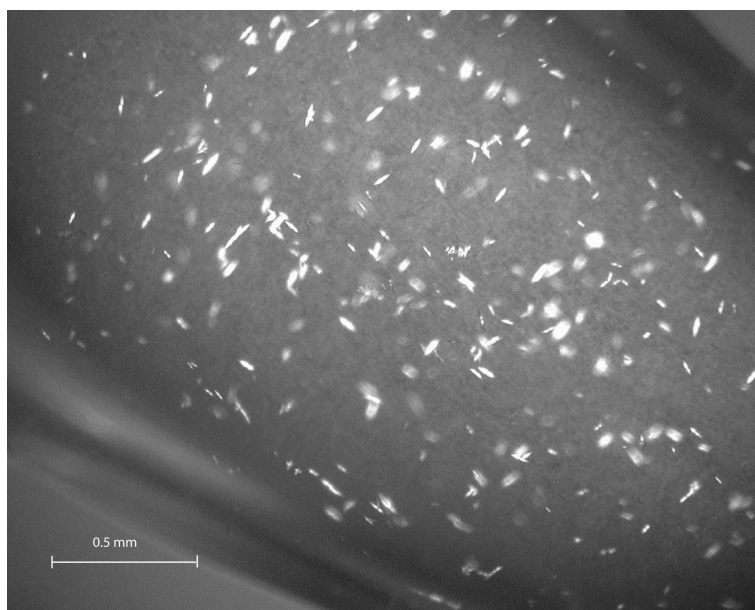


Figure 3.1: Light microscope picture of annealed TX crystals under polarized light

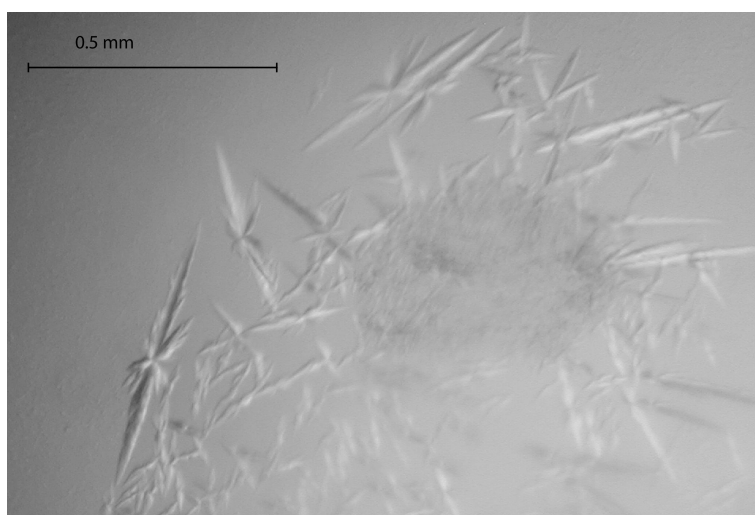


Figure 3.2: Light microscopy picture of TX crystals grown with a combination of slow temperature decrease and hanging drop vapor diffusion.

3.1.2 2D-Assembly of DX Molecules with Short Sticky Ends

At room temperature no arrays out of a two tile TX system could be observed with AFM. When the sample was annealed down to 4°C arrays were found. Fig. 3.3 shows an array and fig. 3.4 a computerized close up. The expected distance between the hairpin loops was 33 nm. 34.8 nm were measured and 32.9 nm were found via a FFT analysis.

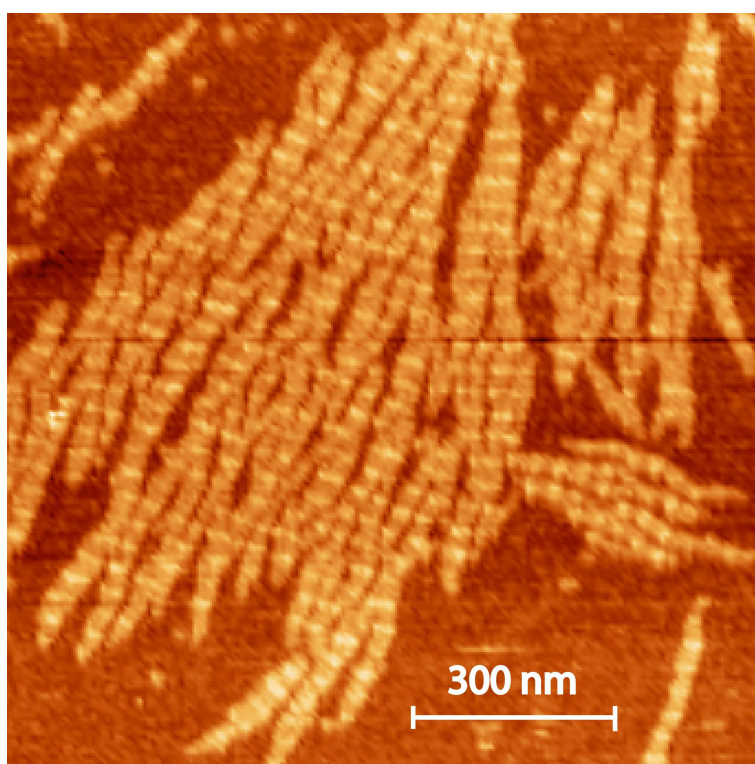


Figure 3.3: AFM picture of a DX array with short sticky ends. Picture scale 1.1 μm x 1.1 μm

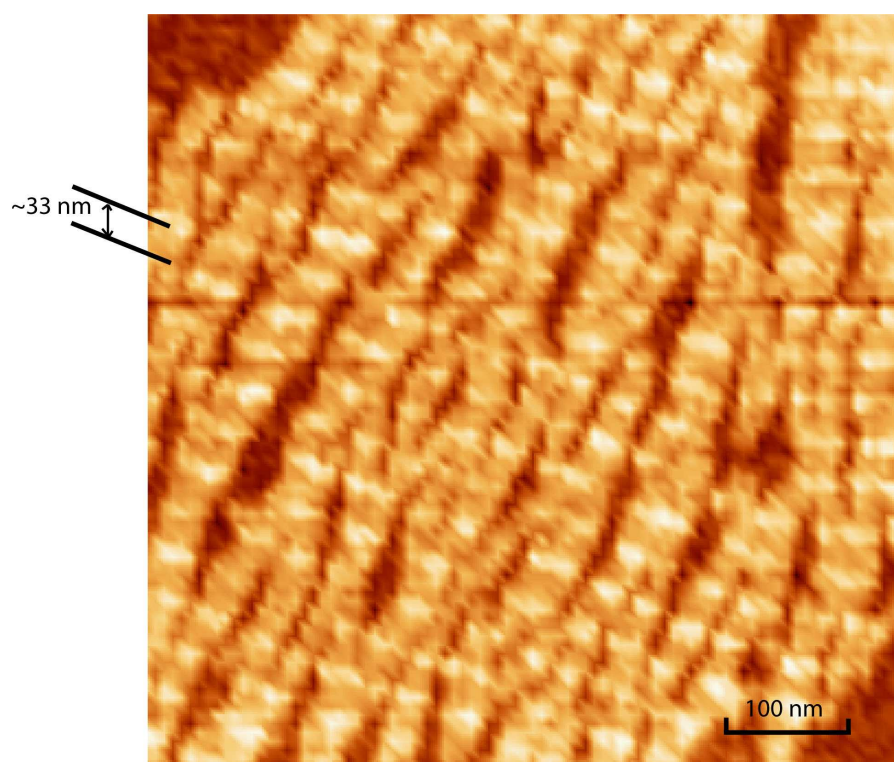


Figure 3.4: AFM picture of a DX array with short sticky ends. Picture scale 595 nm X 595 nm

3.1.3 Crystallization Attempt of Blunt Ended DX Tiles

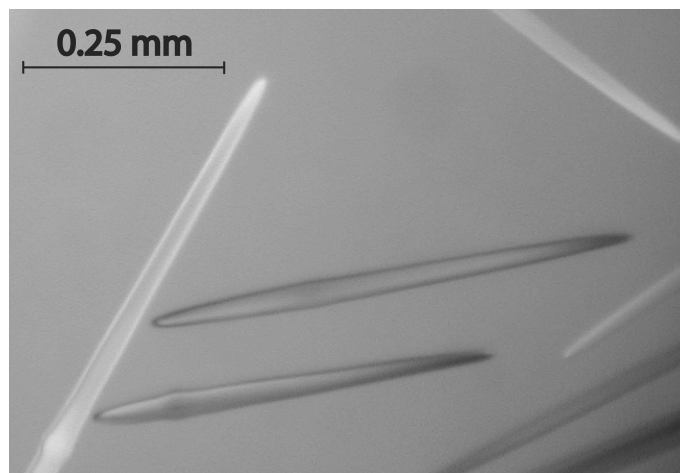


Figure 3.5: Light microscope picture of a crystallization attempt via hanging drop vapor diffusion of a blunt ended DX tile (upper part of the drop). Crystals were grown in Natrix kit buffer 26.

For the crystallization attempt with the Natrix kit (see appendix 6.3) the following results were obtained after 5 days: needle shaped crystals in buffers 5 and 6, needle shaped crystals and a graph like structures (in the lower drop) were found in buffers 10, 17, 25 and 26 (fig. 3.5 and 3.6). Very thin, hair like crystals were found in Natrix buffer 44 (fig. 3.7). All other buffers showed a clear drop or precipitate. The needle shaped crystals singly extinguished under plane polarized light but showed no diffraction when exposed to x-rays.

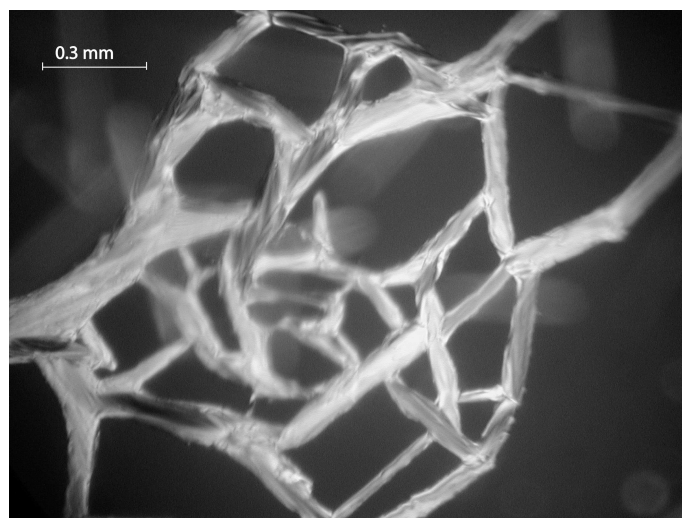


Figure 3.6: Light microscope picture of a crystallization attempt via hanging drop vapor diffusion of a blunt ended DX tile (lower part of the drop). Crystals were grown in Natrix kit buffer 26.

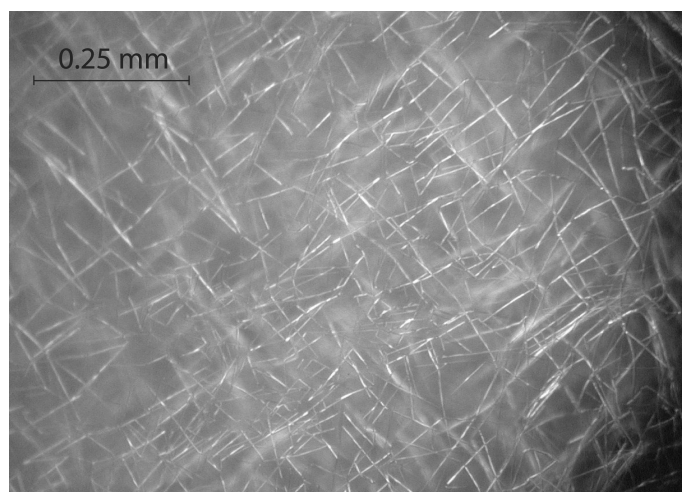


Figure 3.7: Light microscope picture of a crystallization attempt via hanging drop vapor diffusion of a blunt ended DX tile. Crystals were grown in Natrix kit buffer 44.

3.1.4 3D Assembly and Gel Studies of ChengdeMao Triangles

Gel Based Studies of Blunt Ended ChengdeMao Triangles

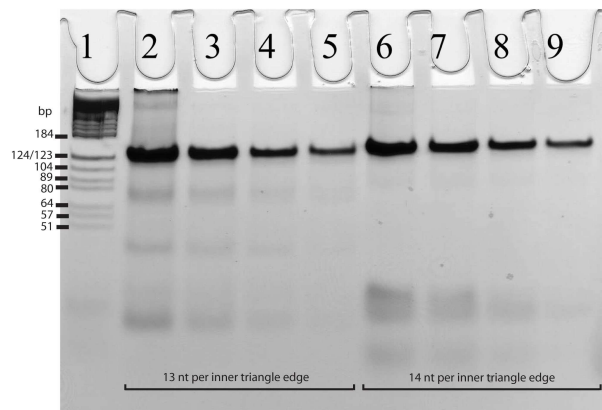


Figure 3.8: Picture of a gel (5% polyacrylamide) study of CDM triangles with 13 nt and 14 nt per inner edge. Lane 1 contains *Hae*III digested pBR marker, lanes 2-5 show the 13 nt triangle with a logarithmically decreasing concentration from 12 μ M to 1.5 μ M, lanes 6-9 show the same for the 14 nt triangle. 10 μ l were loaded.

Fig. 3.8 shows a native gel study of ChengdeMao triangles with 13 and 14 nt per inner triangle edge. Lane 1 shows pBR marker, lanes 2-5 show the 13 nt triangle with a logarithmically decreasing concentration from 12 μ M to 1.5 μ M, lanes 6-9 show the 14 nt triangle with decreasing concentration from 12 μ M to 1.5 μ M. Fig. 3.9 shows the native gel examination of the 15 nt per inner edge ChengdeMao triangle (Lane 1 shows pBR marker, lane 2-5 CDM triangle, 12 μ M to 1.5 μ M logarithmic concentration series). Fig. 3.10 shows the native gel examination of the 17 nt and 18 nt per inner edge ChengdeMao triangle (Lane 1 shows pBR marker, lane 2-5 show the 17 nt triangle, lane 6-9

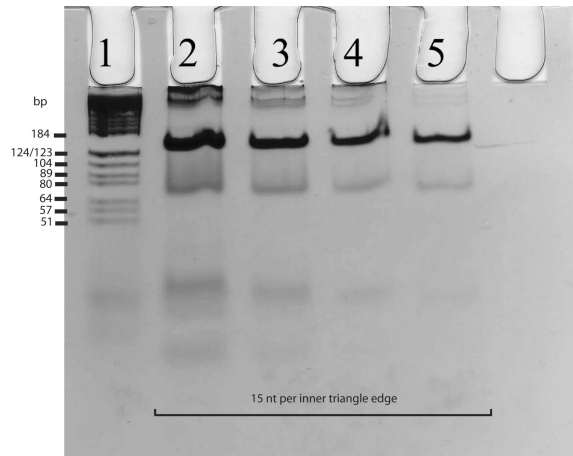


Figure 3.9: Picture of a gel (5% polyacrylamide) study of CDM triangles with 15 nt per inner edge. Lane 1 contains *Hae*III digested pBR marker, lanes 2-5 CDM triangle, 12 μ M to 1.5 μ M logarithmic concentration series). 10 μ l were loaded..

show the 18 nt, both with logarithmically decreasing concentration from 12 μ M to 1.5 μ M). All triangles show lower bands (bands below the molecular weights of the triangles). Significant upper bands are seen for the 13 nt and the 15 nt triangles.

3D Assembly with ChengdeMao Triangles with 14 nt per inner triangle edge

Fig. 3.11 shows the plate like crystals that were obtained from a ChengdeMao Triangle system, based on the assumption of 10.5 nt per helical turn, 14 nt per inner triangle edge, sticky ends consisting of 5 nt, and 2 full helical turns in between triangles. The sample in Fig. 3.11 was crystallized with Natrix Buffer 5 (see appendix 6.3) and a combination between hanging drop and slow temperature decrease (see 2.4.2). Similar plate crystals were obtained

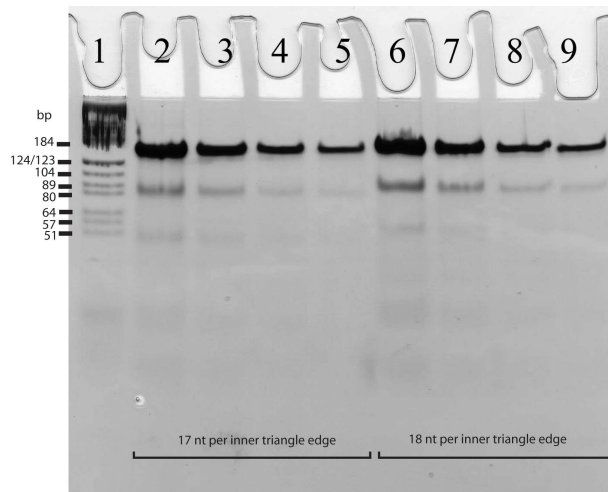


Figure 3.10: Picture of a gel (5% polyacrylamide) study of CDM triangles with 17 nt and 18 nt per inner edge. Lane 1 contains *Hae*III digested pBR marker, lanes 2-5 show the 17 nt triangle, lanes 6-9 show the 18 nt, both with logarithmically decreasing concentration from 12 μ M to 1.5 μ M. 10 μ l were loaded.

with Natrix buffer solutions 4,6,9 and 31 (see appendix 6.3). Fig. 3.12 shows the diamond like crystals that were obtained from a ChengdeMao Triangle system (10 nt per helix full turn, 14 nt per inner triangle edge, sticky ends consisting of 4 nt, 2 full helical turns in between triangles). The sample in Fig. 3.12 was crystallized with Natrix Buffer 45 (see 6.3) and a combination between hanging drop and slow temperature decrease (see 2.4.2). Similar plate crystals were obtained with Natrix buffer solutions 1,2,11,12,13,18,19 and 40 (see 6.3). Fig. 3.13 shows the crystals that were obtained from a ChengdeMao Triangle system (10.5 nt per helix full turn, 14 nt per inner triangle edge, sticky ends consisting of 4 nt, 1 full helical turn in between triangles). The sample in Fig. 3.13 was crystallized with Natrix Buffer 19 (see appendix 6.3) and a combination between hanging drop and slow temperature

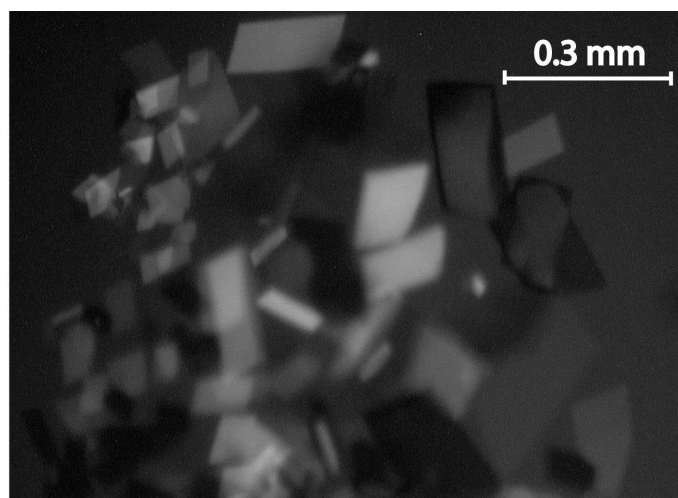


Figure 3.11: Light microscope picture of crystals from system CDM-A (polarized light). Crystals were grown in Natrix kit buffer 5.

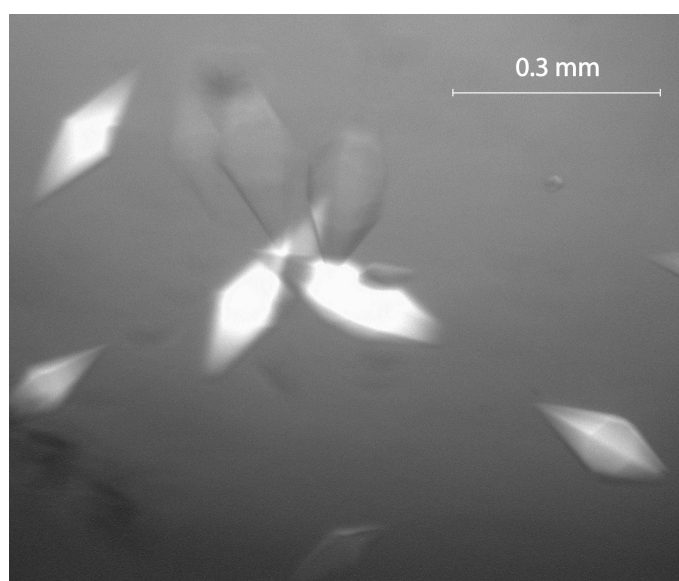


Figure 3.12: Light microscope picture of crystals from system CDM-B (polarized light). Crystals were grown in Natrix kit buffer 45.

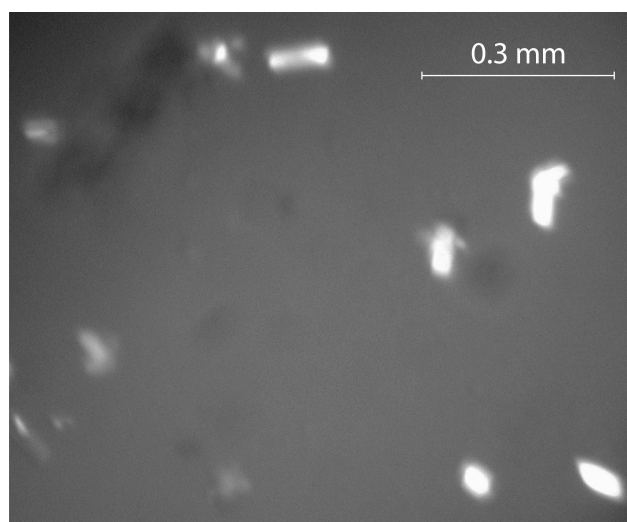


Figure 3.13: Light microscope picture of crystals from system CDM-C (polarized light). Crystals were grown in Natrix kit buffer 19.

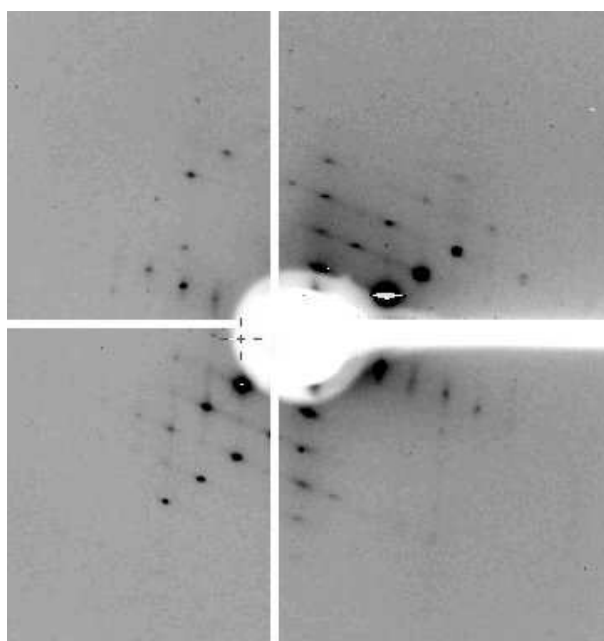


Figure 3.14: X-ray diffraction pattern from a CDM-A triangle system

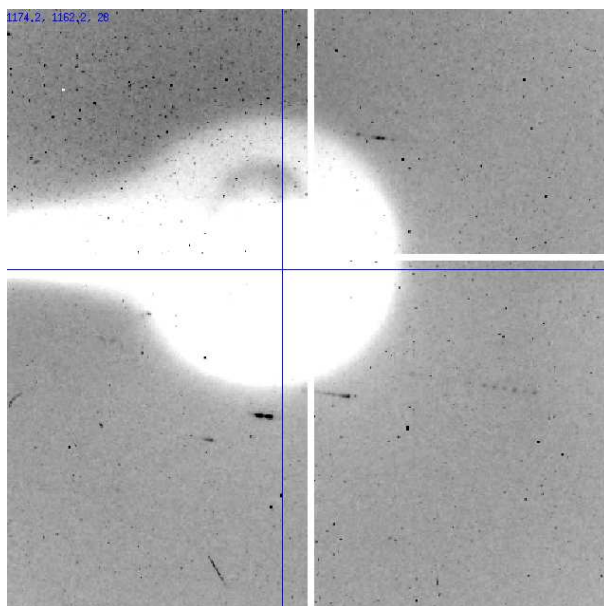


Figure 3.15: X-ray diffraction pattern from a CDM-B triangle system.

decrease (see 2.4.2). It was the only buffer ever showing crystals for system CDM-C. The crystallization process of this system was repeated several times but could never be reproduced.

Fig. 3.14 shows a diffraction pattern collected from system CDM-A. Cell dimensions were $a=132 \text{ \AA}$, $b=133 \text{ \AA}$ and $c=135 \text{ \AA}$. α, β, γ are 108.4° that is close to a rhombohedral/hexagonal cell. The resolution is about 12 \AA .

Fig. 3.15 shows a diffraction pattern collected from system CDM-B. The cell dimensions are around 350 \AA with another axis of 65 \AA or 130 \AA . Resolution down to 13 \AA was achieved. Expected were 109° , a rhombohedral cell and cell dimensions of 142.8 \AA .

3D Assembly of a ChengdeMao Triangle with One Direction Blunted

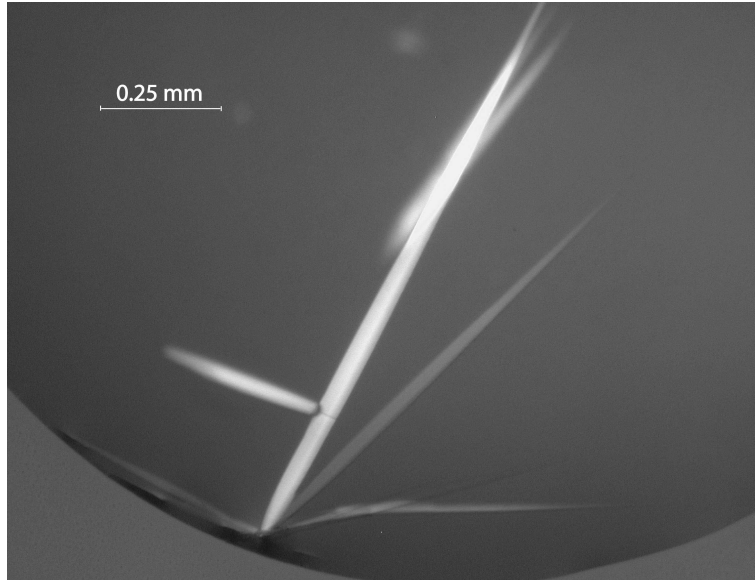


Figure 3.16: Light microscope picture of crystals from system CDM-B_{1BE} (polarized light). Crystals were grown in Natrix kit buffer 19.

Fig. 3.16 shows the diamond like crystals that were obtained from a CDM-B_{1BE} Triangle system (10 nt per helical full turn, 14 nt per inner triangle edge, sticky ends consisting of 4 nt, 2 full helical turns in between triangles) with one direction blunted (one assembly direction out of three was blunt ended, Strand CDM-S1-14B exchanged with strand CDM S1-14). The sample in Fig. 3.16 was crystallized with Natrix Buffer 19 (see appendix 6.3) and a combination between hanging drop and slow temperature decrease (see 2.4.2). Similar plate crystals were obtained with Natrix buffer solutions 11,13 and 40 (see appendix 6.3).

For system CDM-A_{1BE} (based on System CDM-A with one assembly direction blunted), no single extinguishing crystals could be obtained. Fig. 3.17 shows a composite of 10 collected diffraction patterns (each 2°, 20°total). The

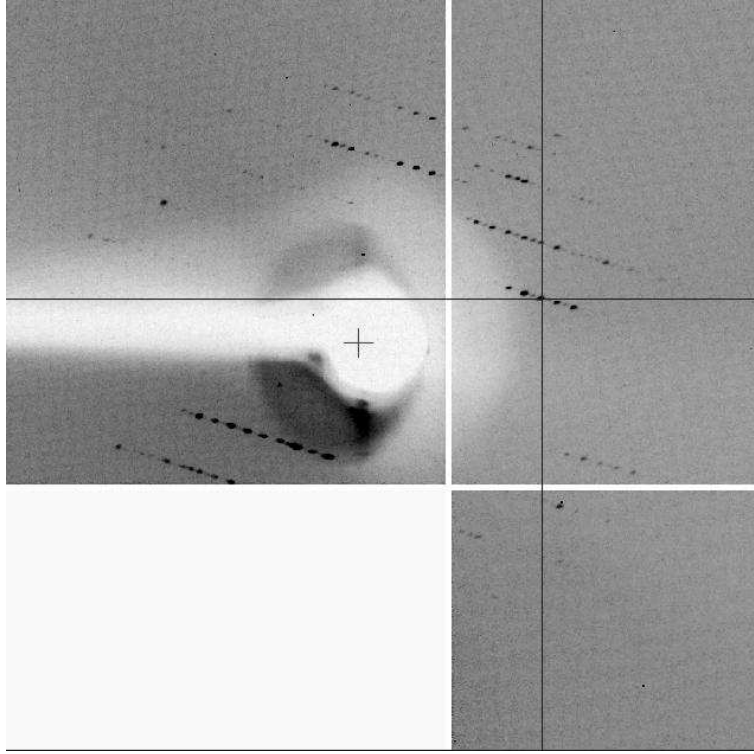


Figure 3.17: Composite of 10 X-ray diffraction patterns collected from system CDM-B_{1BE}

periodicity is around 110 Å to 115 Å in two directions and around 680 Å in the 3rd dimension with a pseudo lattice with distances of approximately 340 Å. The lower left part of the pictures is lost due to a detector malfunction.

3.1.5 3D Assembly with a TXDX triangle motif and 0D, 1D and 2D examination of the motif

Gel Studies of a TXDX Triangle Motif Blunted “Around the Clock” (0D)

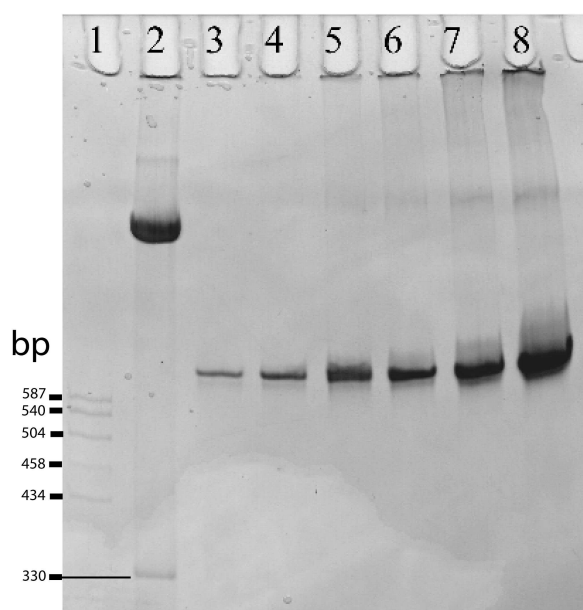


Figure 3.18: Picture of a gel (5% acrylamided) study of the TXDX triangle motif. The motif is blunted “around the clock.” Lane 1 shows *Hae*III digested pBR marker, lane 2 the 10 bp ladder marker, lanes 3-8 contain a logarithmic concentration series of the blunted TXDX triangle 0.1 μ M - 2 μ M. 10 μ l were loaded.

Fig. 3.18 shows the TXDX triangle, all sticky ends are blunted (“blunted around the clock”, 0D). Lane 1 contains pBR marker, lane 2 contains 10bp ladder, lanes 3-8 contain a logarithmic concentration series of the blunted TXDX triangle 0.1 μ M - 2 μ M, 10 μ l were loaded. In well 7 and 8 upper bands (relative to the band that corresponds to the intact triangle motif)

and material that remained in the wells can be seen.

AFM examination of 1D and 2D arrays of the TXDX triangle motif

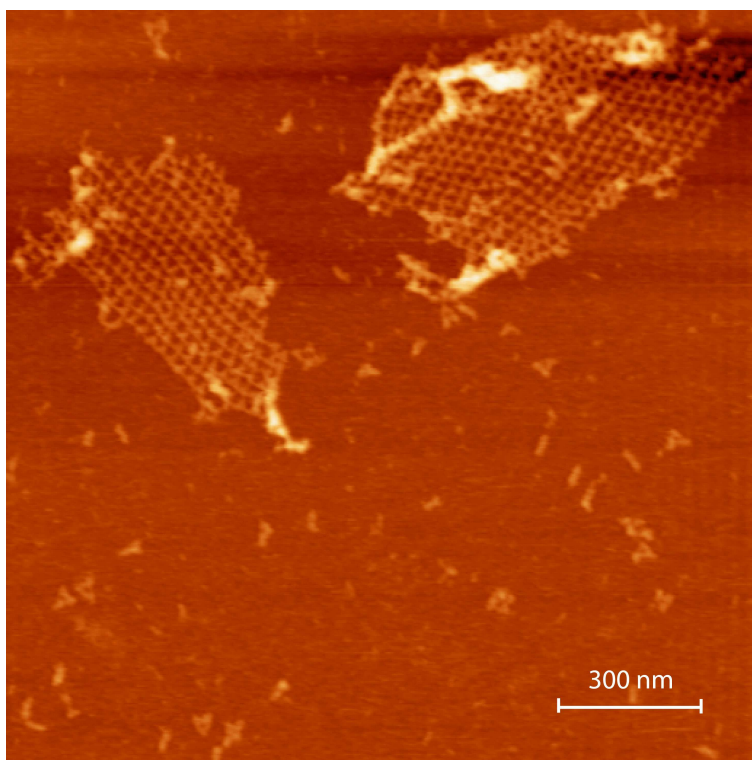


Figure 3.19: Atomic force microscopy picture of 2D arrays consisting of TXDX triangles (flavor A).

At first no 2D TXDX triangle arrays could be observed but 1D arrays could be produced in all possible versions (data not shown). With an increase from 2 minutes to 20 minutes adsorption time on the mica surface 2D arrays with all three flavors could be produced. Fig. 3.19 shows a 2D array with flavor A, fig. 3.20 flavor B and fig. 3.21 flavor C. The expected distances, based on 3.6 nm per DNA helical full turn is approximately 28 nm. Distances found by measurement over several (7-10) triangle lines and distances found

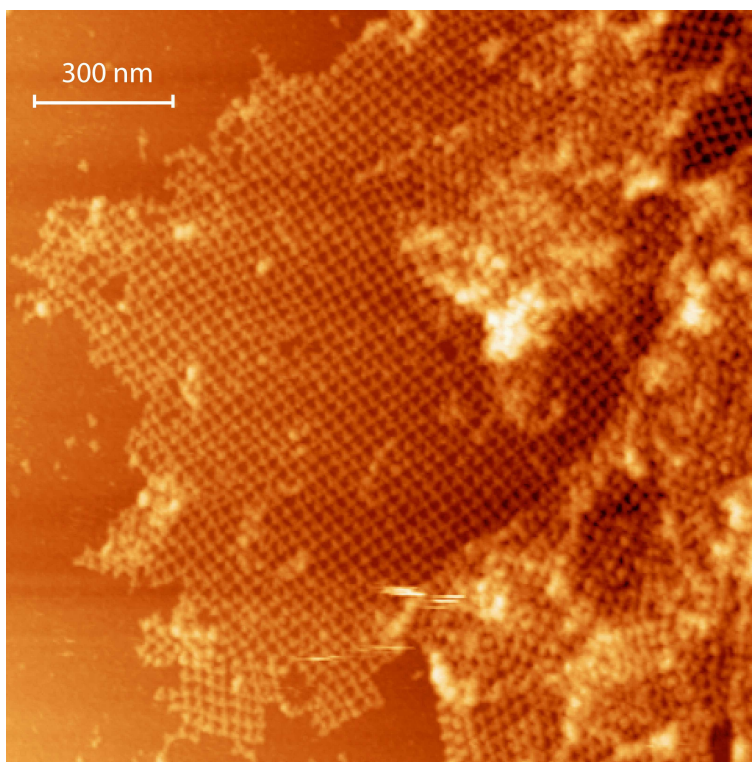


Figure 3.20: Atomic force microscopy picture of 2D arrays consisting of TXDX triangles (flavor B)

by FFT analysis are given in tbl. 3.1. For each triangle flavor, 2 directions were measured (x and y). Please note that, according to the design of the molecule, x and y should be same. The given numbers correspond to the inner diameters of the rhombus like area that is defined by four triangles. The actual triangles could be resolved in some pictures (see fig. 3.22, flavor B).

3D Assembly with TXDX Triangles

All drops of the Natrix Kit were either clear or showed precipitate. Annealing in HEPES, TAE and Cacodylate buffer with 10 mM Mg^{2+} did not give singly

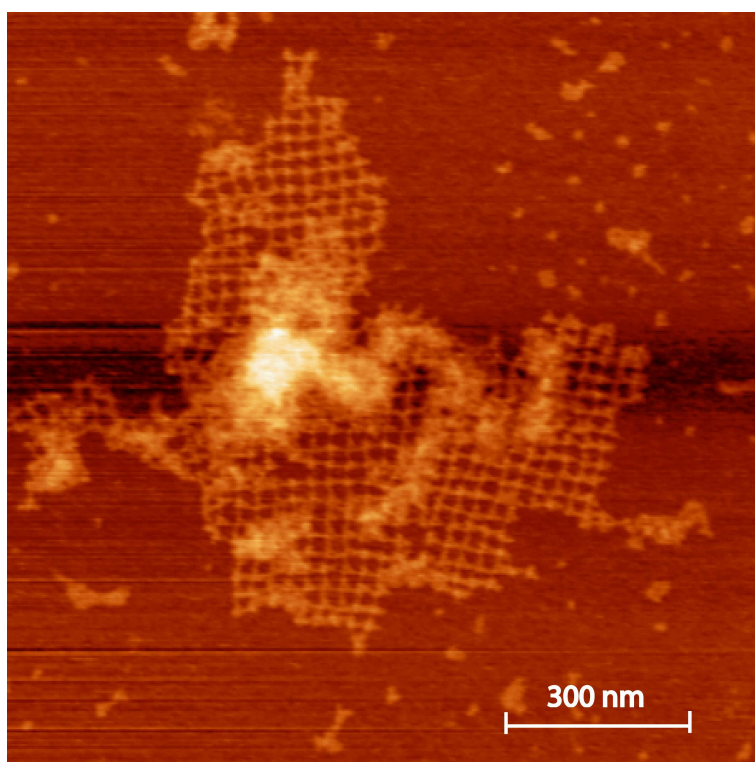


Figure 3.21: Atomic force microscopy picture of 2D arrays consisting of TXDX triangles (flavor C)

extinguishing crystals when viewed with plane polarized light.

Table 3.1: TXDX Triangle distances

Flavor	Distances measured [nm]	Distances found per FFT [nm]
Flavor A x	31.1	31.8
Flavor A y	31.6	31.8
Flavor B x	26.6	29.4
Flavor B y	29.4	29.6
Flavor C x	28.0	29.6
Flavor C y	27.6	32.1

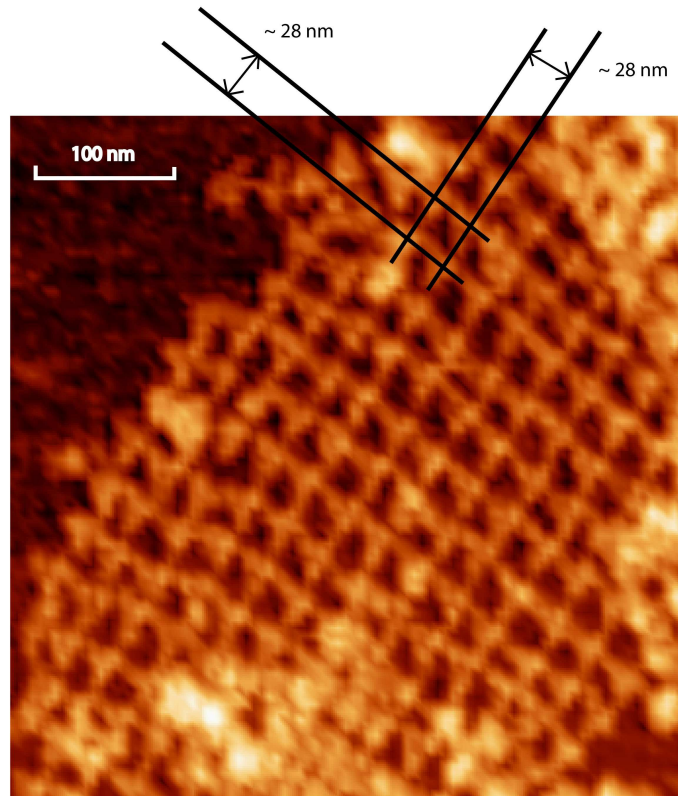


Figure 3.22: Atomic force microscopy picture of 2D arrays consisting of TXDX triangles flavor B

3.2 DNA Nanotubes

3.2.1 DNA Nanotube for Use as an Artificial Ion Channel

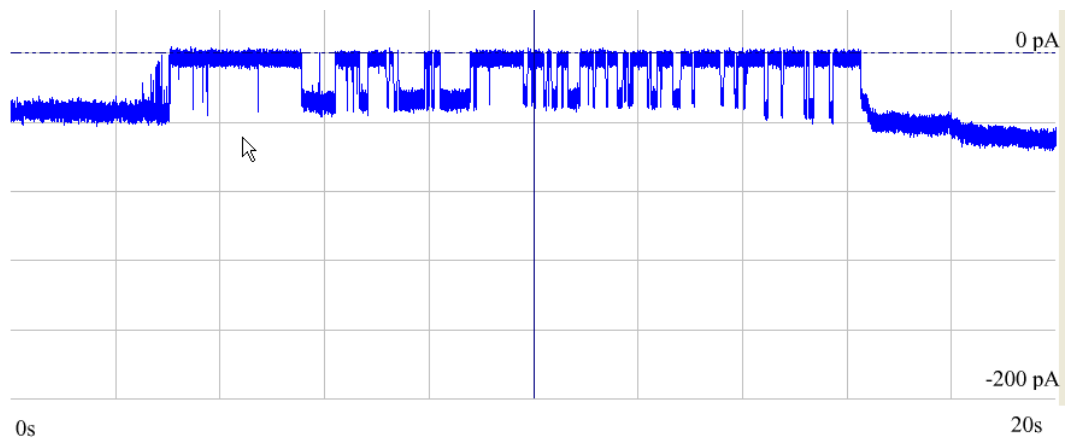


Figure 3.23: Current trace at 50 mV showing ion channel behaviour (800 pS transitions). Sample contained 5 μl 6HB (0.1 μM) and 1 x Netropsin bundle saturation.

Fig. 3.23, fig. 3.24 and fig. 3.25 show recorded channel behaviour. These results were recorded with -50 mV voltage applied to the system and one time netropsin binding site saturation (see calculation in section 2.6.2). Fig. 3.23 shows typical ion channel behaviour, the step sizes are around 40 pA that corresponds to 800 pS. Fig. 3.24 from the same recording shows 800 pS transitions on top of a 800 pS baseline. After approximately 14 seconds (based on the figure, the shown recording is an exported time frame out of a longer recording) the bilayer seems to be disturbed and something is seen that could be interpreted as 2 nS transitions. Fig. 3.25 shows a recording (-50mV, 1x bundle netropsin saturation) that shows a broader range of tran-

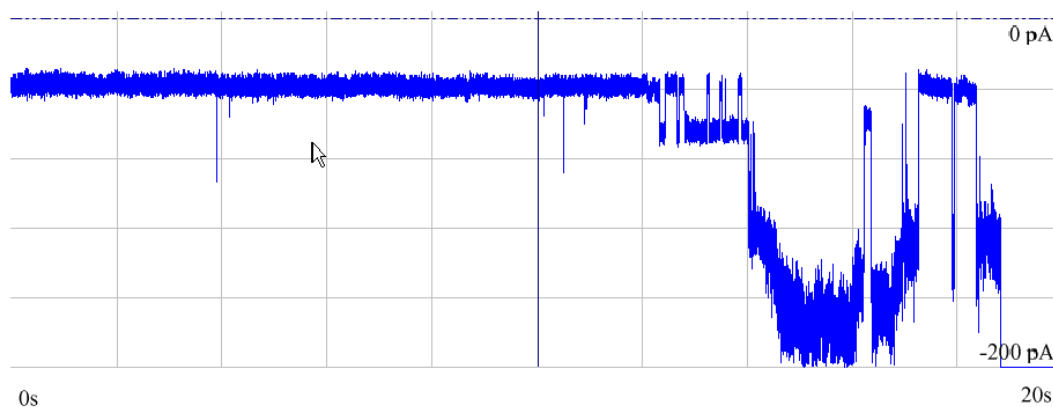


Figure 3.24: Current trace at 50 mV showing ion channel behaviour (800 pS and 2 nS transitions). Sample contained 5 μl 6HB (0.1 μM) and 1 x Netropsin saturation.

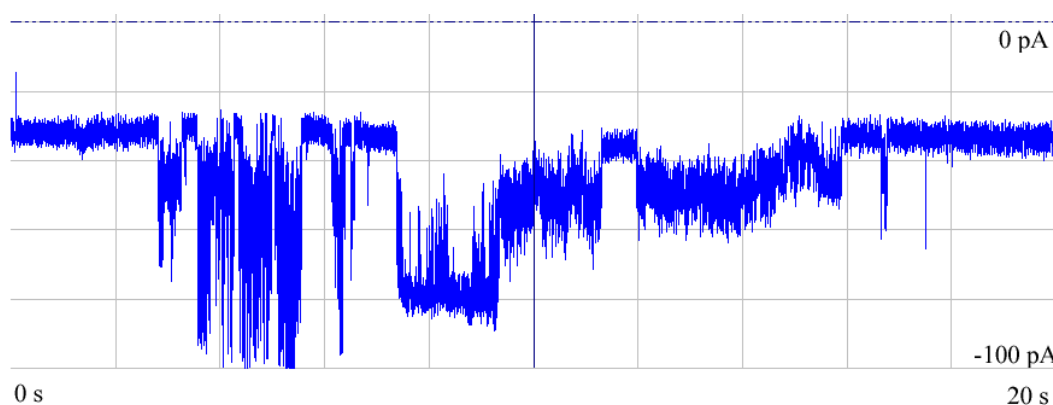


Figure 3.25: Current trace at 50 mV showing ion channel behaviour (200 pS, 600 pS and 1 nS transitions). Sample contained 5 μl 6HB (0.1 μM) and 1 x Netropsin saturation.

sitions. Transitions of 200 pS, 600 pS and 1 nS were observed. Often a bilayer was created (seal test showed insulating behaviour) and immediately current (corresponding to 400 pS to 2 pS) flow was observed but no transitions. During this current flow IV (current-voltage) curves were collected that

showed strong ohmic behaviour (data not shown) with the bundle. If the IV curve was taken under unsymmetrical ion conditions cation selective behaviour was observed. Control experiments were done with the 6 helix bundle but without netropsin. Current flow in similar range but fewer transitions were observed. In bilayer tip-dip experiments with a single 90mer dsDNA helix very few transitions were observed. The experiments with netropsin and no DNA suggest that netropsin can disturb lipid bilayers. 200 pS transitions were observed under all conditions and even with a lipid bilayer membrane without any further substance.

Chapter 4

Discussion

4.1 Crystallization Experiments

4.1.1 3D Assembly with TX Tiles Under High Magnesium Ion Concentration

Singly extinguishing crystals were obtained that indicate periodic organization of the samples down to 400 nm. No diffraction was observed when exposed to x-rays. This suggests disorder on a molecular level.

A key observation from this experiment was that much bigger crystals were obtained by a combination of hanging drop and temperature annealing than by hanging drop or temperature decrease alone.

4.1.2 2D-Assembly of DX Molecules with Short Sticky Ends

2D Arrays consisting of DX molecules with short sticky ends were successfully produced when annealed down to 4°C. This proves that four 3mer sticky ends are sufficient to hold the array, as designed, together at lower temper-

atures. Based on this discovery it was assumed that a 3D array that self assembles with four 4mers in 2D and two 3mers in the 3rd dimension should hold together at room temperature, especially if cooperativity is taken into account.

4.1.3 Crystallization Attempt of Blunt Ended DX Tiles

Blunt ended crystals out of DX tiles gave singly extinguishing crystals with the Natrix kit. This indicates a periodic organized matter of the sample down to 400 nm, the lack of diffraction, when exposed to x-rays, suggest disorder on a molecular level. Pamela Constantinou obtained similar results with a crystallization approach of a blunt ended TX motif.

4.1.4 3D Assembly and Gel Studies of ChengdeMao Triangles

Gel Based Studies of Blunt Ended ChengdeMao Triangles

ChengdeMao Triangles with different number of nucleotides per inner triangle edge were examined via nondenaturing gel electrophoresis. These studies showed that triangles with 14, 17 and 18 nt per inner triangle edge have little to no material above the target band (complete single triangle). This fits surprisingly well to the optimal nucleotide number per inner triangle edge as predicted by the calculations of Dr. William Sherman. Numbers of nucleotides per inner triangle edge that do not correspond to these geometrical requirements may put torsional stress on the motif and may yield triangle multimers. All lower bands (below the complete single triangle motifs) are due to incorrect triangle strand stoichiometry.

A system based on ChengdeMao triangles has proved to be quite difficult for

the creation of two dimensional arrays but 2D assembly was finally reported by Prof. Chengde Mao with a triangle system [55].

3D Assembly with ChengdeMao Triangles with 14 nt per inner triangle edge

Singly extinguishing crystals were obtained from system CDM-A and CDM-B. Both showed diffraction when exposed to X-rays down, system CDM-A down to 12 Å and system CDM-B down to 20Å. The collected data were not sufficient to resolve the molecular structure. Especially little conclusion could be drawn about the 3rd dimension. No definite conclusions can be drawn about the assembly but the ingredients of the Natrix kit moderate DNA helix backbone to backbone interactions. Hence an assembly in two directions (2D) via sticky ends and an assembly in the 3rd dimension by stacking might be possible. Pamela Constantinou got diffraction down to 10Å with her ChengdeMao triangle version, based on 17nt per inner triangle edge.

3D Assembly of a ChengdeMao Triangle with One Direction Blunted

System CDM-B_{1BE} gave singly extinguishing crystals that showed diffraction when exposed to x-rays down to 20Å. This is interesting because the system is designed to assemble only in two dimensions. This might be further indication that assembly in the 3rd dimension is not guided by sticky ends. System CDM-B_{1BE} gave singly extinguishing and diffracting crystals in contrast to system CDM-A_{1BE}. In the crystallization attempt of the one-side-blunted CDM triangle motif, the strand in system CDM-B_{1BE} was blunted that corresponds to the side where the nick of the inner triangle DNA resides. It can not be excluded that this played a major role in the successful crystal for-

mation. On the other hand a 3D assembly approach, undertaken by Pamela Constantinou, with a CDM triangle (sticky ends for all three directions, 18nt per inner triangle edge) with an inner strand containing nick symmetry (the strand is cut down to three strands, hence 3 nicks instead of one) showed no different behavior (same diffraction) compared to her original design with only one nick.

Fractal Assembly with ChengdeMao Triangles

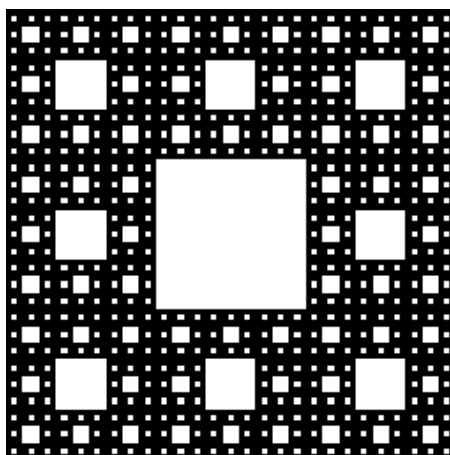


Figure 4.1: Sierpinsky carpet. A 2D fractal derived from a square by cutting it into 9 equal squares with a 3-by-3 grid, removing the central piece and then applying the same procedure ad infinitum to the remaining 8 squares.

DNA fractals¹ were discussed by Erik Winree who used DNA tiles to

¹Fractals are generally irregular (not smooth) in shape, and thus are not objects definable by traditional geometry. That means that fractals tend to have significant detail, visible at any arbitrary scale; when there is self-similarity, this can occur because “zooming in” simply shows similar pictures. Such sets are usually defined instead by recursion. Wikipedia

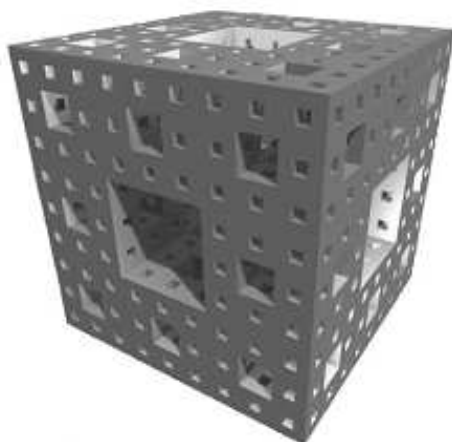


Figure 4.2: The Menger sponge or the Sierpinsky cube fractal[‡] is the 3D version of the Sierpinsky carpet . It may be possible to assemble a version of the sponge out of DNA.

self-assemble the boundary for 2 dimensional Sierpinski triangle [80]. Fractal patterns represent an important class in DNA nanotechnology and prove the ability to assemble complex and aperiodic matter. It was suggested by Carbone and Seeman [10] that the 3 dimensional version of the Sierpinski carpet² (see fig. 4.1), the Menger sponge (see. fig. 4.2) can be assembled out of DNA with the ChengdeMao triangle motif and with aid of protective groups.

²The Sierpinski carpet, named after Waclaw Sierpinski, is a fractal derived from a square by cutting it into 9 equal squares with a 3-by-3 grid, removing the central piece and then applying the same procedure ad infinitum to the remaining 8 squares. From Wikipedia, the free encyclopedia.

4.1.5 3D Assembly with a TXDX Triangle Motif and 0D, 1D and 2D examination of the motif

Gel studies of a TXDX Triangle Motif Blunted Around the Clock (0D)

The non-denaturing examination (0D, see fig. 3.18) of the TXDX triangle shows a clear band for concentrations up to 0.5 μM . A faint upper band can be seen at 1 μM and 2 μM concentrations probably corresponding to a dimer of the motif. For a motif of the size of the TXDX triangle (1260 nt) the behavior of the triangle on the gel is amazingly distinct. The dimer band at the higher concentrations is not unexpected, if considered that 2 μM concentration corresponds to approximately 8 μg (10 μl per well) and that the gel is heavily overloaded.

AFM Examination of 1D and 2D Arrays of the TXDX Triangle Motif

Nice 2D arrays of the TXDX triangle have been produced. Initial difficulties in observing arrays with the AFM can be explained by the different nature of the motif relative to others that have produced 2D arrays observed by AFM. It is a quite huge motif, but relative to its size, very little of the motif hits the mica surface, especially if the skew of the motif is taken into account. The motif minimizes surface (mica) contact and this might explain why adsorption times up to 20 minutes on the mica surface were needed to observe the arrays.

The measured distances are within the predicted length. Some arrays do not seem to have perfect straight lines but it has to be considered that each triangle hits the mica surface with half a floppy DX motif (with the blunted

sticky ends), so it can not be excluded that this might induce some slight disorder in the 2D array. Further the 2D arrays have two possibilities to absorb on the surface. The geometry, as long as sequence independent, should be the same. No differences in the pictures could be observed that would suggest two geometries.

3D Assembly with TXDX Triangles

No crystals were obtained from the TXDX triangles. No ultimate explanation can be given why no crystals could be produced. If the TXDX motif is endowed with sticky ends in a different order, the system is predicted to assemble into hexagonal screw axis. A 3D assembly approach with the modified motif might be undertaken in the future.

4.2 DNA Nanotube as an Artificial Ion Channel

$$R = \frac{l}{\sigma A} \quad (4.1)$$

$$G = \frac{1}{R} \quad (4.2)$$

$$G = \frac{\sigma A}{l} = \frac{\sigma \pi r^2}{l} \quad (4.3)$$

$$G = 100 \frac{mS}{cm} \frac{3.14 \cdot 1 \text{ nm}^2}{30 \text{ nm}} \sim 1 \text{ nS} \quad (4.4)$$

Typical ion channel behaviour could be observed with the 6 helix bundle and netropsin. In a comparison between the 6 helix bundle with and without netropsin no definite conclusions could be drawn, especially if current flow

and less transitions were compared. A noise analysis between current flow through the bilayer membrane (no transitions, variance pA^2 against median frequency Hz) showed no difference. If both systems show similar results concerning current flow (with no transitions) the bundle with netropsin was expected to show less noise due the hydrophobic part of the bundle. This prediction was not observed. The 200 pA transitions that were always observed suggest a contamination of the phospholipid. The disturbance of the bilayer by netropsin alone should not be a big problem because most of it is assumed to bind at the 6 helix bundle in solution. Goudet et al [30] report that a non-peptidal fungal toxin can form ion channel-like structures in presence of magnesium. Fortunately no channel like behaviour was recorded with netropsin alone.

A rough calculation of the expected transition size can be done. We assume the resistance of the ion channel formed by the 6 helix bundle with length of the bundle divided through the conductivity of the solution times the inner area of the bundle (eqn. 4.1). The conductivity is the reciprocal value (eqn. 4.2). Eqn. 4.4 shows the calculation of the expected value (radius 1nm, length 30nm, conductivity of 1M KCl $\sigma = 100 \frac{\text{mS}}{\text{cm}}$) of 1 nS. Transitions around this value were observed and exciting data was collected but it still can not be excluded at this stage that the observed current flow is due to leaks in the lipid bilayer membrane and the transitions are artifacts. On the other hand the recorded transitions (fig. 3.23 and 3.24) have definitive ion channel behaviour. The cationic selective behaviour that was observed is expected due to the anionic backbone of the DNA and might be a further indication that the observed behaviour is caused by the 6 helix bundle.

4.3 Conclusion and Outlook

4.3.1 3D Assembly

I prefer the term 3D assembly to the term crystallization if working with a motif that fills space via sticky end guided assembly. In standard crystallization of macromolecules, molecules are forced out of solution by over saturation and lack of water molecules to assemble into a periodic close packing structure. None of the motifs used so far for sticky ended guided DNA crystallization assembles by design into a close packed structure. The forces that guide conventional crystallization might even fight the forces that are supposed to enable the sticky ended 3D assembly approach.

One of the questions that remain unsolved is the helicity of DNA in such a system. Crystallized B-DNA shows a helicity of 10.0 nt per helical full turn but studies of DNA digestion with enzymes in solution suggest a helicity of 10.5 nt per helical full turn [76, 104]. 3D assembly with sticky ends might reveal which number is more appropriate. Diffraction from crystals were obtained with designs assuming 10.0 nt per helical full turn and 10.5 nt per helical full turn. A final system, diffracting down to high resolution, might suggest a number in between those numbers or might even show that such a system can be created with slightly different helicities.

Major steps in 3D assembly with DNA have been achieved in the last two years. Starting with no motif available that assembles into a crystal that shows any diffraction, crystals with resolutions down to 10 Å are now routinely produced in Prof. Seeman's laboratory. DNA crystals, diffracting down to a few Å seem to be within reach. They could be used to trap biomolecules that are hard to crystallize and might revolutionize the field of macromolecule crystallization. Further, applications in telecommunications

as photonic crystals[113, 112, 43] might be possible.

4.3.2 6 Helix Bundle

Ion Channel

Promising data has been collected in the ion channel experiments that could suggest ion channel behavior. Still, too many unknown factors forbid any final conclusions at this stage. Further experiments are under way and might offer more insight.

Outview to New Motifs based on the 6 Helix Bundle

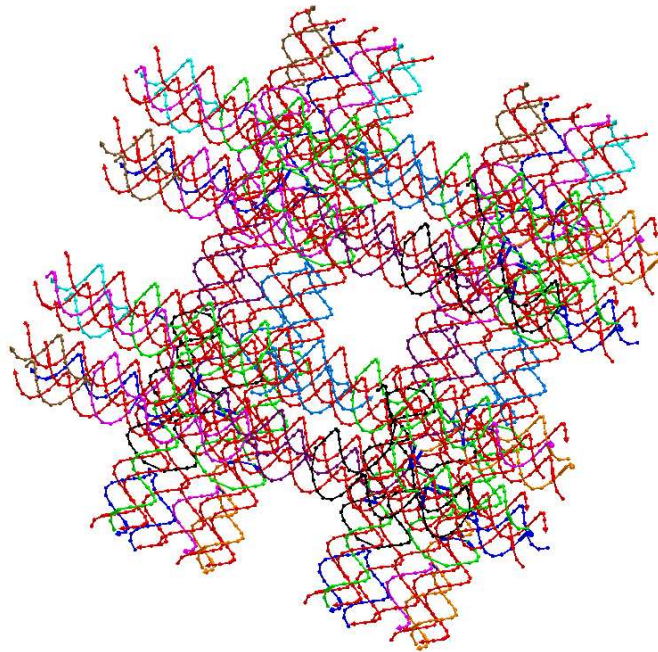


Figure 4.3: A parallelogram consisting of four 6 helix bundles. This might be a promising motif because it may offer the possibility to cross conductor paths on a nanometer scale.

A parallelogram, made out of 6 helix bundles could be used to assemble 2d DNA Arrays and the inner bundle could be filled with a conductor like NanoGoldTM. Concerning the inner diameter of the 6HB it should also be possible to incorporate single walled carbon nanotubes inside the bundle. Due to the geometric properties of a possible 6 helix bundle parallelogram it would be possible to cross conductor paths on a molecular scale.

Chapter 5

Bibliography

Bibliography

- [1] N. G. A. Abrescia, L. Malinina, L. G. Fernandez, T. Huynh-Dinh, S. Neidle, and J. A. Subirana. Structure of the oligonucleotide d(cgtatatacg) as a site-specific complex with nickel ions. *Nucleic Acids Research*, 27(7):1593–1599, 1999. Article.
- [2] L. Adleman, P.W.K. Rothmund, S. Roweis, and E. Winfree. On applying molecular computation to the data encryption. In *DIMACS 2*, 1996.
- [3] L. M. Adleman. Molecular computation of solutions to combinatorial problems. *Science*, 266(5187):1021–1024, 1994.
- [4] S. Arnott and D. W. L. Hukins. Refinement of structure of b-dna and implications for analysis of x-ray-diffraction data from fibers of biopolymers. *Journal of Molecular Biology*, 81(2):93–105, 1973.
- [5] K. Balendiran, S. T. Rao, C. Y. Sekharudu, G. Zon, and M. Sundaralingam. X-ray structures of the b-dna dodecamer d(cgcgttaacgcg) with an inverted central tetranucleotide and its netropsin complex. *Acta Crystallographica Section D-Biological Crystallography*, 51:190–198, 1995. Article Part 2.

-
- [6] E. Biron, N. Voyer, J.C. Meillon, M.E. Cormier, and M. Auger. Conformational and orientation studies of artificial ion channels incorporated into lipid bilayers. *Biopolymers*, 55(7):364–367, 2000. Article.
- [7] T. J. Boggon, E. L. Hancox, K. E. McAuleyHecht, B. A. Connolly, W. N. Hunter, T. Brown, R. T. Walker, and G. A. Leonard. The crystal structure analysis of d(cgcgaasscgcg)(2), a synthetic dna dodecamer duplex containing four 4'-thio-2'-deoxythymidine nucleotides. *Nucleic Acids Research*, 24(5):951–961, 1996. Article.
- [8] T. Brown, W. N. Hunter, G. Kneale, and O. Kennard. Molecular-structure of the g-a base pair in dna and its implications for the mechanism of transversion mutations. *Proceedings of the National Academy of Sciences of the United States of America*, 83(8):2402–2406, 1986. Article.
- [9] T. Brown, G. A. Leonard, E. D. Booth, and J. Chambers. Crystal-structure and stability of a dna duplex containing a(anti).g(syn) base-pairs. *Journal of Molecular Biology*, 207(2):455–457, 1989. Letter.
- [10] A Carbone, CD Mao, PE Constantinou, BQ Ding, J Kopatsch, WB Sherman, and NC Seeman. 3d fractal dna assembly from coding, geometry and protection. *Natural Computing*, 1(4):11–18, 2004. Article.
- [11] F. Cesare-Marincola, G. Saba, and A. Lai. Optical microscopy and multinuclear nmr investigation of the liquid crystalline netropsin-dna complex. *Physical Chemistry Chemical Physics*, 5(8):1678–1681, 2003. Article.

-
- [12] T. Chatake, T. Hikima, A. Ono, Y. Ueno, A. Matsuda, and A. Takenaka. Crystallographic studies on damaged dnas. ii. n-6-methoxyadenine can present two alternate faces for watson-crick base-pairing, leading to pyrimidine transition mutagenesis. *Journal of Molecular Biology*, 294(5):1223–1230, 1999. Article.
- [13] W.H. Chen, M. Nishikawa, S.D. Tan, M. Yamamura, A. Satake, and Y. Kobuke. Tetracyanoresorcin[4]arene ion channel shows ph dependent conductivity change. *Chem. Commun.*, 5(7):872–873, 2004. Article.
- [14] Gan-Moog Chow, Kenneth E. Gonsalves, American Chemical Society. Division of Polymeric Materials: Science, Engineering., and American Chemical Society. Meeting. *Nanotechnology : molecularly designed materials*. ACS symposium series, 622. American Chemical Society, Washington, DC, 1996. Gan-Moog Chow, editor, Kenneth E. Gonsalves, editor. ill. ; 23 cm. "Developed from a symposium sponsored by the Division of Polymeric Materials: Science and Engineering at the 210th National Meeting of the American Chemical Society, Chicago, Illinois, August 20-24, 1995."
- [15] S. N. Cohen, A. C. Y. Chang, H. W. Boyer, and R. B. Helling. Construction of biologically functional bacterial plasmids in-vitro. *Proceedings of the National Academy of Sciences of the United States of America*, 70(11):3240–3244, 1973.
- [16] P. W. R. Corfield, W. N. Hunter, T. Brown, P. Robinson, and O. Kenward. Inosine.adenine base-pairs in a b-dna duplex. *Nucleic Acids Research*, 15(19):7935–7949, 1987. Article.

-
- [17] B. C. Crandall. *Nanotechnology : molecular speculations on global abundance*. MIT Press, Cambridge, Mass., 1996. edited by B.C. Crandall. ill. (some col.) ; 24 cm.
- [18] A. D. Digabriele and T. A. Steitz. A dna dodecamer containing an adenine tract crystallizes in a unique lattice and exhibits a new bend. *Journal of Molecular Biology*, 231(4):1024–1039, 1993. Article.
- [19] K. J. Edwards, D. G. Brown, N. Spink, J. V. Skelly, and S. Neidle. Molecular-structure of the b-dna dodecamer d(cgcaaatttgcg)(2) - an examination of propeller twist and minor-groove water-structure at 2.2-angstrom resolution. *Journal of Molecular Biology*, 226(4):1161–1173, 1992. Article.
- [20] B. F. Eichman, J. M. Vargason, B. H. M. Mooers, and P. S. Ho. The holliday junction in an inverted repeat dna sequence: Sequence effects on the structure of four-way junctions. *Proceedings of the National Academy of Sciences of the United States of America*, 97(8):3971–3976, 2000. Article.
- [21] D. M. Eigler and E. K. Schweizer. Positioning single atoms with a scanning tunneling microscope. *Nature*, 344(6266):524–526, 1990.
- [22] M. Eriksson and P. E. Nielsen. Solution structure of a peptide nucleic acid dna duplex. *Nature Structural Biology*, 3(5):410–413, 1996. Letter MAY.
- [23] D. Fiorani and G. Sberveglieri. *Fundamental properties of nanostructured materials : [proceedings of the] National School of the Condensed Matter Group, Rimini, Italy, September 20-25, 1993*. World Scientific, Singapore ; River Edge, NJ, 1994. National School of the Condensed

- Matter Group (1993 : Rimini, Italy) editors: D. Fiorani, G. Sberveglieri. ill. ; 23 cm.
- [24] O. Flomenbom and J. Klafter. Single stranded dna translocation through a nanopore: A master equation approach. *Physical Review E*, 68(4), 2003. Part 1.
- [25] J. K. Gimzewski, C. Joachim, R. R. Schlittler, V. Langlais, H. Tang, and I. Johannsen. Rotation of a single molecule within a supramolecular bearing. *Science*, 281(5376):531–533, 1998.
- [26] S. L. Ginell, J. Vojtechovsky, B. Gaffney, R. Jones, and H. M. Berman. Crystal-structure of a mispaired dodecamer, d(cgagaattc(o(6)me)gcg)2, containing a carcinogenic o(6)-methylguanine. *Biochemistry*, 33(12):3487–3493, 1994. Article.
- [27] D. S. Goodsell, K. Grzeskowiak, and R. E. Dickerson. Crystal-structure of c-t-c-t-c-g-a-g-a-g - implications for the structure of the holliday junction. *Biochemistry*, 34(3):1022–1029, 1995. Article.
- [28] D. S. Goodsell, M. Kaczorgrzeskowiak, and R. E. Dickerson. The crystal-structure of c-c-a-t-t-a-a-t-g-g - implications for bending of b-dna at t-a steps. *Journal of Molecular Biology*, 239(1):79–96, 1994. Article.
- [29] D. S. Goodsell, M. L. Kopka, D. Cascio, and R. E. Dickerson. Crystal-structure of catggccatg and its implications for a-tract bending models. *Proceedings of the National Academy of Sciences of the United States of America*, 90(7):2930–2934, 1993. Article.
- [30] C. Goudet, A. A. Very, M. L. Milat, M. Ildefonse, J. B. Thibaud, H. Sentenac, and J. P. Blein. Magnesium ions promote assembly of

- channel-like structures from beticolin 0, a non-peptide fungal toxin purified from cercospora beticola. *Plant Journal*, 14(3):359–364, 1998.
- [31] B. Grunbaum and G. C. Shephard. Perfect colorings of transitive tilings and patterns in plane. *Discrete Mathematics*, 20(3):235–247, 1977. Article.
- [32] K. Grzeskowiak, D. S. Goodsell, M. Kaczorgrzeskowiak, D. Cascio, and R. E. Dickerson. Crystallographic analysis of c-c-a-a-g-c-t-t-g-g and its implications for bending in b-dna. *Biochemistry*, 32(34):8923–8931, 1993. Article.
- [33] O. P. Hamill, A. Marty, E. Neher, B. Sakmann, and F. J. Sigworth. Improved patch-clamp techniques for high-resolution current recording from cells and cell-free membrane patches. *Pflugers Archiv-European Journal of Physiology*, 391(2):85–100, 1981. Article.
- [34] U. Heinemann, C. Alings, and M. Bansal. Double helix conformation, groove dimensions and ligand-binding potential of a g/c stretch in b-dna. *Embo Journal*, 11(5):1931–1939, 1992. Article.
- [35] U. Heinemann and M. Hahn. C-c-a-g-g-c-m5c-t-g-g - helical fine-structure, hydration, and comparison with c-c-a-g-g-c-c-t-g-g. *Journal of Biological Chemistry*, 267(11):7332–7341, 1992. Article.
- [36] B. Hille. *Ion Channels of Excitable Membranes*. Sinauer Associates, New York, 2001.
- [37] P. S. Ho and B. F. Eichman. The crystal structures of dna holliday junctions. *Current Opinion in Structural Biology*, 11(3):302–308, 2001. Article.

-
- [38] R. Holiday. A mechanism for gene conversion in fungi. *Genet. Res.*, 5:282–304, 1964.
- [39] Editor Denis Howe. The free online dictionar of computing.
- [40] S. B. Howerton, C. C. Sines, D. VanDerveer, and L. D. Williams. Locating monovalent cations in the grooves of b-dna. *Biochemistry*, 40(34):10023–10031, 2001. Article.
- [41] W. N. Hunter, T. Brown, G. Kneale, N. N. Anand, D. Rabinovich, and O. Kennard. The structure of guanosine-thymidine mismatches in b-dna at 2.5- \AA resolution. *Journal of Biological Chemistry*, 262(21):9962–9970, 1987. Article.
- [42] J. A. Ippolito and T. A. Steitz. The structure of the hiv-1 rre high affinity rev binding site at 1.6 angstrom resolution. *Journal of Molecular Biology*, 295(4):711–717, 2000. Article.
- [43] S. John. Strong localization of photons in certain disordered dielectric superlattices. *PHYSICAL REVIEW LETTERS*, 58(23):2486–2489, 1987. Article.
- [44] C. L. Kielkopf, S. Ding, P. Kuhn, and D. C. Rees. Conformational flexibility of b-dna at 0.74 angstrom resolution: d(ccagtactgg)(2). *Journal of Molecular Biology*, 296(3):787–801, 2000. Article.
- [45] T. H. LaBean, H. Yan, J. Kopatsch, F. R. Liu, E. Winfree, J. H. Reif, and N. C. Seeman. Construction, analysis, ligation, and self-assembly of dna triple crossover complexes. *Journal of the American Chemical Society*, 122(9):1848–1860, 2000.

-
- [46] T. A. Larsen, M. L. Kopka, and R. E. Dickerson. Crystal-structure analysis of the b-dna dodecamer cgtgaattcacg. *Biochemistry*, 30(18):4443–4449, 1991. Article.
- [47] G. A. Leonard, A. Guy, T. Brown, R. Teoule, and W. N. Hunter. Conformation of guanine.8-oxoadenine base-pairs in the crystal-structure of d(cgcgaatt(o8a)gcg). *Biochemistry*, 31(36):8415–8420, 1992. Article.
- [48] G. A. Leonard and W. N. Hunter. Crystal and molecular-structure of d(cgtagatctacg) at 2-center-dot-25-angstrom resolution. *Journal of Molecular Biology*, 234(1):198–208, 1993. Article.
- [49] G. A. Leonard, K. E. McAuleyhecht, N. J. Gibson, T. Brown, W. P. Watson, and W. N. Hunter. Guanine-1,n-6-ethenoadenine base-pairs in the crystal-structure of d(cgcgaatt(epsilon-da)gcg). *Biochemistry*, 33(16):4755–4761, 1994. Article.
- [50] G. A. Leonard, J. Thomson, W. P. Watson, and T. Brown. High-resolution structure of a mutagenic lesion in dna. *Proceedings of the National Academy of Sciences of the United States of America*, 87(24):9573–9576, 1990. Article.
- [51] X. Li, X. Yang, K. Qi, and N.C. Seeman. Antiparallel dna double crossover molecules as components for nanoconstruction. *J. Am. Chem. Soc.*, 33 ? :6131–6140, 1996.
- [52] D. M. J. Lilley and D. G. Norman. The holliday junction is finally seen with crystal clarity. *Nature Structural Biology*, 6(10):897–899, 1999. Article.
- [53] L. A. Lipscomb, M. E. Peek, M. L. Morningstar, S. M. Verghis, E. M. Miller, A. Rich, J. M. Essigmann, and L. D. Williams. X-ray structure

- of a dna decamer containing 7,8-dihydro-8-oxoguanine. *Proceedings of the National Academy of Sciences of the United States of America*, 92(3):719–723, 1995. Article.
- [54] B. Liu, N. B. Leontis, and N. C. Seeman. Bulged 3-arm dna branched junctions as components for nanoconstruction. *Nanobiology*, 3(3-4):177–188, 1994.
- [55] D. Liu, M. S. Wang, Z. X. Deng, R. Walulu, and C. D. Mao. Tensegrity: Construction of rigid dna triangles with flexible four-arm dna junctions. *Journal of the American Chemical Society*, 126(8):2324–2325, 2004. Article MAR 3.
- [56] R. I. Ma, N. R. Kallenbach, R. D. Sheardy, M. L. Petrillo, and N. C. Seeman. 3-arm nucleic-acid junctions are flexible. *Nucleic Acids Research*, 14(24):9745–9753, 1986.
- [57] R.I. Ma, N.R. Kallenbach, R.D. Sheardy, and N.C. Seeman. 3-arm nucleic acid junctions are flexible. *Nucleic Acids Research*, 1986.
- [58] C. D. Mao, W. Q. Sun, and N. C. Seeman. Assembly of borromean rings from dna. *Nature*, 386(6621):137–138, 1997.
- [59] C. D. Mao, W. Q. Sun, Z. Y. Shen, and N. C. Seeman. A nanomechanical device based on the b-z transition of dna. *Nature*, 397(6715):144–146, 1999.
- [60] D. A. Marvin, L. D. Hamilton, M. Spencer, and M. H. F. Wilkins. Molecular configuration of deoxyribonucleic acid .3. x-ray diffraction study of c form of lithium salt. *Journal of Molecular Biology*, 3(5):547–565, 1961. Article.

-
- [61] D. A. Marvin, M. Spencer, M. H. F. Wilkins, and L. D. Hamilton. New configuration of deoxyribonucleic acid. *Nature*, 182(4632):387–388, 1958. Article.
- [62] F. Mathieu, CD Mao, and NC Seeman. A dna nanotube based on a six-helix bundle motif. *Journal of Biomolecular Structure and Dynamics*, 19(3):988, 2001. Abstract.
- [63] K. E. McAuleyhecht, G. A. Leonard, N. J. Gibson, J. B. Thomson, W. P. Watson, W. N. Hunter, and T. Brown. Crystal-structure of a dna duplex containing 8-hydroxydeoxyguanine-adenine base-pairs. *Biochemistry*, 33(34):10266–10270, 1994. Article.
- [64] Alexander McPherson. *Crystallization of biological macromolecules*. Cold Spring Harbor Laboratory Press, Cold Spring Harbor, NY, 1999. lc98026897 A. McPherson.
- [65] G. Minasov, V. Tereshko, and M. Egli. Atomic-resolution crystal structures of b-dna reveal specific influences of divalent metal ions on conformation and packing. *Journal of Molecular Biology*, 291(1):83–99, 1999. Article.
- [66] E. Neher and B. Sakmann. Single channel currents recorded from membrane of denervated frog muscle fibers. *Nature*, 260(4):799–802, 1976. Article.
- [67] H. C. M. Nelson, J. T. Finch, B. F. Luisi, and A. Klug. The structure of an oligo(da).oligo(dt) tract and its biological implications. *Nature*, 330(6145):221–226, 1987. Article.
- [68] Claudio A. Nicolini and Sergei Vakula. *Molecular manufacturing*. Plenum Press, New York, 1996. edited by Claudio Nicolini ; assis-

- tant editor, Sergei Vakula. ill. ; 26 cm. "Proceedings of the 1994 International Workshops on Electronics and Biotechnology Advanced, held March 10-12, 1994, and September 5-15, 1994, on the Isle of Elba, Italy"—T.p. verso. International Workshops on Electronics and Biotechnology Advanced (1994 : Isle of Elba, Italy).
- [69] J. Nowakowski, P. J. Shim, C. D. Stout, and G. F. Joyce. Alternative conformations of a nucleic acid four-way junction. *Journal of Molecular Biology*, 300(1):93–102, 2000. Article.
- [70] M. Ortiz-Lombardia, A. Gonzalez, R. Eritja, J. Aymami, F. Azorin, and M. Coll. Crystal structure of a dna holliday junction. *Nature Structural Biology*, 6(10):913–917, 1999. Article.
- [71] M. L. Petrillo, C. J. Newton, R. P. Cunningham, R. I. Ma, N. R. Kallenbach, and N. C. Seeman. The ligation and flexibility of 4-arm dna junctions. *Biopolymers*, 27(9):1337–1352, 1988.
- [72] N. Peyret, P. A. Seneviratne, H. T. Allawi, and J. SantaLucia. Nearest-neighbor thermodynamics and nmr of dna sequences with internal a center dot a, c center dot c, g center dot g, and t center dot t mismatches. *Biochemistry*, 38(12):3468–3477, 1999. Article MAR 23.
- [73] G. G. Prive, K. Yanagi, and R. E. Dickerson. Structure of the b-dna decamer c-c-a-a-c-g-t-t-g-g and comparison with isomorphous decamers c-c-a-a-g-a-t-t-g-g and c-c-a-g-g-c-c-t-g-g. *Journal of Molecular Biology*, 217(1):177–199, 1991. Article.
- [74] B. Ramakrishnan and M. Sundaralingam. Evidence for crystal environment dominating base sequence effects on dna conformation - crystal-structures of the orthorhombic and hexagonal polymorphs of the a-dna

- decamer d(gcgggcccgc) and comparison with their isomorphous crystal-structures. *Biochemistry*, 32(42):11458–11468, 1993. Article.
- [75] B. Ramakrishnan and M. Sundaralingam. High-resolution crystal-structure of the a-dna decamer d(cccggccggg) - novel intermolecular base-paired g-asterisk(g.c) triplets. *Journal of Molecular Biology*, 231(2):431–444, 1993. Article.
- [76] D. Rhodes and A. Klug. Helical periodicity of dna determined by enzyme digestion. *Nature*, 286(5773):573–578, 1980. Article.
- [77] A. Rich, A. Nordheim, and A. H. J. Wang. The chemistry and biology of left-handed z-dna. *Annual Review of Biochemistry*, 53:791–846, 1984. Review.
- [78] P.W.K. Rothmund, S. Roweis, and E. Winfree. An algorithm for breaking des is designed for the stickers model. size, space, and error rates of the resulting machine are considered. In *Proceedings of the 2nd DIMACS Meeting on DNA based Computers* DIMACS. American Mathematical Society, 1996.
- [79] J. SantaLucia. A unified view of polymer, dumbbell, and oligonucleotide dna nearest-neighbor thermodynamics. *Proceedings of the National Academy of Sciences of the United States of America*, 95(4):1460–1465, 1998. Article FEB 17.
- [80] R Schulman, S Lee, N Papadakis, and E Winfree. One dimensional boundaries for dna tile self-assembly. *DNA Computers*, 2943(9):108–125, 2004. Article.
- [81] W. G. Scott, J. T. Finch, R. Grenfell, J. Fogg, T. Smith, M. J. Gait, and A. Klug. Rapid crystallization of chemically synthesized hammerhead

- rnas using a double screening-procedure. *Journal of Molecular Biology*, 250(3):327–332, 1995. Article JUL 14.
- [82] N. C. Seeman. Denovo design of sequences for nucleic-acid structural-engineering. *Journal of Biomolecular Structure and Dynamics*, 8(3):573–581, 1990.
- [83] N. C. Seeman. Construction of 3-dimensional stick figures from branched dna. *DNA and Cell Biology*, 10(7):475–486, 1991.
- [84] N. C. Seeman and N. R. Kallenbach. Design of immobile nucleic-acid junctions. *Biophysical Journal*, 44(2):201–209, 1983.
- [85] N. C. Seeman, C. D. Mao, T. LaBean, and J. H. Reif. Xor operations by algorithmic assembly of dna tiles. *Biophysical Journal*, 80(1):10A–10A, 2001. Part 2.
- [86] N. C. Seeman, C. D. Mao, and W. Q. Sun. Dna borromean rings. *Mathematical Intelligencer*, 20(3):3–3, 1998.
- [87] X. Q. Shui, L. McFail-Isom, G. G. Hu, and L. D. Williams. The b-dna dodecamer at high resolution reveals a spine of water on sodium. *Biochemistry*, 37(23):8341–8355, 1998. Article.
- [88] X. Q. Shui, C. C. Sines, L. McFail-Isom, D. VanDerveer, and L. D. Williams. Structure of the potassium form of cgcgaattcgcg: Dna deformation by electrostatic collapse around inorganic cations. *Biochemistry*, 37(48):16877–16887, 1998. Article.
- [89] C. C. Sines, L. McFail-Isom, S. B. Howerton, D. VanDerveer, and L. D. Williams. Cations mediate b-dna conformational heterogeneity. *Jour-*

- nal of the American Chemical Society*, 122(45):11048–11056, 2000. Article.
- [90] S.J. Singer and G.L. Nicolson. Fluid mosaic model of structure of cell membranes. *Science*, 175(4023):720–724, 1972. Article.
- [91] J. V. Skelly, K. J. Edwards, T. C. Jenkins, and S. Neidle. Crystal-structure of an oligonucleotide duplex containing g.g base-pairs - influence of mispairing on dna backbone conformation. *Proceedings of the National Academy of Sciences of the United States of America*, 90(3):804–808, 1993. Article.
- [92] T. G. Smith. *Voltage and patch clamping with microelectrodes*. American Physiological Society ; Distributed for the American Physiological Society by the Williams and Wilkins Co., Bethesda, Md. Baltimore, Md., 1985. 84018550 editors, Thomas G. Smith, Jr. ... [et al.] Includes bibliographical references and index. Patch clamping with microelectrodes.
- [93] N. Spink, C. M. Nunn, J. Vojtechovsky, H. M. Berman, and S. Neidle. Crystal-structure of a dna decamer showing a novel pseudo 4-way helix-helix junction. *Proceedings of the National Academy of Sciences of the United States of America*, 92(23):10767–10771, 1995. Article.
- [94] M. Sriram, G. A. Vandermarel, Hlpf Roelen, J. H. Vanboom, and A. H. J. Wang. Conformation of b-dna containing o6-ethyl-g-c base-pairs stabilized by minor groove binding-drugs - molecular-structure of d(cgc e6g aattcgcg complexed with hoechst-33258 or hoechst-33342. *Embo Journal*, 11(1):225–232, 1992. Article.

-
- [95] V. Tereshko, G. Minasov, and M. Egli. The dickerson-drew b-dna dodecamer revisited at atomic resolution (vol 121, pg 470, 1999). *Journal of the American Chemical Society*, 121(29):6970–6970, 1999. Correction.
- [96] B.J. Thompson, M.N. Camien, and R.C. Warner Camien. Kinetics of branch migration in double stranded dna. *Proc. Natl Acad. Sci.*, 73:2299–2303, 1976.
- [97] J. H. Thorpe, S. C. M. Teixeira, B. C. Gale, and C. J. Cardin. Structural characterization of a new crystal form of the four-way holliday junction formed by the dna sequence d(ccggtaccgg)(2): sequence versus lattice? *Acta Crystallographica Section D-Biological Crystallography*, 58:567–569, 2002. Article Part 3.
- [98] Y. Timsit, E. Vilbois, and D. Moras. Base-pairing shift in the major groove of (ca)n tracts by b-dna crystal-structures. *Nature*, 354(6349):167–170, 1991. Article.
- [99] J. M. Vargason and P. S. Ho. The effect of cytosine methylation on the structure and geometry of the holliday junction - the structure of d(ccggtacm(5)cgg) at 1.5 angstrom resolution. *Journal of Biological Chemistry*, 277(23):21041–21049, 2002. Article.
- [100] Donald Voet and Judith G. Voet. *Biochemistry*. Wiley, New York, 1990. 89-16727 Donald Voet, Judith G. Voet ; illustrators, Irving Geis, John and Bette Woolsey. Includes bibliographical references and and index.
- [101] N Voyer, L Potvin, and E Rousseau. Electrical activity of artificial ion channels incorporated into planar lipid bilayers. *J. Chem. Soc.-Perkin Trans. 2*, 10(9):1469–1471, 1997. Article.

-
- [102] N. Voyer and M Robitaille. Novel functional artificial ion channel. *J. Am. Chem. Soc.*, 117(24):6599–6600, 1995. Article.
- [103] P.M.B. Walker, editor. *Dictionary of Science and Technology*. W and R Cambers Ltd and Cambridge University Press, 1988.
- [104] J. C. Wang. Helical repeat of dna in solution. *Proceedings of the National Academy of Sciences of the United States of America*, 76(1):200–203, 1979. Article.
- [105] Y. Wang, J.E. Mueller, B. Kemper, and N.C. Seeman. The assembly and characterization of 5-arm and 6-arm dna junctions. *Biochemistry*, 30:5667–5674, 1991.
- [106] Y. Wang and D. J. Patel. Solution structure of a parallel-stranded g-quadruplex dna. *Journal of Molecular Biology*, 234(4):1171–1183, 1993. Article DEC 20.
- [107] E. Winfree. On the computational power of dna annealing and ligation. in dna based computing. In *Proceedings of the 1st DIMACS Meeting on DNA based Computers*, pages 199–219. Am. Math. Soc., 1995.
- [108] E. Winfree, F. R. Liu, L. A. Wenzler, and N. C. Seeman. Design and self-assembly of two-dimensional dna crystals. *Nature*, 394(6693):539–544, 1998.
- [109] E. Winfree, X. Yang, and N.C. Seeman. Universal computation via self-assembly of dna. In *Proceedings of the 2nd DIMACS Meeting on DNA based Computers*. American Mathematical Society, 1996.
- [110] A. A. Wood, C. M. Nunn, J. O. Trent, and S. Neidle. Sequence-dependent crossed helix packing in the crystal structure of a b-dna

- decamer yields a detailed model for the holliday junction. *Journal of Molecular Biology*, 269(5):827–841, 1997. Article.
- [111] J. C. Xuan and I. T. Weber. Crystal-structure of a b-dna dodecamer containing inosine, d(cgciaattcgcg), at 2.4 a resolution and its comparison with other b-dna dodecamers. *Nucleic Acids Research*, 20(20):5457–5464, 1992. Article.
- [112] E. Yablonovitch. Photonic crystals. *Journal of Modern Optics*, 41(2):173–194, 1984. Article.
- [113] E. Yablonovitch, TJ Gmitter, and R Bhat. Inhibited and enhanced spontaneous emission from optically thin algaas gaas double heterostructures. *PHYSICAL REVIEW LETTERS*, 61(22):2546–2549, 1988. Article.
- [114] H. Yan, S. H. Park, G. Finkelstein, J. H. Reif, and T. H. LaBean. Dna-templated self-assembly of protein arrays and highly conductive nanowires. *Science*, 301(5641):1882–1884, 2003. Article SEP 26.
- [115] B. Yurke, A.J. Tuberfield, AP Mills, F.C. Simmel, and J.L. Neumann. A dna fuelled molecular machine made of dna. *Nature*, 406:605–608, 2000.
- [116] Y. W. Zhang and N. C. Seeman. Construction of a dna-truncated octahedron. *Journal of the American Chemical Society*, 116(5):1661–1669, 1994.

Chapter 6

Appendix

6.1 Gel for XOR Operation

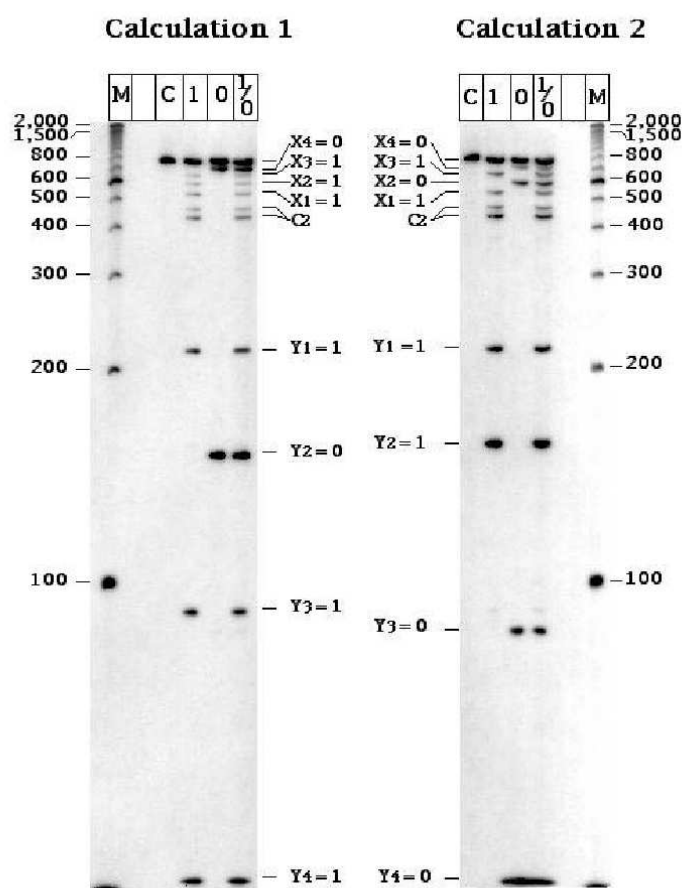


Figure 6.1: XOR calculation with DNA[†].

6.2 Length Marker for Gel Based Studies

DNA Length Markers

Table 6.1: pBR *Hae*III digested marker fragment sizes

Upper Half	Lower Half
587	123
540	104
504	89
458	80
434	64
267	57
234	51
213	21
192	18
184	11
124	8

6.3 Natrix Formulation from Hampton Research

Table 6.2: Natrix Buffer Compositions

Number	Conc.	Unit	Substance
1	0.01	M	magnesium chloride hexahydrate
	0.05	M	MES pH 5.6
	2	M	lithium sulfate monohydrate
2	0.01	M	magnesium acetate tetrahydrate
	0.05	M	MES pH 5.6
	2.5	M	ammonium sulfate
3	0.10	M	magnesium acetate tetrahydrate
	0.05	M	MES pH 5.6
	20	%v/v	MPD
4	0.2	M	potassium chloride
	0.01	M	magnesium sulfate
	0.05	M	MES pH 5.6
	10	%v/v	polyethylene glycol 400
5	0.2	M	potassium chloride
	0.01	M	magnesium chloride hexahydrate
	0.05	M	MES pH 5.6
	5	%w/v	polyethylene glycol 8000
6	0.1	M	ammonium sulfate
	0.01	M	magnesium chloride hexahydrate
	0.05	M	MES pH 5.6

Continued on next page

Table 6.2 – continued from previous page

Number	Conc.	Unit	Substance
	20	%w/v	polyethylene glycol 8000
7	0.02	M	magnesium chloride hexahydrate
	0.05	M	MES pH 6.0
	15	%v/v	iso-propanol
8	0.1	M	ammonium acetate
	0.005	M	magnesium sulfate
	0.05	M	MES pH 6.0
	0.6	M	sodium chloride
9	0.1	M	potassium chloride
	0.01	M	magnesium chloride hexahydrate
	0.05	M	MES pH 6.0
	10	%v/v	polyethylene glycol 400
10	0.005	M	magnesium sulfate
	0.05	M	MES pH 6.0
	5	%w/v	polyethylene glycol 4000
11	0.01	M	magnesium chloride hexahydrate
	0.05	M	sodium cacodylate pH 6.0
	1	M	lithium sulfate monohydrate
12	0.01	M	magnesium sulfate
	0.05	M	sodium cacodylate pH 6.0
	1.8	M	lithium sulfate monohydrate
13	0.015	M	magnesium acetate tetrahydrate
	0.05	M	sodium cacodylate pH 6.0

Continued on next page

Table 6.2 – continued from previous page

Number	Conc.	Unit	Substance
	1.7	M	ammonium sulfate
14	0.1	M	potassium chloride
	0.025	M	magnesium chloride hexahydrate
	0.05	M	sodium cacodylate pH 6.0
	15	%v/v	iso-propanol
15	0.04	M	magnesium chloride hexahydrate
	0.05	M	sodium cacodylate pH 6.0
	5	%v/v	MPD
16	0.04	M	magnesium acetate tetrahydrate
	0.05	M	sodium cacodylate pH 6.0
	30	%v/v	MPD
17	0.2	M	potassium chloride
	0.01	M	calcium chloride dihydrate
	0.05	M	sodium cacodylate pH 6.0
	10	%w/v	polyethylene glycol 4000
18	0.01	M	magnesium acetate tetrahydrate
	0.05	M	sodium cacodylate pH 6.5
	1.3	M	lithium sulfate monohydrate
19	0.01	M	magnesium sulfate
	0.05	M	sodium cacodylate pH 6.5
	2	M	ammonium sulfate
20	0.1	M	ammonium acetate
	0.015	M	magnesium acetate tetrahydrate
	0.05	M	sodium cacodylate pH 6.5

Continued on next page

Table 6.2 – continued from previous page

Number	Conc.	Unit	Substance
	10	%v/v	iso-propanol
21	0.2	M	potassium chloride
	0.005	M	magnesium chloride hexahydrate
	0.05	M	sodium cacodylate pH 6.5
	10	%v/v	iso-propanol
22	0.08	M	magnesium acetate tetrahydrate
	0.05	M	sodium cacodylate pH 6.5
	15	%v/v	polyethylene glycol 400
23	0.2	M	potassium chloride
	0.01	M	magnesium chloride hexahydrate
	0.05	M	sodium cacodylate pH 6.5
	10	%w/v	polyethylene glycol 4000
24	0.2	M	ammonium acetate
	0.01	M	calcium chloride dihydrate
	0.05	M	sodium cacodylate pH 6.5
	10	%w/v	polyethylene glycol 4000
25	0.08	M	magnesium acetate tetrahydrate
	0.05	M	sodium cacodylate pH 6.5
	30	%w/v	polyethylene glycol 4000
26	0.2	M	potassium chloride
	0.1	M	magnesium acetate tetrahydrate
	0.05	M	sodium cacodylate pH 6.5
	10	%w/v	polyethylene glycol 8000
27	0.2	M	ammonium acetate

Continued on next page

Table 6.2 – continued from previous page

Number	Conc.	Unit	Substance
	0.01	M	magnesium acetate tetrahydrate
	0.05	M	sodium cacodylate pH 6.5
	30	%w/v	polyethylene glycol 8000
28	0.05	M	magnesium sulfate aq.
	0.05	M	HEPES-Na pH 7.0
	1.6	M	lithium sulfate monohydrate
29	0.01	M	magnesium chloride hexahydrate
	0.05	M	HEPES-Na pH 7.0
	4	M	lithium chloride
30	0.01	M	magnesium chloride hexahydrate
	0.05	M	HEPES-Na
	1.6	M	ammonium sulfate
31	0.005	M	magnesium chloride hexahydrate
	0.05	M	HEPES-Na pH 7.0
	25	%v/v	polyethylene glycol monomethyl ether 550
32	0.2	M	potassium chloride
	0.01	M	magnesium chloride hexahydrate
	0.05	M	HEPES-Na pH 7.0
	20%	%w/v	1,6-hexanediol
33	0.2	M	ammonium chloride
	0.01	M	magnesium chloride hexahydrate
	0.05	M	HEPES-Na pH 7.0
	30%	%w/v	1,6-hexanediol
34	0.1	M	potassium chloride

Continued on next page

Table 6.2 – continued from previous page

Number	Conc.	Unit	Substance
	0.005	M	magnesium sulfate aq.
	0.05	M	HEPES-Na pH 7.0
	15	%v/v	MPD
35	0.1	M	potassium chloride
	0.01	M	magnesium chloride hexahydrate
	0.05	M	HEPES-Na pH 7.0
	5	%v/v	polyethylene glycol 400
36	0.1	M	potassium chloride
	0.01	M	calcium chloride dihydrate
	0.05	M	HEPES-Na pH 7.0
	10	%v/v	polyethylene glycol 400
37	0.2	M	potassium chloride
	0.025	M	magnesium sulfate aq.
	0.05	M	HEPES-Na pH 7.0
	20	%v/v	polyethylene glycol 200
38	0.2	M	ammonium acetate
	0.15	M	magnesium acetate tetrahydrate
	0.05	M	HEPES-Na pH 7.0
	5	%w/v	polyethylene glycol 4000
39	0.1	M	ammonium acetate
	0.02	M	magnesium chloride hexahydrate
	0.05	M	HEPES-Na pH 7.0
	5	%w/v	polyethylene glycol 8000
40	0.01	M	magnesium chloride hexahydrate

Continued on next page

Table 6.2 – continued from previous page

Number	Conc.	Unit	Substance
	0.05	M	tris hydrochloride pH 7.5
	1.6	M	ammonium sulfate
41	0.1	M	potassium chloride
	0.015	M	magnesium chloride hexahydrate
	0.05	M	tris hydrochloride pH 7.5
	10	%v/v	polyethylene glycol monomethyl ether 550
42	0.01	M	magnesium acetate tetrahydrate
	0.05	M	tris hydrochloride pH 7.5
	5	%v/v	iso-propanol
43	0.05	M	ammonium acetate
	0.01	M	magnesium chloride hexahydrate
	0.05	M	tris hydrochloride pH 7.5
	10	%v/v	MPD
44	0.2	M	potassium chloride
	0.05	M	magnesium chloride hexahydrate
	0.05	M	tris hydrochloride pH 7.5
	10	%w/v	polyethylene glycol 4000
45	0.025	M	magnesium sulfate aq.
	0.05	M	tris hydrochloride pH 8.5
	1.8	M	ammonium sulfate
46	0.005	M	magnesium sulfate aq.
	0.05	M	tris hydrochloride pH 8.5
	35	%w/v	1,6-hexanediol

Continued on next page

Table 6.2 – continued from previous page

Number	Conc.	Unit	Substance
47	0.1	M	potassium chloride
	0.01	M	magnesium chloride hexahydrate
	0.05	M	tris hydrochloride pH 8.5
	30	%v/v	polyethylene glycol 400
48	0.2	M	ammonium chloride
	0.01	M	calcium chloride dihydrate
	0.05	M	tris hydrochloride pH 8.5
	30	%w/v	polyethylene glycol 4000

6.4 Crystall Mounting in Capillaries

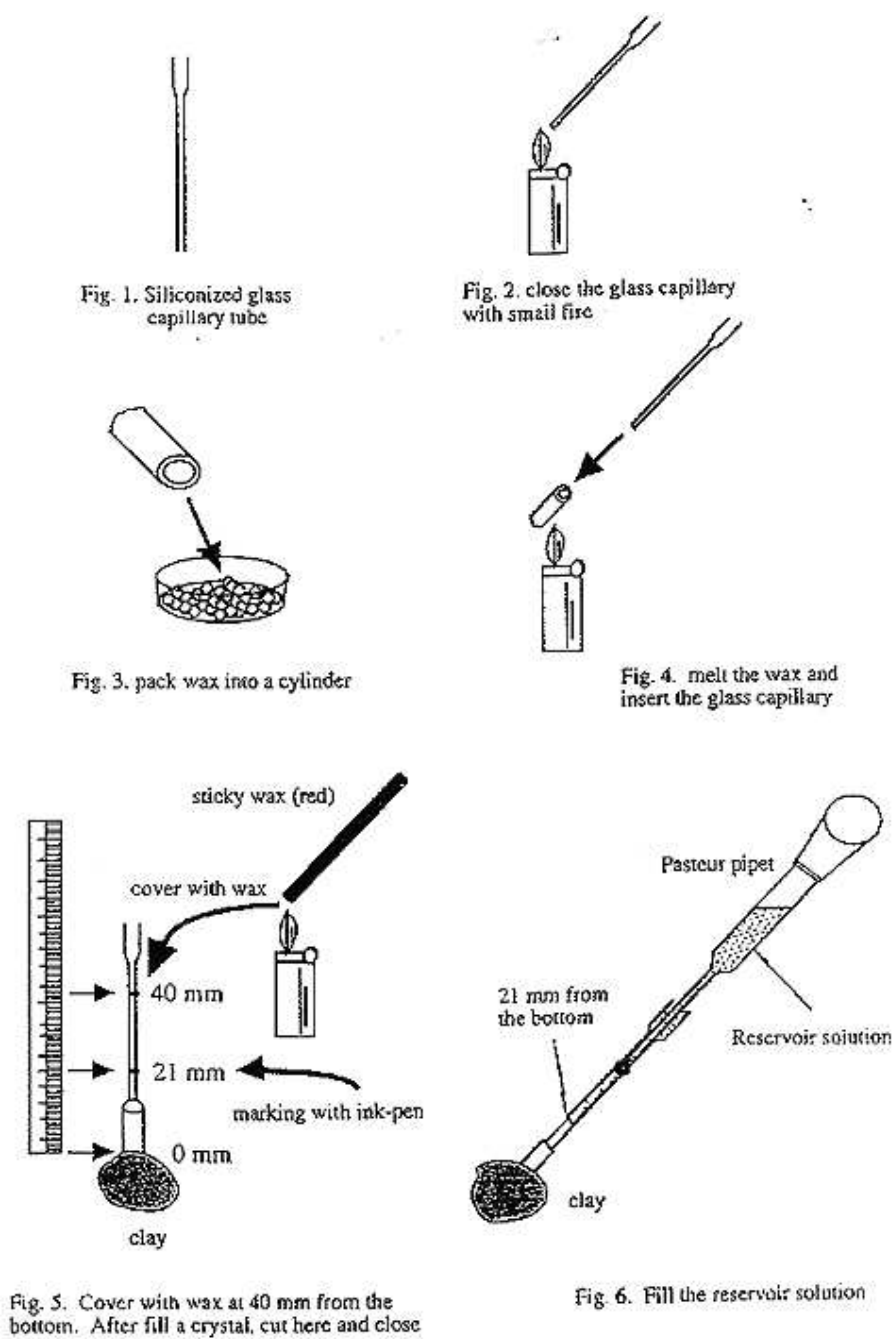


Figure 6.2: Capillary crystal mounting step 1*

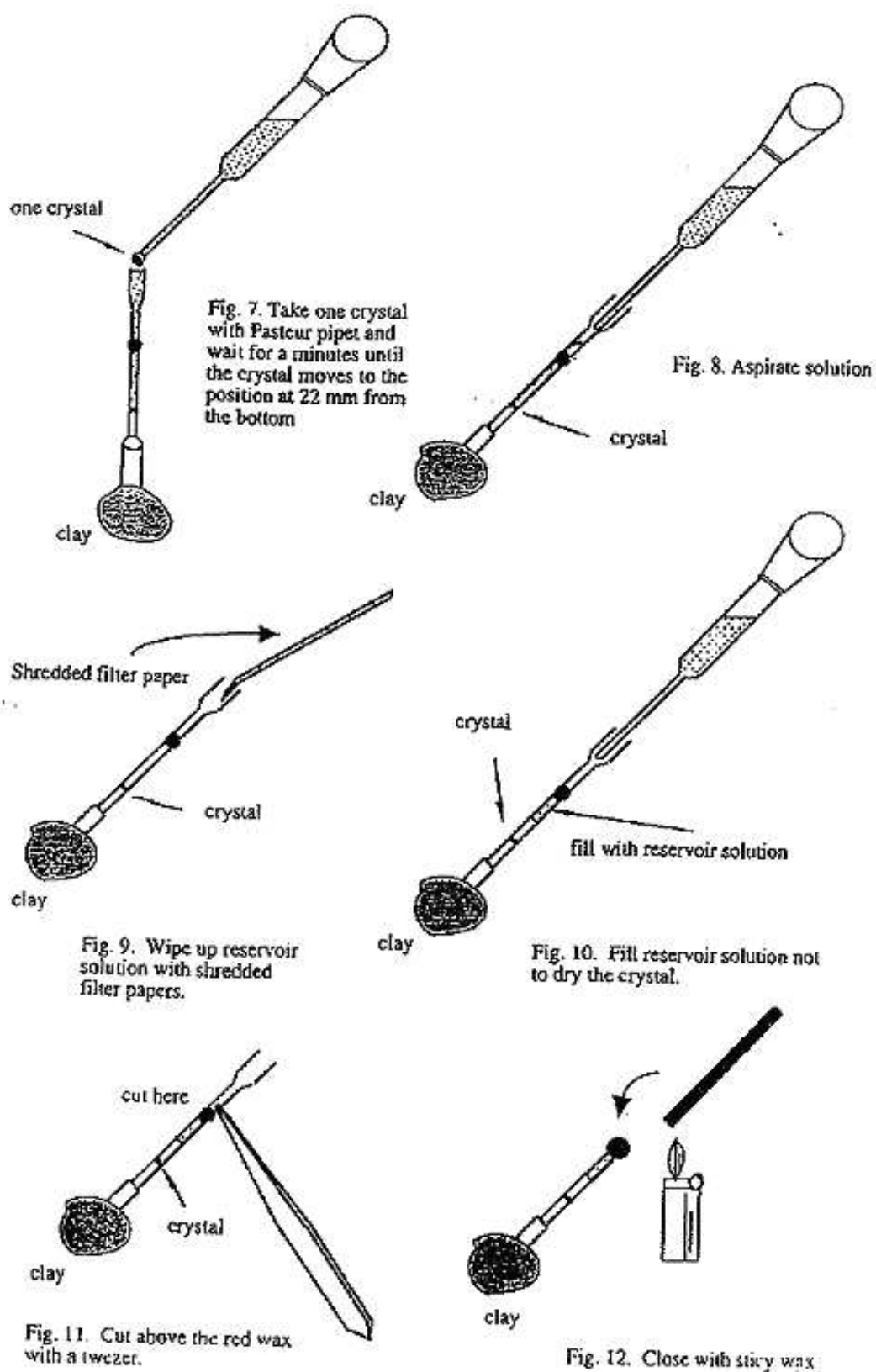


Figure 6.3: Capillary crystal mounting step 2*

6.5 Netropsin Binding Thermodynamics

Table 6.3: Sequence dependent Netropsin binding energies.

DNA Duplex	ΔG [$\frac{kcal}{mol}$]	ΔH [$\frac{kcal}{mol}$]	ΔS [$\frac{kcal}{mol}$]
polyd(AT) polyd(AT)	-12.7	-11.2	5.0
polyd(A) polyd(T)	-12.2	-2.2	33.0
polyd(GC) polyd(GC)	-7.1	-4.3	9.3
d(GCGAATTTCGC)2	-11.5	-9.3	-7.5

6.6 Properties and Sequences of Used Sticky Ends

Table 6.4: Sticky ends for the DX Motif for 2D Arrays

Sequence 5'-3'	$\Delta G_{37.0^\circ C}^O [\frac{kcal}{mol}]$	$\Delta H^O [\frac{kcal}{mol}]$	$\Delta S^O [\frac{cal}{K}]$
GAT	-0.17	-13.00	-41.37
GTA	-0.01	-13.20	-42.53
ACG	-1.60	-16.60	-48.36
ACC	-1.27	-14.00	-41.05

Table 6.5: Sticky ends for the CDM Triangle Motif for 3D Assembly

Motif	Sequence 5'-3'	$\Delta G_{37.0^\circ C}^O [\frac{kcal}{mol}]$	$\Delta H^O [\frac{kcal}{mol}]$	$\Delta S^O [\frac{cal}{K}]$
System A	CATAC	-2.39	-31.10	-92.57
System A	GTTCT	-3.01	-29.90	-86.70
System A	TAGAT	-1.98	-25.80	-76.80
System B	CATC	-1.67	-23.70	-71.03
System B	ACAG	-2.16	-22.30	-64.94
System B	TAGC	-2.09	-22.40	-65.48
System C	CATC	-1.67	-23.70	-71.03
System C	ACAG	-2.16	-22.30	-64.94
System C	TAGC	-2.09	-22.40	-65.48

Table 6.6: Sticky ends for the TxDx Triangle Motif

Sequence 5'-3'	$\Delta G_{37.0^\circ C}^O [\frac{kcal}{mol}]$	$\Delta H^O [\frac{kcal}{mol}]$	$\Delta S^O [\frac{cal}{K}]$	$T_M [^\circ C]$
GATGGC	-5.75	-41.50	-115.27	37.5
GA CTGC	-5.75	-42.50	-118.49	37.5
G TAGCG	-5.75	-43.60	-122.04	37.5
CTGACG	-5.68	-43.30	-121.30	37.0
TCGTTG	-5.35	-41.20	-115.59	34.6
GCTGTG	-5.90	-42.80	-118.98	38.6

Table 6.7: Sticky Ends for the TXA Motif for 3D Assembly

Sequence 5'-3'	$\Delta G_{37.0^\circ C}^O [\frac{kcal}{mol}]$	$\Delta H^O [\frac{kcal}{mol}]$	$\Delta S^O [\frac{cal}{K}]$
GCT	-1.51	-15.20	-44.14
CTC	-0.62	-15.80	-48.94
CATG	-1.39	-24.00	-72.89

Sequence

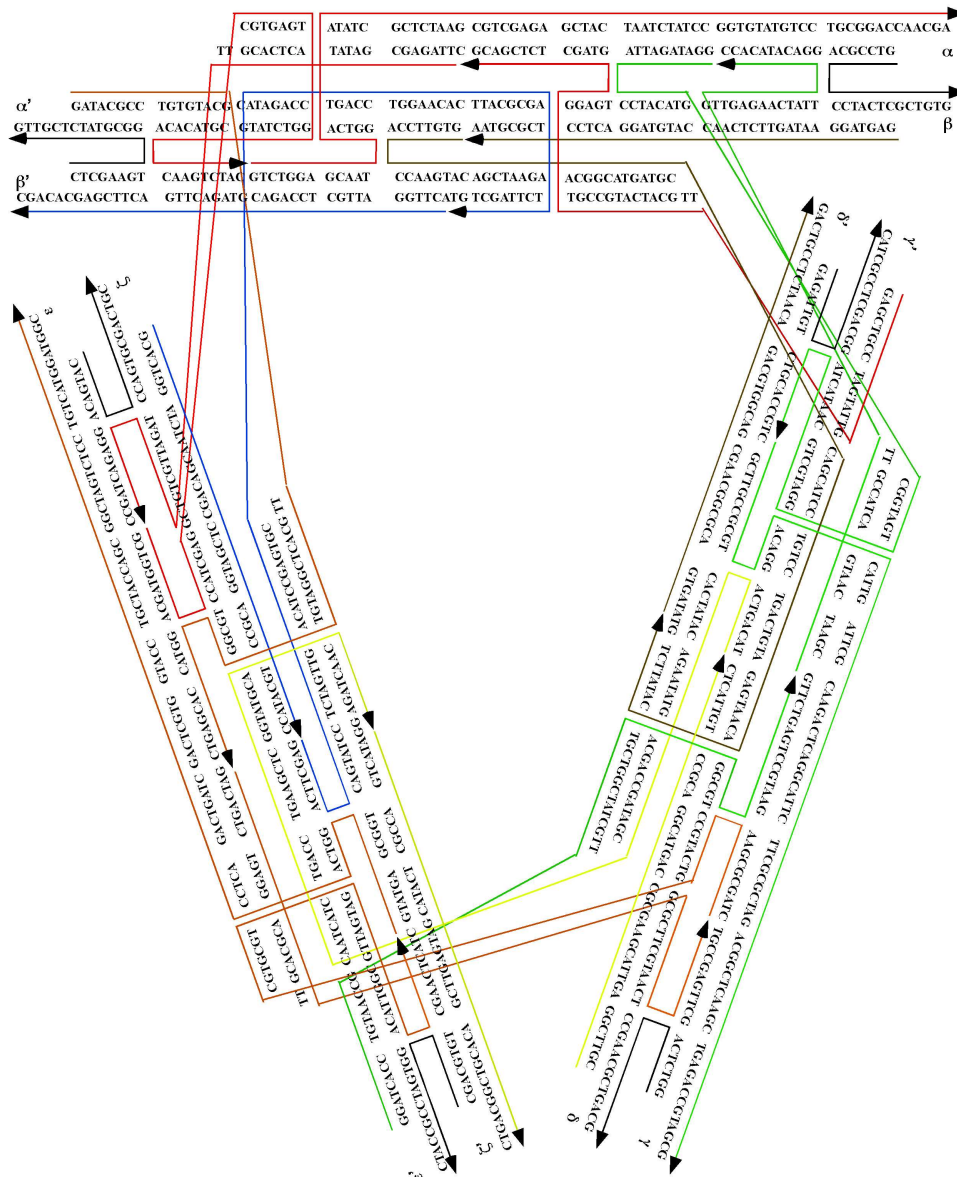


Figure 6.4: Sequence and strand structure of TXDX triangle.

6.8 Pipetting Strand Combinations for the TXDX Triangle

Table 6.8: Strand combinations for the 3D TXDX Triangle

Strand	0D	1D-A	1D-B	1D-C	2D-A	2D-B	2D-C	3D
TXDXtri-1-22	0	0	1	1	0	1	1	1
TXDXtri-2-41	1	1	1	1	1	1	1	1
TXDXtri-3-73	1	1	1	1	1	1	1	1
TXDXtri-4-43	1	1	1	1	1	1	1	1
TXDXtri-5-48	1	1	1	1	1	1	1	1
TXDXtri-6-46	1	1	1	1	1	1	1	1
TXDXtri-7-50	1	1	1	1	1	1	1	1
TXDXtri-8-77	1	1	1	1	1	1	1	1
TXDXtri-9-20	0	0	1	1	0	1	1	1
TXDXtri-10-22	0	1	0	1	1	0	1	1
TXDXtri-11-41	1	1	1	1	1	1	1	1
TXDXtri-12-73	1	1	1	1	1	1	1	1
TXDXtri-13-43	1	1	1	1	1	1	1	1
TXDXtri-14-51	1	1	1	1	1	1	1	1
TXDXtri-15-43	1	1	1	1	1	1	1	1
TXDXtri-16-51	1	1	1	1	1	1	1	1
TXDXtri-17-76	1	1	1	1	1	1	1	1
TXDXtri-18-20	0	1	0	1	1	0	1	1
TXDXtri-19-22	0	1	1	0	1	1	0	1

Continued on next page

Table 6.8 – continued from previous page

Strand	0D	1D-A	1D-B	1D-C	2D-A	2D-B	2D-C	3D
TXDXtri-20-41	1	1	1	1	1	1	1	1
TXDXtri-21-73	1	1	1	1	1	1	1	1
TXDXtri-22-43	1	1	1	1	1	1	1	1
TXDXtri-23-48	1	1	1	1	1	1	1	1
TXDXtri-24-44	1	1	1	1	1	1	1	1
TXDXtri-25-53	1	1	1	1	1	1	1	1
TXDXtri-26-76	1	1	1	1	1	1	1	1
TXDXtri-27-20	0	1	1	0	1	1	0	1
TXDXtri-1BE-22	1	0	1	1	1	0	0	0
TXDXtri-9BE-20	1	0	1	1	1	0	0	0
TXDXtri-10BE-22	1	1	0	1	0	1	0	0
TXDXtri-18BE-20	1	1	0	1	0	1	0	0
TXDXtri-19BE-22	1	1	1	0	0	0	1	0
TXDXtri-27BE-20	1	1	1	0	0	0	1	0

6.9 Calculation of Unique 7mers for the AT-rich sequence

Table 6.9: Calculation of unique 7 mers

No.	Binary	Eliminate	Compl.	Invert	Replace	Sort	Unique
0	0000000						
1	0000001						
2	0000010						
3	0000011						
4	0000100						
5	0000101						
6	0000110						
7	0000111						
8	0001000	0001000	1110111	1110111	AAATAAA	AAATAAA	AAATAAAT
9	0001001	0001001	1110110	0110111	AAATAAT	AAATAAT	AAATAATT
10	0001010	0001010	1110101	1010111	AAATATA	AAATATA	AAATATAT
11	0001011	0001011	1110100	0010111	AAATATT	AAATATT	AAATATTA
12	0001100	0001100	1110011	1100111	AAATTAA	AAATTAA	AAATTAAT
13	0001101	0001101	1110010	0100111	AAATTAT	AAATTAT	AAATTATA
14	0001110	0001110	1110001	1000111	AAATTTA	AAATTTA	AAATTTAT
15	0001111					AATAAAT	AATAATAT
16	0010000					AATAATA	AATATAAT
17	0010001	0010001	1101110	0111011	AATAAAT	AATAAAT	AAATAAAT
18	0010010	0010010	1101101	1011011	AATAATA	AATATAA	AATTAAAT
19	0010011	0010011	1101100	0011011	AATAATT	AATATAT	AATTTAAA
20	0010100	0010100	1101011	1101011	AATATAA	AATATTA	ATAAATAA
21	0010101	0010101	1101010	0101011	AATATAT	AATTTAA	ATAAATAA
22	0010110	0010110	1101001	1001011	AATATTA	AATTAAT	ATAATTAA
23	0010111	0010111	1101000	0001011		AATTATA	TATATAAA
24	0011000	0011000	1100111	1110011	AATTAAA	AATTTAA	ATATTAAA

Continued on next page

Table 6.9 – continued from previous page

No.	Binary	Eliminate	Compl.	Invert	Replace	Sort	Unique
25	0011001	0011001	1100110	0110011	AATTAAT	AATTTAT	ATATTTAA
26	0011010	0011010	1100101	1010011	AATTATA	ATAAATA	ATTAATAA
27	0011011	0011011	1100100	0010011		ATAATAA	ATTATTTAA
28	0011100	0011100	1100011	1100011	AATTTAA	ATAATAT	ATTTATAT
29	0011101	0011101	1100010	0100011	AATTTAT	ATAATTA	
30	0011110					ATATAAA	
31	0011111					ATATAAT	
32	0100000					ATATATA	
33	0100001					ATATTAA	
34	0100010	0100010	1011101	1011101	ATAAATA	ATATTTA	
35	0100011	0100011	1011100	0011101		ATTAAAT	
36	0100100	0100100	1011011	1101101	ATAATAA	ATTAATA	
37	0100101	0100101	1011010	0101101	ATAATAT	ATTATAA	
38	0100110	0100110	1011001	1001101	ATAATTA	ATTATTA	
39	0100111	0100111	1011000	0001101		ATTTAAA	
40	0101000	0101000	1010111	1110101	ATATAAA	ATTTATA	
41	0101001	0101001	1010110	0110101	ATATAAT	TAAATAA	
42	0101010	0101010	1010101	1010101	ATATATA	TAAATTA	
43	0101011	0101011	1010100	0010101		TAATAAA	
44	0101100	0101100	1010011	1100101	ATATTAA	TAATATA	
45	0101101	0101101	1010010	0100101		TAATTAA	
46	0101110	0101110	1010001	1000101	ATATTTA	TATAATA	
47	0101111					TATATAA	
48	0110000					TATTTAA	
49	0110001	0110001	1001110	0111001	ATTAAAT	TATTTAA	
50	0110010	0110010	1001101	1011001	ATTAATA	TTAATAA	
51	0110011	0110011	1001100	0011001		TTATAAA	
52	0110100	0110100	1001011	1101001	ATTATAA	TTATTAA	
53	0110101	0110101	1001010	0101001		TTTATAA	
54	0110110	0110110	1001001	1001001	ATTATTA		

Continued on next page

Table 6.9 – continued from previous page

No.	Binary	Eliminate	Compl.	Invert	Replace	Sort	Unique
55	0110111	0110111	1001000	0001001			
56	0111000	0111000	1000111	1110001	ATTTAAA		
57	0111001	0111001	1000110	0110001			
58	0111010	0111010	1000101	1010001	ATTTATA		
59	0111011	0111011	1000100	0010001			
60	0111100						
61	0111101						
62	0111110						
63	0111111						
64	1000000						
65	1000001						
66	1000010						
67	1000011						
68	1000100	1000100	0111011	1101110	TAAATAA		
69	1000101	1000101	0111010	0101110			
70	1000110	1000110	0111001	1001110	TAAATTA		
71	1000111	1000111	0111000	0001110			
72	1001000	1001000	0110111	1110110	TAATAAA		
73	1001001	1001001	0110110	0110110			
74	1001010	1001010	0110101	1010110	TAATATA		
75	1001011	1001011	0110100	0010110			
76	1001100	1001100	0110011	1100110	TAATTAA		
77	1001101	1001101	0110010	0100110			
78	1001110	1001110	0110001	1000110			
79	1001111						
80	1010000						
81	1010001	1010001	0101110	0111010			
82	1010010	1010010	0101101	1011010	TATAATA		
83	1010011	1010011	0101100	0011010			
84	1010100	1010100	0101011	1101010	TATATAA		

Continued on next page

Table 6.9 – continued from previous page

No.	Binary	Eliminate	Compl.	Invert	Replace	Sort	Unique
85	1010101	1010101	0101010	0101010	TATTAAA		
86	1010110	1010110	0101001	1001010			
87	1010111	1010111	0101000	0001010			
88	1011000	1011000	0100111	1110010			
89	1011001	1011001	0100110	0110010			
90	1011010	1011010	0100101	1010010	TATTTAA		
91	1011011	1011011	0100100	0010010			
92	1011100	1011100	0100011	1100010			
93	1011101	1011101	0100010	0100010			
94	1011110						
95	1011111				TTAATAA		
96	1100000						
97	1100001						
98	1100010	1100010	0011101	1011100			
99	1100011	1100011	0011100	0011100			
100	1100100	1100100	0011011	1101100	TTATAAA		
101	1100101	1100101	0011010	0101100			
102	1100110	1100110	0011001	1001100			
103	1100111	1100111	0011000	0001100			
104	1101000	1101000	0010111	1110100			
105	1101001	1101001	0010110	0110100	TTATTAA		
106	1101010	1101010	0010101	1010100			
107	1101011	1101011	0010100	0010100			
108	1101100	1101100	0010011	1100100			
109	1101101	1101101	0010010	0100100			
110	1101110	1101110	0010001	1000100			
111	1101111						
112	1110000						
113	1110001	1110001	0001110	0111000			
114	1110010	1110010	0001101	1011000			

Continued on next page

Table 6.9 – continued from previous page

No.	Binary	Eleminate	Compl.	Invert	Replace	Sort	Unique
115	1110011	1110011	0001100	0011000	TTTATAA		
116	1110100	1110100	0001011	1101000			
117	1110101	1110101	0001010	0101000			
118	1110110	1110110	0001001	1001000			
119	1110111	1110111	0001000	0001000			
120	1111000						
121	1111001						
122	1111010						
123	1111011						
124	1111100						
125	1111101						
126	1111110						
127	1111111						

6.10 DNA Crystallization Conditions from Literature

Table 6.10: DNA Crystals and Crystallization Conditions

DNA Type	Length [nt]	Conc.[mM]	Conc. [$\frac{mg}{ml}$]	Helicity	Reference
C-DNA	1 x 10 nt	2		$9 \frac{1}{3}$	[60]
B-DNA	1 x 10 nt	2	6.6	10	[34]
B-DNA	1 x 12 nt	0.8	3.2		[94]
B-DNA	2 x 12 nt	0.2	1.6	10	[67]
Holliday Junc.	1 x 10 nt	0.25	0.8		[20]
B-DNA	1 x 12 nt	3/4	2.5	10	[19]
B-DNA	1 x 10 nt	n.a.	9-10		[73]
B-DNA	1 x 12 nt	0.5	2		[9]
B-DNA	1 x 12 nt	0.5 Duplex	4		[16]
B-DNA	1 x 12 nt	n.a.	1.2-1.3		[111]
B-DNA	1 x 10 nt	0.2 Duplex	1.3		[1]
B-DNA	1 x 12 nt	0.5	2		[7]
Holliday Junc.	1 x 10 nt	0.5	1.7		[99]
B-DNA	1 x 12 nt	1.8	7.1		[87]
Crossed Junc.	1 x 10 nt	3 Duplex	19.8	10.1	[110]
B-DNA	1 x 12 nt	1	4		[50]
B -DNA	1 x 12 nt	1	4		[88]
B-DNA	1 x 12 nt	0.23	0.9		[46]
B-DNA	1 x 12 nt	1	4		[40]

Continued on next page

Table 6.10 – continued from previous page

DNA Type	Length [nt]	Conc.[mM]	Conc. [$\frac{mg}{ml}$]	Helicity	Reference
Holliday Junc.	1 x 10 nt	1 Duplex	6.6		[97]
B-DNA	1 x 12 nt	2.6	10.3		[91]
B-DNA	1 x 12 nt	1	4		[47]
Pseudo Junc.	1 x 10 nt	1.2	4		[93]
28 nt	1 x 28 nt	0.5	4.6		[42]
B-DNA	1 x 12 nt	n.a.			[12]
B-DNA	1 x 12 nt	0.8-1.2	3.2-4.8		[65]
B-DNA	2 x 12 nt	n.a.	5		[18]
B-DNA	1 x 10 nt	0.6	2	10	[44]
B-DNA	1 x 10 nt	n.a.		10	[35]
B-DNA	1 x 12 nt	0.5 Duplex	4	10	[41]
B-DNA	1 x 12 nt	1	4		[89]
Holliday Junc.					[52]
B DNA	1 x 10 nt	0.37 Duplex	1.2		[32]
B-DNA	1 x 12 nt	1	4		[63]
A DNA	1 x 10 nt	2	6.6	11.1	[74]
B-DNA	1 x 12 nt	0.5 Duplex	4		[8]
B-DNA	1 x 10 nt	1.9	6.3		[53]
B-DNA	1 x 10 nt	0.54 Duplex	1.8		[29]
Holliday Junc.	1 x 10 nt	0.333	1.1		[70]
A DNA	1 x 10 nt	1	3.3		[75]
B-DNA	1 x 12 nt	n.a.			[5]
B-DNA	2 x 12 nt	1 Duplex	7.9		[98]
B-DNA	1 x 12 nt	0.93	3.7		[26]

Continued on next page

Table 6.10 – continued from previous page

DNA Type	Length [nt]	Conc.[mM]	Conc. [$\frac{mg}{ml}$]	Helicity	Reference
Holliday Junc.	n.a.	n.a.	n.a.	9.7	[37]
B-DNA	1 x 10 nt	0.39	1.3		[28]
Cross arrang.	1 x 10 nt	1.34	4.4		[27]
B-DNA	1 x 12 nt	1	4		[49]
B-DNA	1 x 12 nt	1.2	4.8		[95]
RNA/DNA	68+20 duplex	n.a.	n.a.		[69]
B-DNA	1 x 12 nt	n.a.			[48]

6.11 Calculation of CDM Triangle Properties

Table 6.11: CDM Triangle Properties with Minimal Turns.

Helicity	INNER			MINIMAL TURNS			
	Bases	DNA Angle	Geom. Angle	Bases	DNA Angle	Total DNA	Total Geom.
10.5	13	86	116	8	274.3	0.0	30.3
10.5	13	86	116	8	274.3	0.0	30.3
10.5	13	86	116	7	240.0	-34.3	-4.0
10.5	14	120	119	7	240.0	0.0	-1.0
10.5							
10.5	15	154	121	6	205.7	0.0	-33.3
10.5	15	154	121	7	240.0	34.3	1.0
10.5							
10.5	16	189	236	5	171.4	0.0	47.4
10.5	16	189	236	4	137.1	-34.3	13.1
10.5							
10.5	17	223	234	4	137.1	0.0	11.1
10.5	17	223	234	13	445.7	-51.4	-40.3
10.5							
10.5	18	257	232	3	102.9	0.0	-25.1
10.5	18	257	232	4	137.1	34.3	9.1
10.5							
10.5	19	291	230	2	68.6	0.0	-61.4

Continued on next page

Table 6.11 – continued from previous page

Helicity	INNER			MINIMAL TURNS			
	Bases	DNA Angle	Geom. Angle	Bases	DNA Angle	Total DNA	Total Geom.
10.5	19	291	230	4	137.1	68.6	7.1
10	13	108	116	7	252.0	0.0	8.0
10	14	144	118	6	216.0	0.0	-26.0
10	14	144	118	7	252.0	36.0	10.0
10	15	180	x				
10	16	216	236	4	144.0	0.0	20.0
10	16	216	236	3	108.0	-36.0	-16.0
10	17	252	234	3	108.0	0.0	-18.0
10	17	252	234	4	144.0	36.0	18.0
10	18	288	232	2	72.0	0.0	-56.0
10	18	288	232	4	144.0	72.0	16.0
10	19	324	230	7	252.0	-144.0	122.0

Table 6.12: CDM Triangle Properties with 1 Turn.

Helicity	INNER			ONE TURN			
	Bases	DNA Angle	Geom. Angle	Bases	DNA Angle	Total DNA	Total Geom.
10.5	13	86	116	19	651.4	17.1	47.4
10.5	13	86	116	18	617.1	-17.1	13.1
10.5	13	86	116	18	617.1	-17.1	13.1
10.5	14	120	119	18	617.1	17.1	16.1
10.5	14	120	119	18	617.1	17.1	16.1
10.5	15	154	121	17	582.9	17.1	-16.1
10.5	15	154	121	17	582.9	17.1	-16.1
10.5	16	189	236	15	514.3	-17.1	30.3
10.5	16	189	236	14	480.0	-51.4	-4.0
10.5	17	223	234	14	480.0	-17.1	-6.0
10.5	17	223	234	13	445.7	-51.4	-40.3
10.5	18	257	232	14	480.0	17.1	-8.0
10.5	18	257	232	14	480.0	17.1	-8.0
10.5	19	291	230	13	445.7	17.1	-44.3
10.5	19	291	230	14	480.0	51.4	-10.0

Continued on next page

Table 6.12 – continued from previous page

Helicity	INNER			ONE TURN			
	Bases	DNA Angle	Geom. Angle	Bases	DNA Angle	Total DNA	Total Geom.
10	13	108	116				
10	14	144	118	18	648.0	72.0	46.0
10	14	144	118				
10	15	180	x				
10	16	216	236				
10	16	216	236				
10	17	252	234	13	468.0	0.0	-18.0
10	17	252	234	14	504.0	36.0	18.0
10	18	288	232				
10	18	288	232	14	504.0	72.0	16.0
10	19	324	230				

Table 6.13: CDM Triangle Properties with 1 Turn.

Helicity	INNER			$1\frac{1}{2}$ TURNS			
	Bases	DNA Angle	Geom. Angle	Bases	DNA Angle	Total DNA	Total Geom.
10.5	14	120	118	23	788.6	8.6	6.6
10.5	14	120	118	22	754.3	-25.7	-27.7
10.5	14	120	118	21	720.0	-60.0	-62.0
10.5	17	223	234	20	685.7	8.6	19.7
10.5	17	223	234	19	651.4	-25.7	-14.6
10.5	17	223	234	19	651.4	-25.7	-14.6
10.5	17	223	234	19	651.4	-25.7	-14.6
10.5	18	257	232	19	651.4	8.6	-16.6
10.5	18	257	232	18	617.1	-25.7	-50.9
10.5	18	257	232	17	582.9	-60.0	-85.1
10.5	18	257	232	16	548.6	-94.3	-119.4
10	14	144	118	21	756.0	0.0	-26.0
10	14	144	118	22	792.0	36.0	10.0
10	14	144	118	23	828.0	72.0	46.0
10	17	252	234	18	648.0	0.0	-18.0
10	17	252	234	19	684.0	36.0	18.0

Continued on next page

Table 6.13 – continued from previous page

Helicity	INNER			1.5 TURNS			
	Bases	DNA Angle	Geom. Angle	Bases	DNA Angle	Total DNA	Total Geom.
10	17	252	234	19	684.0	36.0	18.0
10	18	288	232	17	612.0	0.0	-56.0
10	18	288	232	18	648.0	36.0	-20.0
10	18	288	232	19	684.0	72.0	16.0
10	18	288	232	19	684.0	72.0	16.0

Table 6.14: CDM Triangle Properties with 1 Turn.

Helicity	INNER			TWO TURNS			
	Bases	DNA Angle	Geom. Angle	Bases	DNA Angle	Total DNA	Total Geom.
10.5	14	120	118	28	960.0	0.0	-2.0
10.5	14	120	118	27	925.7	-34.3	-36.3
10.5	14	120	118	26	891.4	-68.6	-70.6
10.5	17	223	234	25	857.1	0.0	11.1
10.5	17	223	234	25	857.1	0.0	11.1
10.5	17	223	234	24	822.9	-34.3	-23.1
10.5	17	223	234	23	788.6	-68.6	-57.4
10.5	18	257	232	25	857.1	34.3	9.1

Continued on next page

Table 6.14 – continued from previous page

Helicity	INNER			TWO TURNS			
	Bases	DNA Angle	Geom. Angle	Bases	DNA Angle	Total DNA	Total Geom.
10.5	18	257	232	24	822.9	0.0	-25.1
10.5	18	257	232	23	788.6	-34.3	-59.4
10.5	18	257	232	22	754.3	-68.6	-93.7
10	14	144	118	26	936.0	0.0	-26.0
10	14	144	118	27	972.0	36.0	10.0
10	14	144	118	28	1008.0	72.0	46.0
10	17	252	234	23	828.0	0.0	-18.0
10	17	252	234	24	864.0	36.0	18.0
10	17	252	234	25	900.0	72.0	54.0
10	18	288	232	22	792.0	0.0	-56.0
10	18	288	232	23	828.0	36.0	-20.0
10	18	288	232	24	864.0	72.0	16.0
10	18	288	232	25	900.0	108.0	52.0

6.12 All DNA Strand Sequences used in 5'to 3' Direction

6.12.1 Strands for DX 2D Array with Short Sticky Ends

STRAND NTA1-47nt G A T G G C G A C A T C C T G C C G C T A T
G A T T A C A C A G C C T G A G C A T T G A C A C

STRAND NTA2-42nt T G T A G T A T C G T G G C T G T G T A
A T C A T A G C G G C A C C A A C T G G C A

STRAND NTA3-29nt A C C G T G T C A A T G C T C A C C G A
T G C A A C C A G

STRAND NTA4-24nt G T A G C G C C G T T A G T G G A T G T C G C C

STRAND NTA5-48nt A C G C T G G T T G C A T C G G A C G A
T A C T A C A T G C C A G T T G G A C T A A C G G C G C

STRAND NTB1-25nt C G T C A G G C T G C T G T G G T C G T
G C G A C

STRAND NTB2-43nt A G T A C A A C G C C A C C G A T G C G
G T C A C T G G T T A G T G G A T T G C G T

STRAND NTB3-28nt A T C C G T C G A T A C G G C A C C A T
G A T G C A C G

STRAND NTB4-69nt T A C C G T G C A T C A T G G A C T A A
C C A G T G C T C G C T G A T T T T T C A G C G A G T T A C C
G C A T C G G A C A G C A G C C T G

STRAND NTB5-70nt G G T G T C G C A C G A C C T G G C G T
C T G T T G A C T T T T G T C A A C A G T T T G T A C T A C G
C A A T C C T G C C G T A T C G A C G

6.12.2 Strands used for 3D project with TX Motif

STRAND TX-1-60nt G A G C A T T C A G C A A G C G T G G A G T
G G C A G A C C G C A T A G G T A T C T G A C G G A C A A C A
T C G G C A C

STRAND TX-2-65nt G T A C G A C A T A C G T T G G A C T C
C T G A T A G C T C G C C A G T G G T C A C A G T A G T C G G
A C G C T T G C T G A A T G

STRAND TX-3-62-nt C A T G A C T T G A G C C T G A G G A C
T G G C G A G C T A T C A C C G A C T A C T G T G A C C T G C
G A A C T G C T A C C

STRAND TX-4-60nt G C T G G T A G C A G T T C G C A C C T
C A C C G T C A G A T A C C T A T G C G G T C T G C C T G T A
G A C A G A A T C

STRAND TX-5-28nt A G C G A T T C T G T C T A C A C C A A
C G T A T G T C

STRAND TX-6-25nt C T C G T G C C G A T G T T G T G G C T
C A A G T

6.12.3 Strands for Crystallization of Blunt ended DX Motif

STRAND DX1-20nt G C G A T C T A C A C C G T T C T C C G

STRAND DX2-40nt C G G A T G A G C C T G A C G A G A C T
A T T G A T A A C C T G T A G A T C G C

STRAND DX3-40ntA G T C T C G T C A C C A C A A C T C G G
G T A C T A T G T G G T T A T C A A T

STRAND DX4-40nt C G G A G A A C G G A C A T A G T A C C
C G A G T T G T G G A C T G G C A C G C

STRAND DX5-20nt G C G T G C C A G T G G C T C A T C C G

STRAND DXBR1-20nt G C G A T C T A C A C C G T A T G C C
G

STRAND DXBR2-40nt C G G A t G A G C C T G A c G A G A C t
A T t G A t A A C C T G t A G A t C G C

STRAND DXBR3-40nt T G G T A C T A T G T G G T T A T C A
A T A G T C T C G T C A C C A C A A C T C

STRAND DXBR-4-40nt C G G c A t A C G G A C A t A G t A C c
A G A G t T G t G G A C T G G c A c G C

STRAND CDBR5-20nt G C G T G C C A G T G G C T C A T C C
G

6.12.4 DNA Triangle Strands Designed by Prof. ChengDe Mao

STRAND CDMT1-18nt G C T G C T A C A C C G T G T T C G

STRAND CDMT2-38nt C G T G A G C C T G A C G A G T G T C
A T T G A T A A C C T G T A G C A G C

STRAND CDMT3-42nt G G T A C T A T G T G G T T A T C A A
T G A C A C T C G T C A C C A C A A C T C G C

STRAND CDMT4-38nt C G A A C A C G G A C A T A G T A C C
G C G A G T T G T G G A C T G G C G C

STRAND CDM5-16nt G C G C C A G T G G C T C A C G

6.12.5 DNA Strands for Gel-based studies of Triangles

STRAND CDM13-1-31nt C A G A C A G C C T G C T C T C G A T T G
G A C G A A G C C A

CDM-G2-18nt C C G C C A A G T G G C T G T C T G

STRAND CDM13-3-39nt C G A G A G C A C C G T C T A T T A
T C A C C T G A A C T C A C C A C C A A T

STRAND CDM13-4-31nt G A C T G T A C C T G G T G A G T T
C A G G A C G C T A C G A

STRAND CDM-G5-18nt T G G C T T C G T G G T A C A G T C

STRAND CDM13-6-31nt G G C A G T G C C T G A T A A T A G
A C G G A C T T G G C G G
CDM-G7-18nt T C G T A G C G T G G C A C T G C C

STRAND CDM14-1-32nt C A G A C A G C C T G C T C T C G C A
T T G G A C G A A G C C A

STRAND CDM14-3-42nt C G A G A G C A C C G T C A T A G C
A T C A C C T G T C A C T C A C C A C C A A T G

STRAND CDM14-4-32nt G A C T G T A C C T G G T G A G T G
A C A G G A C G C T A C G A

STRAND CDM14-6-32nt G G C A G T G C C T G A T G C T A T
G A C G G A C T T G G C G G

STRAND CDM15-1-33nt C A G A C A G C C T G C T C T C G C A
T C T G G A C G A A G C C A

STRAND CDM15-3-45nt C G A G A G C A C C G T C A A G C T
T A T C A C C T G A A C A C T C A C C A C C A G A T G

STRAND CDM15-4-33nt G A C T G T A C C T G G T G A G T G
T T C A G G A C G C T A C G A

STRAND CDM15-6-33nt G G C A G T G C C T G A T A A G C T
T G A C G G A C T T G G C G

STRAND CDM17-1-35nt C A G A C A G C C T G C T C T C G G
A T C G A C G G A C G A A G C C A

STRAND CDM17-3-51nt C G A G A G C A C C G T C A A C C T
A T T A T C A C C T G A A C G T A C T C A C C A C C G T C G A
T C

STRAND CDM17-4-35nt G A C T G T A C C T G G T G A G T A
C G T T C A G G A C G C T A C G A

STRAND CDM17-6-35nt G G C A G T G C C T G A T A A T A G

G T T G A C G G A C T T G G C G G

CDM18-1-36nt C A G A C A G C C T G C T C T C G G T A T C G
A C G G A C G A A G C C A

STRAND CDM18-3-54nt C G A G A G C A C C G T C A A C C A G A
T T A T C A C C T G A A C T C T A C T C A C C A C C G T C G A T A C

STRAND CDM18-4-36nt G A C T G T A C C T G G T G A G T A
G A G T T C A G G A C G C T A C G A

STRAND CDM18-6-36nt G G C A G T G C C T G A T A A T C T
G G T T G A C G G A C T T G G C G G

6.12.6 DNA Stands for 3D Triangle with 14nt per Edge

STRAND CDM3D-1-14A-42nt G T T C T G A T A G A C G A C C T G
C T G A C G C A T A G G A C G A T A G T C A T C

STRAND CDM3D-2-14A-27nt T A G A T G T C C G A C A A G T G
G T C G T C T A T C

STRAND CDM3D-3-GEN-42nt G T C A G C A C C G T C A T A G
C A T C A C C T G T C G T A C A C C A C C T A T G C

STRAND CDM3D-4-14A-42nt C A T A C G T G A C T G T A C C T
G G T G T A C G A C A G G A C G C T A A C A C T G

STRAND C5-14A-28nt A G A A C G A T G A C T A T C G T G G
T A C A G T C A C

STRAND C6-14A-42nt A T C T A C G A T T C A G T G C C T G
A T G C T A T G A C G G A C T T G T C G G A C

STRAND C7-14A-29 nt G T A T G C A G T G T T A G C G T G G
C A C T G A A T C G

STRAND C1-14B-40nt G C T A G A C G T G T C T C C T G C T
G A C G C A T A G G A C A G A C C A T A C

STRAND C2-14B-26nt A C A G A G T C G C G T A G T G G A G
A C A C G T C

STRAND C4-14B-40nt G A T G T A G T T G C G A C C T G G T
G T A C G A C A G G A C G A T G A C T G C

STRAND C5-14B-26nt T A G C G T A T G G T C T G T G G T C
G C A A C T A

STRAND C6-14B-40nt C T G T G A G T G C A T A C C T G A T
G C T A T G A C G G A C T A C G C G A C T

STRAND C7-14B-26nt C A T C G C A G T C A T C G T G G T A
T G C A C T C

STRAND C1-14C-32nt G C T A G A T A G C C T G C T G A C G
C A T A G G A C G A T A C

STRAND C2-14C-18nt A C A G T C T G A G T G G C T A T C

STRAND C4-14C-32nt G A T G T C G C T C C T G G T G T A C
G A C A G G A C A T G G C

STRAND C5-14C-18nt T A G C G T A T C G T G G A G C G A

STRAND C6-14C-32nt C T G T G A G T A C C T G A T G C T A
T G A C G G A C T C A G A

STRAND C7-14C-18nt C A T C G C C A T G T G G T A C T C

STRAND C4-A1SE-42nt C G T G A C T G T A C C T G G T G T A
C G A C A G G A C G C T A A C A C T G C A T A

STRAND C1-B-BE-40nt G A C G T G T C T C C T G C T G A C G
C A T A G G A C A G A C C A T A C G C T A

STRAND C6-A-BE-42nt C G A T T C A G T G C C T G A T G C T
A T G A C G G A C T T G T C G G A C A T C T A

6.12.7 DNA Strands for 6 Helix Bundle with Netropsin Binding Sites

STRAND 6HBNE-1-20nt G C A G A A C C G T C C A T A C A T C C

STRAND 6HBNE-2-90nt C G C A T A G T A C G A C G T C C A
C T C G C T G G A G C T T T A A A T A G T C T A A T A T T T C
C A T T T A T T T G A G G C C G T G G C A T C C A G A G G T C
A C G G T T C T G C

STRAND 6HBNE-3-90nt G G T A C G A G C G G A T C T C C T
G C C G C A G A C C T C T G G A T G C C T G G C G C A G G T C
C T A G G C A

STRAND 6HBNE-4-36nt G C T G T T C G G T C A C G G T C G
A T T C G G A C G G C C T C A A A T

STRAND 6HBNE-5-36nt A A A T G G A A A T A T T A G A G A
A A T A A T A G G T A T T T T A T C A G A T A A T A T A G

STRAND 6HBNE-6-37nt G A T T A T A A A G G C T T A A T A
A T C G C T T T T A A T T C C A T A A

STRAND 6HBNE-7-54nt T A A A G C C T C T G A C C T A T G A G G
T C G A G T A C C T G A C G C A G G A C G T C G T A C T A T G C G

STRAND 6HBNE-8-55nt C G G A G T A G A T C G A A T G G A C T G A
C C T G T C T C C G G T G C T A A G C G A G T T C A C G T T G G C

STRAND 6HBNE-9-37nt T C A T T A T A T T C C T A T T T A A
A G C T C C T A A T T T G G T A T A

STRAND 6HBNE-10-83nt T A T T G G C T A A T T A T T C G T
A A A T A T A C G C T A A A A T T T C C T T T A A T A T C A G G
A G G C G T A C G G T C T C A C G C G T T A A A A T T C T G C C G

STRAND 6HBNE-11-55nt A C C A T C G T G G A C C G C G T C
G C A C A A C A G A G C C T G C G A G T C A G C T C G A C T C
A C G T C C

STRAND 6HBNE-12-90nt G G A T G T A T G G T G C G G C A C
C A C G A T G G T C G G C A G A A T T T A T A C C T A T T A T
T T C G A A T A T A A T G A G C C A A C G T G A T G C G T C A
C C T T G A C T G G

STRAND 6HBNE-13-20nt C C A G T C A A G G A G C A A C T G
C G

STRAND 6HBNE-14-90nt C G C A G T T G C T G G T A C T C G
A C C T C A C C T T T A T A A T C C T A T A T T A T C T G A T A
A A T A A C G C G T G A G A C C A C G C G G T G G A G A T C C
G C T C G T A C C

STRAND 6HBNE-15-90nt G C G A T G A T G T G G C T C T G T
T G T G C G G T A C G C C T C C T G A T A T T A A A G G A A A

T T T A A G C G A T T A T T A A G T A G G T C A C C A T T C G
A T C T A C T C C G

STRAND 6HBNE-16-20nt G C G G T G T C G G A C A T C A T C
G C

STRAND 6HBNE-17-90nt C C A G T A T C C T G G T C A G T G
A G G C T T T A T T A T G G A A T T A A T A G C G T A T A T T
T A C A C C G A A C A G C T G C C T A G G A C C A C T C G C A
C C G A C A C C G C

STRAND 6HBNE-18-90nt G G A C G T G A G T C G A G C T G T
G C G C C A C C G A A T C G A C C G T G G A A T A A T T A G C
C A A T A T A T A C C A A A T T A T A G C A C C G G A G A C A
C C A C T A G T C C

STRAND 6HBNE-19-20nt G G A C T A G T G G A G G A T A C T
G G

Strands for 90mer DNA Duplex control:

STRAND 90m46hb1-90 G G A T G T G G T A T C G T G A T T G A C
G A C G A T T G C G T A T C C G A G G A T G C A A G C G T T G
A T A C A G C C A G T G G A G A C T A T G C G G T A C T T G G
A T G A A C G

STRAND 90m46hb2-90 C G T T C A T C C A A G T A C C G C A
T A G T C T C C A C T G G C T G T A T C A A C G C T T G C A T

C C T C G G A T A C G C A A T C G T C G T C A A T C A C G A T
A C C A C A T C C

6.12.8 DNA Strands for the TXDX Triangle Motif

STRAND TXDX_{tri-1-22} C T C G A A G T G G C G T A T C T C G T T G

STRAND TXDX_{tri-2A-41} G C A C T G G A T C T A A C G A C A
G C C T C G A T G G A C G C C T G C A T A C C

STRAND TXDX_{tri-2B-73} G A G C T T C A C A G T A T C C T C
T A G T T G A C A T C C G A G T G C C A T A G A C C T G A C C
T G G A A C A C T T A C G C G A T C T T A G C T

STRAND TXDX_{tri-2C-43} G T A C T T G G A T T G C T C C A G
A C G T A G A C T T G A C T T C G A G C A C A G C

STRAND TXDX_{tri-3A-48} G A G C T G C C T A G T A T T G T T
G C A T C A T G C C G T G G A G T G T A G C T C T C G A C G

STRAND TXDX_{tri-3B-46} C T T A G A G C G A T A T A C T C A
C G T T G C T G T C G T T A G A T G G A G A C T A G C C

STRAND TXDX_{tri-3C-50} G C T G G T A G C A C C A T C G A G
C G T G A G T G G T C T A T G C G T A C A C A C A A G T C T A C

STRAND TXDX_{tri-3D-77} G T C T G G A G C A A T G G T C A A

T A T C G C T C T A A G C G T C G A G A G C T A C T A A T C T
A T C C G G T G T A T G T C C T G C G G A C C A A C G A

STRAND TXDXtri-4-20 G T C C G C A C C T A C T C G C T G T
G

STRAND TXDXtri-5-22 G A G A T T G T G G C A G C T C C G C T A C

STRAND TXDXtri-6A-41 G A G T A G G A A T A G T T C T C A
A C C A T G T A G G A C T C C T C G C G T A A

STRAND TXDXtri-6B-73 G T G T T C C A C C A A G T A C A G
C T A A G A A C G G C A T G A T G C C A G C A T C C T G T C C
T G A C T G T A G A G T A A C A C A T A T T C T

STRAND TXDXtri-6C-43 G T A T A G T G A C G C G G C A A G
C G A C G G T G C A G A C A A T C T C C G T C A G

STRAND TXDXtri-7A-51 G G A T C A C C T G T A A C C G T T
G C T A T C G G T C G T G G C G T G A A T G C C T G A G T C T
T G

STRAND TXDXtri-7B-43 C G A A T C A A T G A C T A C C G T
T G T T G A G A A C T A T T G G A C A T A C A C C

STRAND TXDXtri-7C-51 G G A T A G A T T A C C T A C A T G
C G G T A G T G G A T G C T G C A A T A C T A C T G C A C C G

T C

STRAND TXDXtri-7D-76 G C T T G C C G C G T G G A C A C A
T T G A T T C G C A A G A C T C A G G C A T T C T T C G C G C
T A G A C G G C T C A A G C T G A G A C C G T A G C G

STRAND TXDXtri-8-20 G G T C T C A C C G A A C G C T G A C
G

STRAND TXDXtri-9-22 C G A C G T G T G G T G A T C C G C C A T C

STRAND TXDXtri-10A-41 C G T T C G G A G T T A C G A A G C
G C C A G T A C G G A C G C C T G T T A C T C

STRAND TXDXtri-10B-73 T A C A G T C A C A C T A T A C A G
A A T A T G A C G A C C G A T A G C C A A T C A T C T G A C C
T G A A G C T C G G T A T G C A C A A C T A G A

STRAND TXDXtri-10C-43 G G T A T G C A C A A C T A G A G G
A T A C T G A C C G C T C A T A C G A T G A G T T C G A C A C
G T C G G C A G T C

STRAND TXDXtri-11A-48 G A T A C G C C T G T G T A C G T T
G C A C T C G G A T G T G G C G T G G T A C G A C G A G T C

STRAND TXDXtri-11B-44 G A T C A G T C T G A G G A C G C A
C G T T G C G C T T C G T A A C T G C T T G A G C C

STRAND TXDXtri-11C-53 G T C T A G C G C G A A C C G T A C
T G C G T G C G T G A T G A T T G C G G T T A C A C G A A C T
C A T C

STRAND TXDXtri-11D-76 G T A T G A G C G G T G G T C A C C
T C A G A C T G A T C G A C T C G T C G T A C C T G C T A C C
A G C G G C T A G T C T C C T G T C A T G G A T G G C

STRAND TXDXtri-12-20 C A T G A C A C C A G T G C G A C T
G C

STRAND TXDXtri-1BE-22 G C T G T G C T C G A A G T G G C
G T A T C

STRAND TXDXtri-4BE-20 T C G T T G G T C C G C A C C T A C
T C

STRAND TXDXtri-5BE-22 C T G A C G G A G A T T G T G G C
A G C T C

STRAND TXDXtri-8BE-20 C G C T A C G G T C T C A C C G A A
C G

STRAND TXDXtri-9BE-22 G A C T G C C G A C G T G T G G T
G A T C C

STRAND TXDXtri-12BE-20 G C C A T C C A T G A C A C C A G
T G C

6.13 Lebenslauf - Curriculum Vitae

Name: Jens Kopatsch

Geburtsdatum: 3. September 1972

Geburtsort: Salmünster

1979-1983 Philipp-Reis Grundschule, Gelnhausen

1983-1985 Rudolf-Steiner Schule, Loheland

1985-1993 Grimmelshausen Gymnasium, Gelnhausen

06/1993 Abitur am Grimmelshausen Gymnasium, Gelnhausen

10/1993 Aufnahme des Studiums der Biotechnologie an der TU Berlin

07/1997-11/1997 Studienarbeit an der Dongseo University in Süd Korea
(Pusan) über kontinuierliche Kultivierung von Mikroalgen

04/1998-10/1998 Diplomarbeit an der New York University im Institut für
Chemie über Self Assembly of 2-dimensional DNA Arrays

10/1999 Abschluss des Studiums an der TU Berlin als
Diplom Ingenieur Fachrichtung Biotechnologie

09/2004 Promotion an der TU Berlin, Fakultät für Prozesswissenschaften.

Die Forschungsarbeit wurde an der der New York University im Institut
für Chemie bei Prof. Dr. Nadrian C. Seeman durchgeführt. Betreuer an der
TU Berlin war Prof. Dr. Ulf Stahl.